POLITECNICO DI MILANO

SCUOLA DI INGEGNERIA CIVILE, AMBIENTALE E TERRITORIALE

CORSO DI LAUREA MAGISTRALE IN INGEGNERIA CIVILE – CIVIL ENGINEERING

Enhancing the use of externally bonded FRP laminates with FRP anchor spikes

Relatore: *Prof. Carlo Poggi*

Co-Relatore: *Prof. Antonio Nanni*

Elaborato di:

Angiolo Berneschi Matr. 818275

Anno accademico 2014/2015

To my parents,

for always supporting me

and pushing me towards my dreams.

TABLE OF CONTENTS

TABLE OF FIGURES

TABLE OF TABLES

ABSTRACT

Fiber reinforced polymer (FRP) is an ideal composite material system for the repair and strengthening of existing concrete and masonry structures. The efficiency of the strengthening system largely depends on adequate bond between the FRP laminate and the concrete substrate. Among all the anchoring techniques which could improve the bond, carbon FRP anchor spikes are studied in details in this research, due to their efficiency, easy handling, high strength, compatibility with FRP laminates and their capability to avoid stress concentration.

An FRP anchor consists of bundles of strands of carbon fibers with one end inserted into an epoxy-filled hole in the concrete substrate and the other end fanned out on the externally bonded FRP laminate. Currently, no specific criteria or guidelines exist to help the designer to understand the improvement in terms of strengthening of the existing concrete structure after the installation of FRP anchors.

The aim of this research is to deepen the knowledge of the fundamental behavior of the FRP anchor spikes and to identify the key parameters that affect the performance of the FRP laminates using FRP anchors. The experimental campaign is composed by three different types of test performed in the laboratory, followed by a comparison with analytical models present in literature. The first test is a pullout test in which the resistance of the anchor under pure tension load is measured. The second test is another pullout test in which the chamfer radius of curvature of the concrete at the hole is analyzed. The last test is a double shear test in which different anchor fan configurations are studied. Based on the research, design guidelines for carbon FRP anchor spikes are developed. These guidelines intend to provide engineers with the necessary information to make design decisions when incorporating FRP anchors to enhance the bond of externally bonded FRP laminates.

ABSTRACT

I sistemi compositi FRP (materiali compositi fibrorinforzati a matrice polimerica) sono materiali ideali per il rinforzo di strutture esistenti in calcestruzzo. L'efficienza del sistema di rinforzo dipende principalmente da un'adeguata adesione tra la lamina di FRP ed il substrato di calcestruzzo. Tra tutte le tecniche di ancoraggio che potrebbero migliorare tale legame, in questa tesi vengono analizzati gli ancoraggi in CFRP (Carbon Fiber Reinforced Polymer) per la loro efficienza, facile maneggevolezza ed alta resistenza. Questo tipo di anoraggio permette alla lamina di raggiungere deformazioni ben oltre quelle di "debonding", creando così i presupposti per una miglior efficienza del rinforzo strutturale. Inoltre, essendo le lamine fabbricate con lo stesso materiale degli ancoraggi stessi, questi ultimi hanno un ulteriore pregio, cioè quello di non essere corrosivi e pericolosi per il sistema di rinforzo.

Un ancoraggio in FRP consiste in un fascio di fibre di carbonio con un'estremità inserita nel foro nel substrato di calcestruzzo precedentemente riempito di resina epossidica, e con l'altra aperta a ventaglio sulla lamina di FRP. In generale, gli ancoraggi sono sottoposti a due tipi di azione: trazione e taglio. La loro efficacia largamente dipende dalla loro resistenza a tali sollecitazioni. Attualmente non esistono criteri progettuali o linee guida che possano aiutare il progettista a quantificare il miglioramento, in termini di resistenza della struttura esistente, in seguito all'installazione degli ancoraggi nei sistemi di rinforzo esterno in FRP.

Lo scopo della mia ricerca è di comprendere a fondo il comportamento di tali ancoraggi e di identificare i parametri chiave che ne influenzano l'efficacia. La campagna sperimentale prevede quindi diversi tipi di esperimenti volti allo studio del loro funzionamento. Inizialmente viene effettuato un primo pullout test volto alla determinazione della resistenza degli ancoraggi sottoposti a pura trazione. A questo è seguito un altro pullout test in cui il parametro analizzato è il raggio di curvature della smussatura del foro. Infine, viene eseguito un double shear test in cui vari tipi di

configurazione del ventaglio dell'ancoraggio sono stati analizzati. Sulla base dei risultati ottenuti, verrà redatta una linea guida per l'utilizzo degli ancoraggi in FRP che possa dare informazioni agli ingegneri riguardo l'utilizzo degli ancoraggi durante la fase di progettazione del rinforzo strutturale per strutture esistenti.

1. INTRUDUCTION

After a briefly description of the main goal of this research, an overview of the historical background of the FRP materials, from the evolution after World War II to the present day, is provided. The second objective of this chapter is to introduce the characterization of FRP composite systems, beginning with the properties of the fibers and the resins, arriving to the properties of the composite material. Particular attention is given to the FRP composite systems made of carbon fiber and epoxy resin. In addition, an introduction to the main objective of this thesis, which is the enhance of externally bonded FRP laminas with FRP anchor spikes, is presented

1.1 Research Significance

In the last decades, the construction industry has been drove by environmental, sustainability and economical concerns to make profound and radical changes in its structures. The approach for new constructions has turned towards the repair and renovation of buildings or infrastructure rather than demolishing and rebuilding. For these reasons, alternative techniques for structural rehabilitation have become of critical importance for the safety and preservation of the world's habitable inheritance. Researchers have work for many years to find new materials capable of meeting these needs. Externally bonded FRP is a specific material that has an optimal behavior from a structural point of view and it is sensitive from an environmental prospective. The capability of this kind of material to repair the structures even in cases where damage is caused by extreme natural events, such as earthquakes and hurricanes, is a property that should not be underestimated. On the other hands, despite promising developments in applications of FRP for the repair and retrofit of reinforced concrete structures, many challenges exist that have limited the growth of this market. Such problems include: brittle failure of FRP-strengthened RC structures due to sudden failure modes such as FRP rupture or debonding (Galal and Mofidi, 2010); deterioration of the mechanical properties of FRP due to harsh environmental conditions such as wet-dry cycles and freeze-thaw conditions (Belarbi and Bae, 2007); a reduction in strength due to the effects of improper installation procedures

(Orton, 2007); and lack of agreement among debonding behavior and bond length models (Ben Ouezdou et al., 2009). In general, the success of the external bonded FRP strengthening systems largely depends on adequate bond between FRP sheets and concrete substrate. The debondig occurs at strain considerably lower than the ultimate strain of the FRP and, for this reason, the current approach to preclude debonding failure is to limit the design strain in the FRP to levels much less than the rupture strain. The anchorage system may be used in order to limit or delay this problem because they allow the development of higher forces in the FRP sheets beyond those causing debonding. Unfortunately, no one guideline or criteria exist to help engineers to include this technology in the design of strengthening systems for reinforced concrete structure. This work aims to fully understand the behavior of a particular anchorage system, called FRP anchor spikes, through an experimental campaign composed by different types of test.

1.1.1 Broader Impact

The goal of this research is the characterization of externally bonded FRP composite materials, anchored with FRP anchor spikes, intended for the rehabilitation and retrofit of structural elements such as RC elements including beams, slabs, columns, and masonry walls. In most cases, it is more economical to rehabilitate the structure and make the building improvements instead of demolishing and constructing a new building in the same space. Additionally, there are cases where the existing buildings have historical significance and many city-states and national regulations prevent demolition. For this reason, the enhancing given by externally bonded FRP composite systems is fundamental. These materials allow the rehabilitation of structures protecting them from further damage, they can be use for reinforcement of deficient members or for a life span extension and restoration of safety requirements. As already mentioned, it is necessary to prevent or delay one of the most dangerous problems of the FRP strengthening systems, the sudden and premature debonding of the lamina from the concrete substrate. The anchorages could have a fundamental role in the future in the enhancing of reinforced concrete structures, but further studies are necessary. In fact, no one guidelines or criteria exist which could help engineering to include them into the design of strengthening systems. This research focus on a particular type of anchorage system, the FRP anchor spikes. Some parameters are studied through an experimental campaign, in order to fully understand the enhancing

given by these new technologies. Moreover, the innovation of the present research resides in the results of the performed tests and in the experimental procedure that will serve as an initial base for further studies.

1.2 Composite Material: Historical Background

The idea of composite material is a really old concept. The ancient Egyptian thought about the possibility to combine two different materials in order to make a new one with better properties. They used to reinforce mud bricks with straw to make them stronger (Nanni 1999). Later, in 1200 AD, the Mongols invented the first composite bow. They combined wood, bone and animal glue and wrap everything with birch bark. The result was an extremely accurate and powerful bow. Due to composite technology the Mongolian Army lead by Genghis Khan had the most efficient and strongest weapon on heart.

Many more historical examples could be find in the literature, such as mud wall reinforced with bamboo, glued laminated wood or laminated metals (Kaw 2005).

In early 1900s, with the invention and development of plastic, such as vinyl, polystyrene or polyester, the modern era of composite begins. Due to the low strength and rigidity of plastic, it could not be used alone and there was the need to reinforce it. In 1935, Owes Corning made the first GFRP (Glass Fiber Reinforced Polymer), a combination of plastic polymer and fiberglass. The result was an incredible strong and light material.

During the Second War World there was a huge improvement of FRP due to the need to have lightweight material in military aircraft. In this period scientist and researcher tried to find new solution in order to satisfy the high demand of the aerospace industry.

Another really important application for this new type of material was the boat construction. The first commercial boat hull made by composite material was released in the 1946 and little by little many more applications were developed, such as the automotive, defense and sporting goods industries (Kaw 2005).

In the 1970s better plastic resins and new reinforcing fibers were developed, due to the improvement of the industry. Aramid fiber, known as Kevlar, and carbon fibers started to be used because of their high tenacity around this period.

FRP is currently being used in the construction industry to strengthen concrete and masonry structures. It competes directly with the traditional strengthening techniques due to its suitable properties. Furthermore, the specific mechanical properties of FRP can be easily modified by changing the type and the direction of the fibers or the composition of the polymer (Nanni 1999).
The composite industry is still evolving, thank to dedicated university programs and research institutions. Composite materials are becoming more eco-friendly and recycle plastics and bio-based polymer are going to be used to create new types of "green" resin.

1.3 Fiber Reinforced Polymer

Fiber reinforced polymer (FRP) materials are composite material consisting of fibers in a polymer matrix. FRPs have excellent characteristic, such as high strength, lightweight, resistance to corrosion, easy handling and installation. In addition FRP does not need to be covered by a protection, as in the case of steel reinforcement, and can be exposed to many more environments. On the other hand, the presence of the polymer matrix limits its fire resistance. FRP materials are commonly used wherever high strength-to weight ratio and rigidity is required, such as aerospace, automotive and civil engineering. The fields in which this material can be applied are increasing due to its incredible properties. The most important application, for what concerns civil engineering, is the strengthening of concrete, masonry, steel, cast iron and timber structures. Increasing the load capacity of old structures which were designed for a lower service loads then they are expecting today, seismic retrofitting or repairing damaged structures are some very common example of application. Two techniques are typically adopted to enhance the shear or flexure strength of structure. In the first case FRP are usually wrapped around the section. It causes an increasing of the ductility of the section which means even enhancing the resistance to collapse under earthquake loading. In the second case, the application of the FRPs has a large impact on the strength but only a moderate increasing in the stiffness. This happens because the fiber reinforced polymer materials used for this application are usually very strong and not particularly stiff. As a consequence, just a small cross-section area of the material is used. Fig. 1.1 illustrates a common application of FRPs for flexure. In

many cases both the two techniques written above may be provided in the same structure.

Fig. 1. 1 – Application of FRPs

The fibers are the element of the composite material that carries the load, due to their high strength and stiffness when pulled in tension. The most common are made by glass (GFRP), carbon (CFRP) and aramid (AFRP). Glass fibers are the most commonly used reinforcing fibers for polymeric matrix composite. They have some good properties, such as low cost, high strength, high chemical resistance and they are a good insulating. Unfortunately they have a low elastic modulus, high specific gravity, sensitivity to abrasion, poor adhesion to polymers and low fatigue strength. Carbon fibers have some advantages, such as high fatigue strength and low coefficient of thermal expansion. The tensile strength and modulus are high and remain stable as temperature rises. The most important disadvantages is their high cost, following by high electrical conductivity and low impact resistance. Aramid fibers are organic fibers which have the lowest specific gravity and the highest tensile strength-to-weight ratio among the current reinforcing fibers. In addition, they have a low cost and high impact resistance. The disadvantages of Aramid fibers are the low compressive properties and their sensitivity to UV light . Nowadays, some other types

of fibers are used, like for example Basalt fibers. They are significantly cheaper than carbon fibers and they have some advantages such as fire resistance, significant capability of acoustic insulation and resistance to chemically active environments (Fib 2007). The following table (Table 1.1) shows the typical properties of the most common fibers (Nanni 1999), where ρ is density of the material, E is the elastic modulus, σ is the strength, ε_{ult} is the ultimate tensile strain and μ is the Poisson's ratio.

Table 1. 1- Typical properties of fibers (single filament)

Type of Fiber	ρ [kg/m^3]	σ [Mpa]	E [Gpa]	ε_{ult} [÷]	μ -
E-glass	2450	3445	72.4	2.4	0.22
S-galss	2450	4547	85.5	3.3	0.22
AR-glass	2253	1793÷3447	69.6÷75.8	2.0÷3.0	N/A
High-modulus carbon	1951	2482÷3999	349.6÷650.2	0.5	0.2
Low-modulus carbon	1749	3496	239.9	1.1	0.2
Aramid (Kevlar 29)	1440	2758	62.1	4.4	0.35
Aramid (Kevlar 49)	1440	3620	18.0	2.2	0.35
Aramid (Kevlar 149)	1440	3447	124.1	1.4	0.35
Basalt	2799	4826	88.9	3.1	N/A

The polymer matrix binds together the fibers and protects their surface from damage during handling, fabrication and service life of the composite. In addition, it keeps the fibers straight and transfers the stresses to them avoiding intensification (Nanni 1999). In general, a polymer is called resin system during processing and matrix after the polymer has cured. The polymer matrix should be chemically and thermally compatible with the fibers and it affects also the failure mode and the fracture toughness of the overall composite material. There are two types of polymeric matrices used in FRP composite: thermosetting and thermoplastic resin. Thermoset materials are usually liquid or malleable prior to curing. The raw uncured resin molecules are crossed linked through a catalytic chemical reaction. This reaction is most often exothermic and the resin creates really strong bonds to one another changing state from liquid to solid. Once hardened a thermoset resin cannot be reheated and melted to get the original shape. Because of this, the recycling of

thermoset composite is extremely difficult. Thermoplastic material can be converted back to the original liquid form. Usually thermoset materials are stronger than thermoplastic due to their three-dimensional network of bonds and are also better suited to high temperature applications. Usually traditional reinforced polymer composites use a thermosetting resin as a matrix. Common thermosetting resins include: Polyester Resin, Vinyl Ester Resin, Epoxy, Phenolic, Urethane. They are popular even because uncured, at room temperature, they are in a liquid state. This allows for convenient impregnation of reinforcing fibers such as fiberglass, carbon fiber o aramid fiber. Although thermosetting resins remain a low cost material, they have the excellent properties, such that: good resistance to solvent and corrosives, resistance to heat and high temperature, fatigue strength, tailored elasticity, excellent adhesion, excellent finishing. The table below (Table 1.2) lists the most important properties of Epoxy, Polyester and Vinyl Ester (Nanni 1999).

Table 1. 2 – Typical properties of resin matrices

Type of Resin Matrix	ρ [kg/m^3]	σ [Mpa]	E [Gpa]	μ -	CTE [10^{-6}/°C]	Moisture content [÷]	Tg [°C]
Epoxy	1186÷1423	2067÷3445	35÷103	2.88÷5.4	0.35÷0.39	0.15÷0.60	95÷175
Polyester	1186÷1423	2756÷4134	48÷131	2.34÷3.42	0.38÷0.40	0.08÷0.15	70÷100
Vinylester	1127÷1364	2997÷3445	69÷76	2.7÷3.96	0.36÷0.39	0.14÷0.30	70÷165

Where ρ is density of the material, E is the elastic modulus, σ is the strength, μ is the Poisson's ratio, CTE is the coefficient of thermal expansion and Tg is the glass transition temperature.

Epoxy is the most used matrix material for FRP due to its good properties, such as high strength, low viscosity, low flow rate, low volatility during curing, low shrinkage rates and low cost. Thermoplastic resin is naturally in a solid state and it must be heated to the melting point to impregnate the fibers. This operation is really complex and required technique and expensive special tooling. For the reason written above thermoplastic resins are most commonly used without reinforcement. They are formed into shape and used to create a lot of different products. Examples of product manufactured with them include: PET (Water and soda bottles), Polypropylene

(Packaging containers), Polycarbonate (Safety glass lenses), PBT (Children's Toys), Vinyl (Window frames), and PVC.

FRP materials are anisotropic, linear elastic until failure and characterized by an high tensile strength in the direction of the reinforcing fibers (Nanni 1999). The properties of this type of material depend on the layouts of the carbon fiber and the proportion of the carbon fibers relative to the polymer. Another important and very complex aspect of composite material is the fiber-matrix interface. The mechanical performance of FRP materials is largely influenced by the interaction between the fiber reinforcement and the polymer matrix. There are three type of interfacial interaction: mechanical interlocking, intermolecular interactions and chemical bonds between the adhesive (matrix) and the adherent (fiber). Thanks to interfacial interface, applied load is transferred from the matrix to the fiber (Nicolas and Borzachiello 2012).

After this briefly introduction of FRPs, the next sections describe more specifically the two FRP constituents used for this research, carbon fiber and epoxy resin.

1.3.1 Carbon Fiber

Carbon fiber is a material composed by fibers are are about 5-10 μm in diameter. The carbon atoms are bonded together in crystals that are aligned to the major axis of the fiber. It gives to the carbon fiber a high resistance compared to its volume. Thousands of fibers are then bundle together and woven to create a fabric. The atomic structure of carbon fiber is similar to that of graphite; it consists in sheets of carbon atoms arranged in a regular hexagonal pattern.

The first one that was able to develop carbon fibers was Thomas Edison in 1879, who used an all-carbon fiber filament to create the first incandescent light bulb. He generated carbon fiber by carbonizing cotton threads or bamboo slivers at high temperature in a controlled atmosphere. The result was a material able to conduct electricity. The process used by Edison is still followed today and it is called pyrolysis. At the end of the 1950' Rayon became the first precursor used to create these modern fibers, obtaining high tensile strength carbon fibers. Ultimately, Rayon was replaced by more effective materials such ads polyacrylonitrile (PAN) and pitch. Carbon fibers became commercially available just at the end of the 1960', representing a breakthrough in really high performance, low-density material production.

Carbon fibers, in the industrial production, are classified into three different types depending on the type of precursor: PAN-based (polyacrylonite), pitch-based and rayon-based (regenerated cellulosic fibers). Among them PAN-based is the most produced. It is characterized by high strength and relatively high modulus and it is the most used type of carbon fibers in civil engineering applications. Pitch-based carbon fiber has higher modulus but lower strength; for these properties it fits better in aerospace applications. Finally rayon-based carbon fibers have a very low modulus. Based on the previous characteristics carbon fibers can be classified as high modulus or low modulus. In general carbon fibers has high fatigue strength, high resistance to alkali or acid attack, low coefficient of thermal expansion, relatively low impact resistance and high electrical conductivity.

There are typically five steps in the manufacturing of carbon fiber PAN-based. The first phase is the so-called spinning, in which the polyacrylonite is mixed with other ingredients and spun into fiber, which are washed and stretched. This operation allows a better chain orientation and, consequently, better mechanical properties. The second step is the stabilization of the fibers. Before the fibers are carbonized, they need to be chemically altered to convert their linear atomic bonding to a more thermally stable ladder bonding. This operation is done by heating the fibers in air to 200-300°C for 30-120 min; the fibers pick up oxygen molecules from the air and rearrange their atomic pattern. During this operation the fibers change color from white to yellow to brown and finally to black. After the fibers are stabilized, they are heated to a temperature of about 1000-3000°C for several minutes in an inert atmosphere. The lack of oxygen prevents the fibers from burning in the very high temperature. This operation is called carbonization; the precursor fibers are transformed into carbon fibers and the impurities are eliminated. After carbonizing, the fibers have a surface that does not bond well with the epoxy resins and other material used for composite materials. To give to fibers better bonding with the adhesive, their surface is slightly treated by oxygenation. The addition of oxygen atoms gives to the surface better chemical and mechanical properties; if this treatment was not done the inter laminar shear between epoxy resin and carbon fiber would be very low. The last step is called sizing; in this phase the fibers are coated to protect them from damage during winding or weaving. The coating materials are chosen to be compatible with the adhesive used to form the composite material.

The Fig. 1.2 schematizes the manufacturing process of carbon fibers (PAN-base).

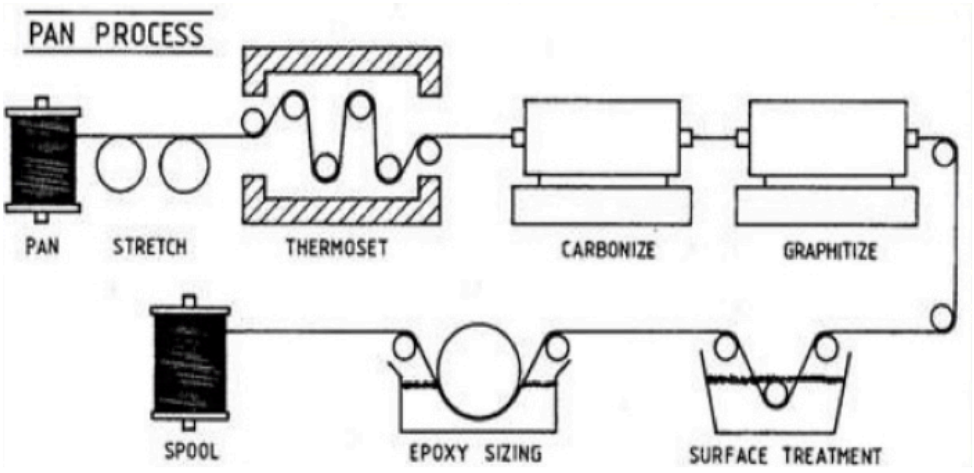

Fig. 1. 2 - Schematic illustration of PAN process

1.3.2 Epoxy Resin

Epoxy resins are the most commonly used thermoset plastic in polymer matrix composites. This polymer was synthesized for the first time in the early 1900' but it was commercialized in the late 1930'. The primary industrial application of epoxy resin was in the coating, due to its high resistance to chemicals, durability and toughness. Later epoxy started to be used to encapsulate electrical and electronic component, due to its resistance and durability at high temperature and high electrical resistance. Nowadays epoxy resins can be used as a strong adhesive in metal and construction material; they are strong enough to be used in place of rivets and welds in certain applications. Currently this material has been used to create tools, replacing metal, wood and other materials.

Epoxy resins must be cross-linked in order to develop required characteristics. This cross-linking process is achieved by chemically reacting the resin with a suitable curing agent or hardener. The reactive groups of molecules in the epoxy resin formulations are the terminal epoxide groups and the hydroxyl groups.

Epoxy resin does not give off reaction products during the curing period and so it has low cure shrinkage and no volatiles release that can lead to voids. It has an excellent adhesion to a wide variety of substrate, good chemical and environmental resistance, and good insulating properties. While other

thermosetting resins offer resistance to a specific class of chemicals, epoxy resins can resist to caustics, solvents and acids. Other important properties that make this material largely used are its compatibility with glass, carbon, aramid and basalt fibers (Nanni 1999).

Epoxy resins, also know as polyepoxides, may be reacted (cross-linked) either with themselves through catalytic homopolymerisation, or with a wide range of co-reactants including polyfunctional amines, acids, phenols, alcohols and thiols. These co-reactants are often referred to as hardeners or curatives, and the cross-linking reaction is commonly referred to as curing. Nowadays two-part epoxy adhesives for home, shop or hobby are available in stores and present a wide range of properties, depending on the final use.

Different types of Epoxy resins can be created just using different types of materials as curing agents. For example, the chemistry can be adjusted to perfect the molecular weight or viscosity as required by the end use, the curing rate can be modified from very fast (second) to slow (hours) or one can obtain the final desired properties from soft, flexible compositions to hard, tough materials.

Deeping into details, epoxy resins are low molecular weight pre-polymers or higher molecular weight polymers, which usually are characterized by the presence of at least two epoxide groups.

In general epoxy resins are composed by a long chain molecular structure similar to vinyl ester in which the reactive sites are at the end. Epoxy groups instead of ester groups form these two reactive sites. The epoxy group is sometimes referred to as a glycidyl or oxirane group. It is important to underline the fact that the absence of the ester group makes epoxy resins a really good water resistance. As shown in the Fig. 1.3, the presence of the two rings at the center of the epoxy molecule is really important because it makes the epoxy able to absorb both mechanical and thermal stresses. It gives to this material toughness, stiffness and heat resistance properties. The three most common type of epoxy resin are the following: cycloaliphatic resin, epoxidized oils and glycidated resin.

In particular, the last are the most used in most commercial applications.

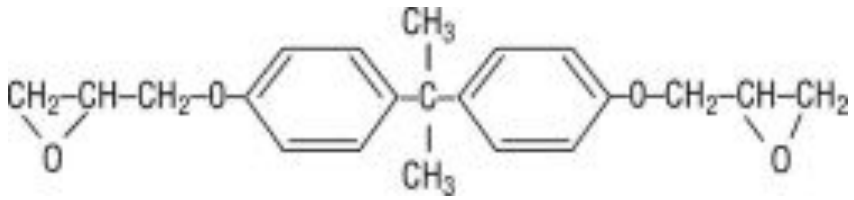

Fig. 1. 3 - Idealized chemical structure of a typical epoxy

The different between epoxies and polyester resins is that the first one must be cured by a hardener rather that a catalyst. Adding a hardener, often an amine, to the epoxy, an additional reaction takes place in which both the materials are involved. Amines are usually organic materials containing a nitrogen atom linked to two hydrogen atoms (-NH2). In epoxy formulations, the active hydrogen of the amine is what reacts with the epoxide group of the resin. The structure of the amine-containing organic compound and the number and type of amine groups in the compound is what determine the rate of cross-linking and the coating's properties. There are some other types of chemical curing agents, like for example acid anhydrides and lewis bases or lewis acid. This phase is fundamental because the two-epoxy groups bind to the amine forming a complex three-dimensional molecular structure. It is really important to underline how important is the mix ratio of the two material involving in the reaction due to the fact that the amine molecules react with the epoxy molecules in a fixed ratio. We must pay attention in this phase if we want to get a complete reaction; if amine and epoxy are not mixed together in the correct way, unreacted epoxy or hardener will remain inside the matrix. It will affect the final properties of the material after the curing period. Every company, which produces epoxy resins, provides the precise mixing ratio (by weight or by volume) to help the clients during the applications.

After a brief introduction about FRP materials and their main components, the next section introduces how they are mostly applied in civil engineering.

1.4 Use of Fiber Reinforced Polymer

1.4.1 Externally Bonded Fiber Reinforced Polymer

In the last two decades the use of FRP materials for repairing, strengthening and retrofitting existing reinforced concrete structure has increased all over the world. Deterioration due to ageing, degradation such as corrosion of steel reinforcement, lack of maintenance, accidental events such as earthquakes, increasing in service load or change to the structural system are just some cases in which strengthening or retrofitting existing civil structures is needed.

Some examples of traditional solutions to the problems written above are externally bonded steel plate, steel or concrete jacket or externally post-tensioning. Steel plate bonded with epoxy to the external surface are usually applied in the tension zone of plates and beams and are a simple and cost-effective solution to the strengthening and the flexural resistance of a structure. Unfortunately this technique has many disadvantages, such as the problem of the steel corrosion and thus the bond degradation, the difficulty to handle heavy steel plates at the construction site and the limitation on the length of the plates. Steel jacket are able to increase the ductility of section as well as enhance the resistance of the structure. On the other hand this technique is really invasive because enlarges the cross section of the beam in which is applied. Moreover the weight of the jacket could be a dangerous permanent load.

Externally bonded FRP is considered a really efficient alternative to the traditional technique written above. It has many advantages, such as low weight and therefore easier application, unlimited availability in FRP sizes, very high strength/weight and stiffness/weight ratio, good fatigue resistance and high resistance to corrosion (Nanni 1999). The FRP sheet or fabric can be applied, for example, in the tension zone with fibers parallel to the RC member longitudinal axis or wrapped around the RC members with the fibers perpendicular to the longitudinal axis, depending on the type of structural problem to solve. Typical applications of externally bonded FRP are: flexural strengthening of slabs and beams (strips or sheets), shear strengthening of beam (angles, sheets, fabrics), shear strengthening and confinement od column (sheets, fabrics, shells), wrapping of concrete tank (sheets, fabrics) and shear strengthening of beam-column joint (strips, sheets., fabrics). In addition, this

technique can be used even to restore to their original ultimate flexural capacity damaged pre-stressed concrete girders that require repairing or strengthening.

The application of the FRP composite in the field of strengthening started in the 1980' providing addition confinement to RC columns (Fardis and Khalili 1981, katsumanata et al. 1987) and flexural strengthening for RC bridges (Meier 1987, Rostasy 1987, Meier et al. 1992). It was observed a sudden increase in the use of FRP in Japan after the 1995 and later in Europe and North America (ACI 440 R 2007, Bakis et al. 2002). Codes, guideline and standards were developed for the first time in Europe (FIB 2001, CNR 2013, Istructe 1999), Japan (JSCE 1996, JSCE 2001), Canada (CSA 2000) and United States (ACI 440 2008) at the beginning of the 1980'. They were created in order to make the design of FRP reinforcement for concrete structure safe.

The following figures show some of the applications written above.

Fig. 1. 4 - Some Application of FRPs

1.4.1..1 Mechanical Properties of FRP Materials

It is necessary to know the mechanical properties of the FRP, such as ultimate strength; ultimate tensile strain and modulus of elasticity to better understand and analyze the shear bond strength between the FRP and the substrate. In general the mechanical performance of a unidirectional fiber reinforced composite material is dominated by the properties of the fiber since the load is carried by the carbon. In the case of an unimpregnated bundle of fiber, if a single fiber breaks, the load is equally redistributed among the remaining entire fibers in the bundle. This is commonly called equal load sharing (Phoenix and Taylor 1973). In the case of a fiber reinforced polymer, in which the fibers are impregnated, if a single fiber breaks, the load distribution is restrained by the matrix. The stress is redirected back to the broken fiber by plain shear interaction with the matrix at the interface. The matrix localizes and redistributes the load. The overload is then carried by the fibers nearest to the broken fiber (Harlow and Phoenix 1978). A standard procedure was developed in the last years to analyze the in-plane tensile characteristic polymer matrix composite material reinforced by high-modulus fibers. The test method used to determine those properties is the ASTM D3039 (2008). It consists in a tensile test performed on a thin flat strip of material having a constant rectangular cross section. This strip is gripped at the two ends by a mechanical testing machine and monotonically loading in tension. The ultimate strength can be calculated from the maximum load carried before failure and the tensile modulus of elasticity, Poisson's ratio and transition strain can be calculated using strain transducers. Fig. 1.5 illustrates a typical set-up for a tensile test.

Another important aspect of the test is the failure modes of the specimens. Fig. 1.6 illustrates the different failure modes given by ASTMD3039 (2008), which can be used to compare the type of failures obtained by testing.

Fig. 1. 5 - Typical Set-Up for the tensile test

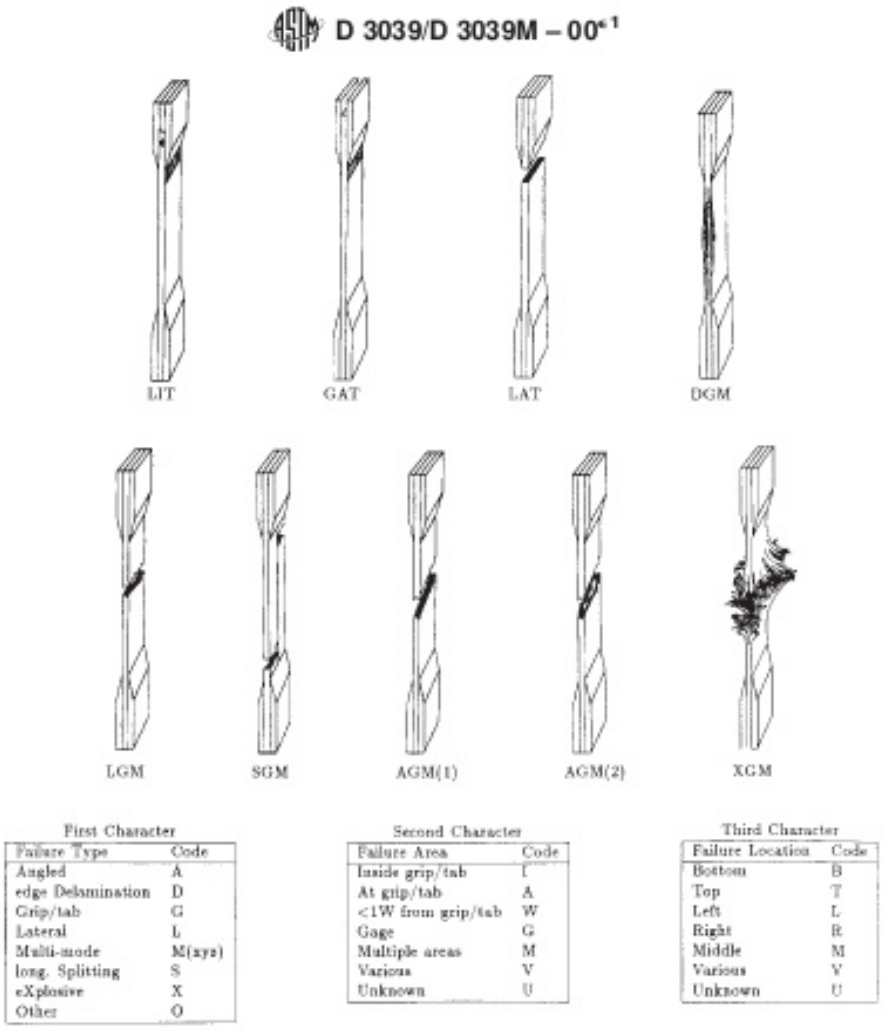

First Character

Failure Type	Code
Angled	A
edge Delamination	D
Grip/tab	G
Lateral	L
Multi-mode	M(xyz)
long. Splitting	S
eXplosive	X
Other	O

Second Character

Failure Area	Code
Inside grip/tab	I
At grip/tab	A
<1W from grip/tab	W
Gage	G
Multiple areas	M
Various	V
Unknown	U

Third Character

Failure Location	Code
Bottom	B
Top	T
Left	L
Right	R
Middle	M
Various	V
Unknown	U

Fig. 1. 6 - Typical failure modes (ASTM D3039 2008)

1.4.1..2 Shear Bond Strength

Nowadays, externally bonded fiber reinforced polymers are a common and efficient technique for the strengthening and reinforcement of concrete structures. The bond mechanism is fundamental because is responsible to transfer the load from the concrete to the FRP material. The main challenge for this type of strengthening system is to design against the various debonding failure modes. Many theoretical formulations have been proposed to evaluate the bond strength in a concrete element with externally bonded reinforcement (FIB 2001, CNR 2004, ACI committee 440 2008, Chen and Teng 2001, De Lorenzis et al. 3001, Smith and Teng 2002, Brosens and Van Gement 1999, Oejilers et al. 2007, Taljsten 1997, Bilotta et al. 2011). The main part of these formulations are usually similar and the differences are in some numerical coefficients calibrates by experimental results and bond tests and in some safety factor (Nicolais and Borzaccheillo 2012).

The bond behavior between FRP and concrete is related to the interfacial stress diffusion and thus, to the mechanical characteristic that influence it, such as the geometry or the properties of the materials. This bond is usually represented by a shear stress (τ) – slip (s) relationship (Nicolais and Borzachiello 2012) and many simplified model exist in literature. The following figure (Fig. 1.7) shows some examples of stress-slip relationship present in literature.

The bi-linear behavior, graph (b), is the most largely adopted due to its good correspondence with the experimental results. As shown in Fig. 1.8, it is characterized by a linear increasing until the maximum shear stress, followed by a linear softening. The softening is due to the gradually damage of the materials at the interface that occurs as the stress transferred from concrete to FRP increases. After this stage, the debonding initiates and the deformation increases rapidly with a small increment in applied load.

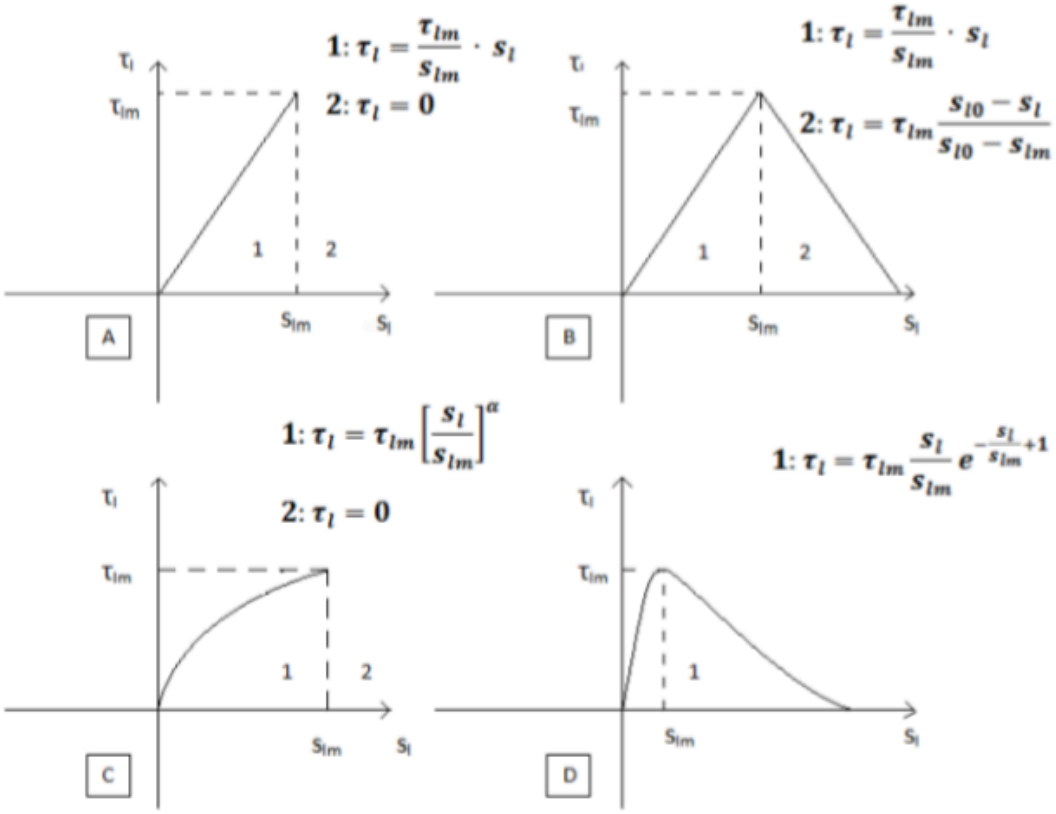

Fig. 1. 7 - Stress-Slip relationship

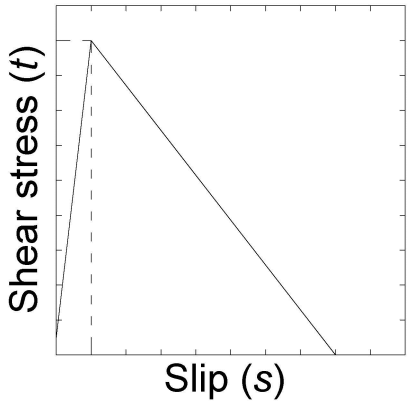

Fig. 1. 8- Bilinear constitutive law (Nicolais and Borzachiello 2012)

Bond failure modes represent an important factor that must be taken into account in the designing of the strengthening system (Nicolas and Borzachiello 2012). Several bond tests has been performed in the last years to evaluate experimentally the maximum tensile stress in the FRP reinforcement. These tests consist in a pure shear

test, as shown in Fig. 1.9, in which the FRP is glued to the concrete and loaded in tension (Yap et al. 2005).

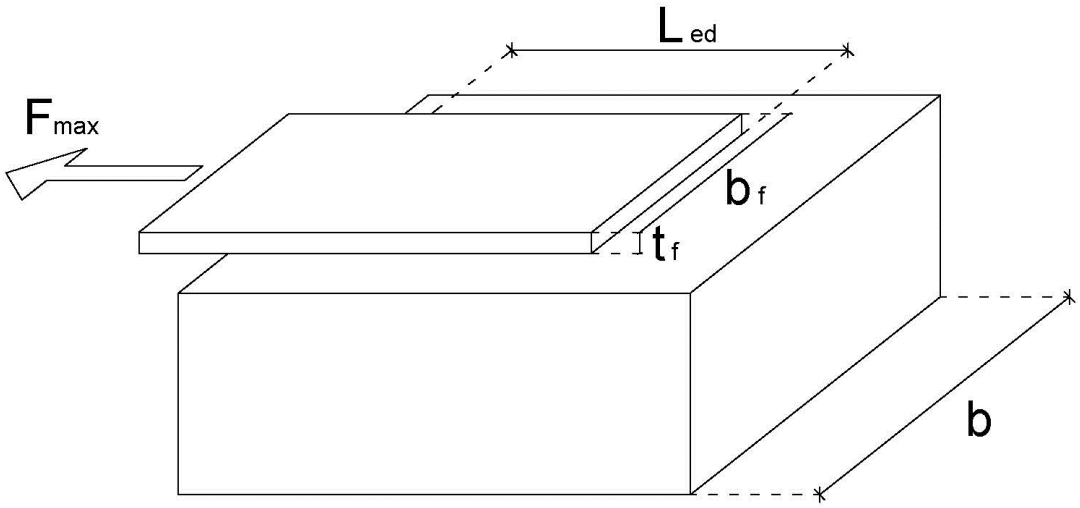

Fig. 1. 9 - Maximum force transferred between FRP and concrete (CNR-DT200 R1/2013)

Based on the existing studies, it was found that the bond strength of the strengthening system mainly depends on the concrete strength and on the FRP-to-concrete member width ratio. The maximum tensile stress, in the case of FRP strengthening, is affected by the length of bonded area and increases up to maximum corresponding to a certain length, also known as *effective length* (FIB 2001, N, Chen and Teng 2001). This aspect represents the main different between internal and external reinforcement; in the second case a sufficiently long anchorage length can always be found that the full tensile strength of the reinforcement can be achieve (Yao et al. 2005). Being the effective length the minimum bonded length that ensures the transmission of the bonding forces, any longer bonded length does not produce any force increase. Based on the previous tests, it was found that effective length is proportional to the axial stiffness of the reinforcement, in particular Young's modulus and thickness, and inversely proportional to the strength properties of the support. If for example the stiffness of the reinforcement (FRP sheet) increases, a longer bonded length is required to ensure a condition in which the debonding load is fully transferred. If the effective length increases, the load that is possible to transfer increases asymptotically up to a maximum value, depending on the mechanical and geometrical properties of the FRP sheet and on the fracture energy of the interface law

1.4.1..3 Failure Mechanisms due to Debonding

The role of the bond between the concrete and FRP is of great relevance in the strengthening of reinforced concrete members with FRP composites, due to the brittle failure mechanism associated with debonding (loss of adhesion). According to the capacity design criteria, failure due to debonding shall not proceed flexural or shear failure of the strengthened member. The loss of adhesion between FRP and concrete may concern both the laminates or sheets applied to reinforced concrete beams for flexural and/or shear strengthening (CNR-DT200 R1/2013). As shown in Fig. 1.10, debonding may take place within the adhesive, between the concrete and the adhesive, in the concrete itself, or within the FRP reinforcement (e.g. at the interface between two adjacent layers bonded each other). When proper installation is performed, the adhesive strength is typically much higher than the concrete tensile strength, therefore failure occurs within the concrete itself in the form of removal of a layer of material (thickness may range from few millimeters to the whole concrete cover).

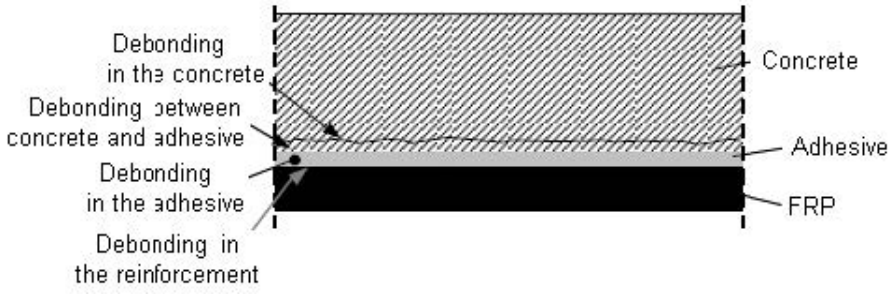

Fig. 1. 10 - Debonding between FRP and concrete

Debonding failure modes for flexural strengthening are schematically represented in Fig. 1.10 and may be classified in the following four categories.

· Mode 1 (Laminate/sheet end debonding)

· Mode 2 (Intermediate debonding, caused by flexural cracks)

· Mode 3 (Debonding caused by diagonal shear cracks)

· Mode 4 (Debonding caused by irregularities and roughness of concrete surface)

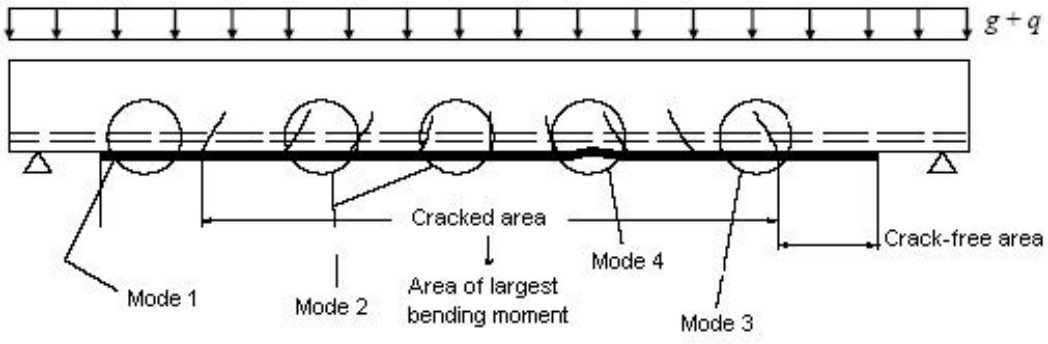

Fig. 1. 11 - FRP flexural strengthening: debonding failure modes (CNR-DT200 R1/2013)

In general, before designing for flexural and shear, the evaluation of the maximum force transferred from the concrete to the FRP, as well as the evaluation of shear and normal stresses at the concrete-FRP interface, is required. The CNR DT-200 gives several simplified expression for the calculation of these quantities that are analyzed in chapter 4.

1.4.2 FRP Anchorage Systems

The success of the external bonded FRP strengthening system largely depends on adequate bond between FRP sheets and the concrete substrate. In general, the flexural and shear stresses generated in the interface between concrete and FRP sheet may cause detachment of the sheet limiting its capacity to develop higher stress. Moreover, there are some harsh environmental conditions that could affect the efficient of the FRP strengthening system, such as wet-dry cycles and freeze-thaw conditions or a reduction in strength due to effects to improper installation. As a consequence, the debonding occurs at strain considerably lower than the ultimate strain of the FRP and, for this reason, the current approach to preclude deboning failure is to limit the design strain in the FRP to levels much less than the rupture strain.

Because of this limiting design condition, on the basis of the fracture energy formulation previously given and on the experimental results of bond tests, many theoretical formulations have been proposed to evaluate the bond strength in a concrete element with external bonded reinforcement (FIB 2001, CNR 2004, ACI Committee 440 2008, Chen and Teng 2001, De Lorenzis et al. 2001, Smith and Teng 2002, Brosens and Van Gemert 1999, Oejlers et al. 2007, Taljsten 1997, Bilotta et al.

2011, Bilotta et al. 2011). The layout of these formulations is often similar and the differences are essentially related to the numerical coefficient calibrated by experimental results of bond tests and to the presence of safety factors (Nicolais and Borzacchiello 2012).

Several studies, in terms of stress distribution, have been done in order to develop design equations for external bonded FRP sheets, which have led to the definition of stress transfer zone (Bizindavyi and Neale 1999, Subramaniam et al. 2007). The stress transfer zone is defined as the length over which peak strains and stresses are developed in an FRP sheet as increased loading is applied (Brena and Mc Guirk, 2013). The stress transfer zone is directly related to the optimal bond length of the FRP sheet. Debonding of FRP sheets typically initiates after maximum stresses are reached at the end of the stress transfer zone at peak force applied to the FRP sheet. The debonding front propagates along the bonded sheet at approximately constant force without a change in the effective length until the debonding front reaches the end of the sheet (Brena and Mc Guirk, 2013). The stress transfer zone translates toward the unloaded end of the FRP sheet without a significant increase in the force.

Increasing the bonded length of an adhesive bonded FRP sheet beyond the optimal bonded length does not increase the bond strength since propagation of debonding occurs at same load once the stress transfer zone is fully established (Subramaniam et al. 2007). However, the debonding process occurs gradually as the debonding front propagates toward the unloaded end of the sheet, so an increase in bonded length beyond the optimal length results in ductility enhancement of the bonded FRP system (Brena and Mc Guirk, 2013). The stresses that can be developed in FRP sheets bonded to concrete represent only a fraction of the rupture strength of the sheet. In order to make the FRP strengthening application more efficient, debonding from the concrete surface must be eliminated or delayed. Stress distribution has been determines using experimental investigations or analytical modeling. One of the limitations of these studies is that researcher have primarily focused on studying stress developed in the centerline of the FRP sheets. A non-uniform stress distribution is generated across the width of the FRP sheet bonded to concrete with higher stresses near the middle of the sheet that decrease toward the sheet edges. This phenomenon, which has important implications in the performance of bonded sheets, has not been studied in detail in the literature except for studies reported by Subramaniam et al. (2007). Past researcher have firstly approached the FRP sheet-concrete interfacial

shear stress problem developing models to accurately predict the onset of debonding and calculating the maximum force that can be transferred into the FRP sheet to develop design equations (Niemitz, James and Brena, 2010). Following this approach, several models have been created to determine the maximum interfacial shear stress that can be developed given fundamental properties of the FRP sheet system and the concrete substrate. Some of these models are based on statistical reduction of available test while others on fracture mechanics theory (Niemitz, James and Brena, 2010). In addition, anchoring system to allow the development of higher forces in the FRP sheets beyond those causing debonding have been created. Various ways of anchoring the FRP sheet to concrete have been investigated, including the use of transverse sheet or straps (Brena et al. 2008, Coronado and Lopez 2008, Kotynia et al. 2008), using mechanical anchors (Elsayed et al. 2009), wrapping the end of sheets in rods embedded in grooves formed into the concrete (Eshwar et al. 2008, Khalifa et al. 1999), or forming and anchoring the FRP sheets using FRP anchors (Eshwar et al. 2008, Ozbakkaloglu and Saatcioglu 2009, Orton et al. 2008).

Many of these anchoring methods have shown promising results but unfortunately, information has not been provided in sufficient details that would allow development of design procedures (Niemitz, James and Brena, 2010).

1.4.2..1 Role of the FRP Anchorage Systems

A literature review of the performance of different mechanical anchorage systems used in FRP strengthening applications is presented in this paragraph.

In general, the primary role of the FRP anchorage system is to prevent or delay the process of debonding, which occurs when externally bonded FRP detaches from the reinforced concrete substrate because of low tensile strength concrete (Ceroni et al. 2008). This type of anchorage system is mostly used along the length of the cantilever to arrest the propagation of debonding towards the free end of the member resulting from the formation of the major crack. The beams containing anchor spikes usually fail by anchor spike pullout and FRP debonding or rupture and achieve higher peak load than similar strengthened beams without anchorage. Another important role of the anchorage system is to provide a load transfer mechanism at critical locations of structural members where no bond length is available. In this case the anchors are

really important because the FRP strengthening system can be considered to have to contribution to the strength without their inclusion. In some cases the anchorage system are used to provide a ductile failure for structural member instead of the typical brittle and sudden failure mode of the FRP debonding and rupture. The anchorage systems can be use even to increase the total available interfacial shear stress transfer, by increasing the area over which the shear stress is transferred, or to reduce the length of the FRP used by increasing the interfacial stress transfer. Fig. 1.12 and Fig. 1.13 illustrate examples of anchorage device. On the other hands, the performance of the anchorage system becomes critical in the design of FRP strengthening system and in some cases they may limit the strength of the FRP system. Failure modes including global anchorage failure or FRP rupture due to a local stress concentration may happen. As a consequence, a through understanding of the behavior of anchorage system is essential for a safe and reliable design.

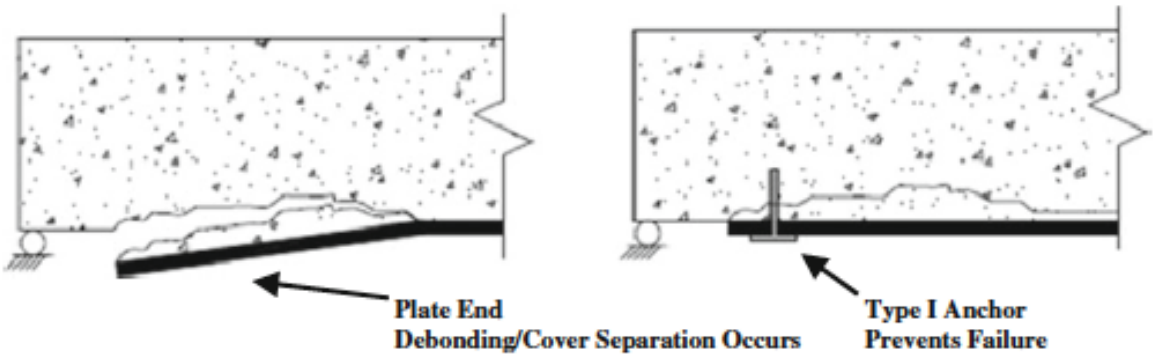

Fig. 1. 12 - Examples of Anchorage Devices (Galle and Sneed, 2013)

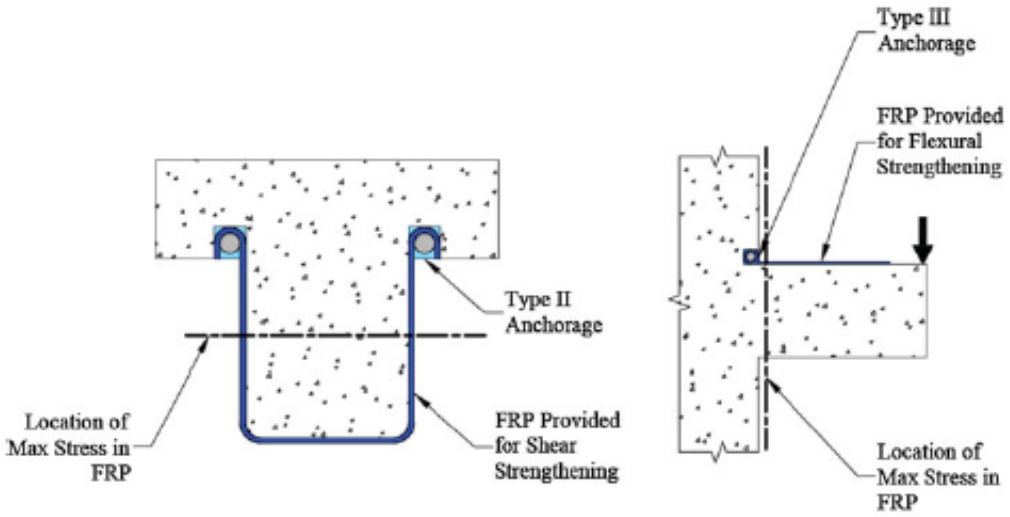

Fig. 1.13 - Example of Anchorage Device (Galle and Sneed, 2013)

1.4.2..2 Existing FRP Anchorage System

Many types of FRP anchorage system have been already studied in past researches, such as anchors spike, transversal wrapping, U-Anchors, longitudinal chases, FRP strips, plate anchors, bolted angles, cylindrical hollow section and ductile anchorage system and. Each of these types present different geometry, installation limits and force transfer characteristic (Galle and Sneed, 2013). A briefly description of each type of anchorage system is briefly reported in this paragraph.

1.4.2..2.1 Anchor Spike

The anchors spikes are made either of metal or FRP composite material. The metal anchor spikes are used to mechanically fasten FRP sheet to concrete. The low shear resistance of FRP composites, however, commonly results in bearing failures of the composites under stress concentrations associated with the use of metal anchors. The problem was then overcome using FRP anchors having the same physical characteristic as those of FRP sheets used to retrofit the structural element (Ozbakkaloglu and Saatcioglu, 2013). Moreover, another important advantage of using anchor spikes made of FRP is that they can be fabricated in the field with the same FRP materials as the externally bonded fabric, which facilitates the construction and eliminates potential corrosion hazards from dissimilar material, and make the

whole anchorage system homogenous. The FRP anchor spikes are strands of bundle fibers with one end embedded in the concrete substrate and the other one fanned out over the FRP sheet. They are usually installed orthogonal to or in plane with the FRP, although other orientation can exist. 90° anchor spikes are installed with the bundle of fiber embedded into the concrete substrate and the remaining fibers fanned out on the FRP sheet. They are commonly assumed to resist axial forces (pullout) and shear force. 180° anchor spikes are typically installed in plane with anchored FRP so that the fibers in the anchors can transfer the tensile force in the anchored FRP to the anchor. The following figures illustrate the 90° and 180° anchor spikes.

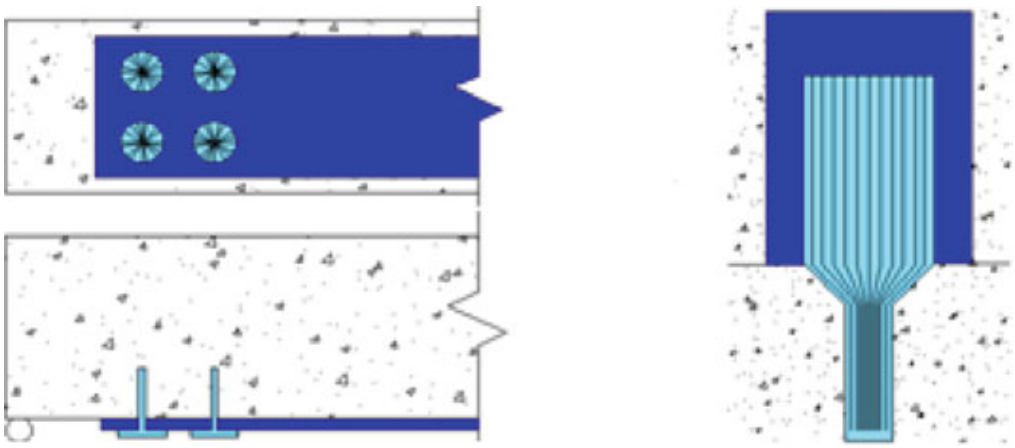

Fig. 1. 14 - 90° Anchor Spike (Left) and 180° Anchor Spike (Right)
(Galle and Sneed, 2013)

1.4.2..2.2 Transverse Wrapping

Wrapping bonded FRP transversally with other FRP sheet provide a clamping effect in the wrapped FRP and can be considered a form of anchorage system. Transverse wrapping can be in form of discrete strips located at the end or along the length. The orientation of the fiber may be perpendicular to the longitudinal axis or having a different angle. As in the case of anchor spike, the material used to wrap the beam can be the same as the strengthing material, eliminating the potential problem of corrosion that can result using different materials. Installation may be a challenge for this type of anchorage system due to the geometry of the member or access to its adjacent side. Another disadvantage of this anchoring technique is that transverse wrapping is not effective until a certain level of tensile stress is reached in the wrap; it may be

necessary to prestress the transverse wraps before the installation. The following figure illustrates an example of transverse wrapping anchorage.

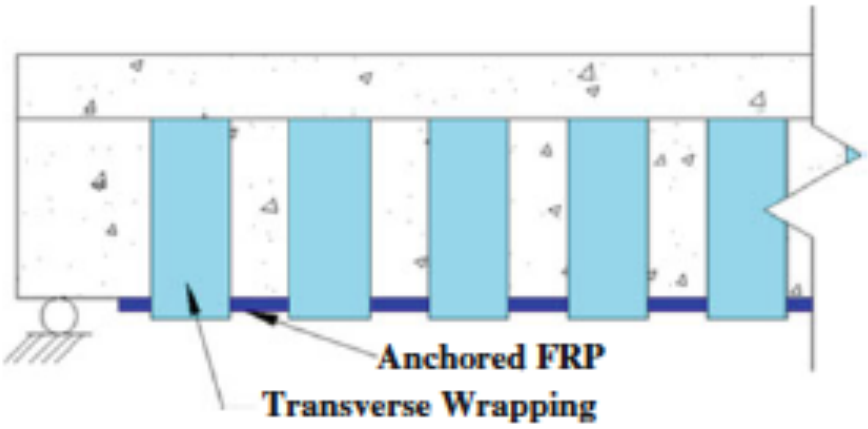

Fig. 1. 15 - Example of transverse wrapping anchorage
(Galle and Sneed, 2013)

1.4.2..2.3 FRP Strips

FRP strips are a simple type of anchorage system installed on the top of the FRP sheet used to strengthen the reinforced concrete member. They are installed in the plane of the FRP sheet and perpendicular to the longitudinal axis of the beam. Due to the fact that the FRP strips are loaded in direction orthogonal to the FRP strips fibers, they have limited efficiency. Even if this type of anchorage system may be similar to the transverse wrapping, the behavior can be distinguished because the strips do not provide a clamping effect to the FRP sheet. As in the previous case, the material used to strength the beam is the same used to anchor the FRP sheet. It eliminates the potential problem of corrosion that can result using different materials, facilitates the construction and minimizes the anchorage fabrication efforts. The following figure illustrates an example of FRP strips anchorage system.

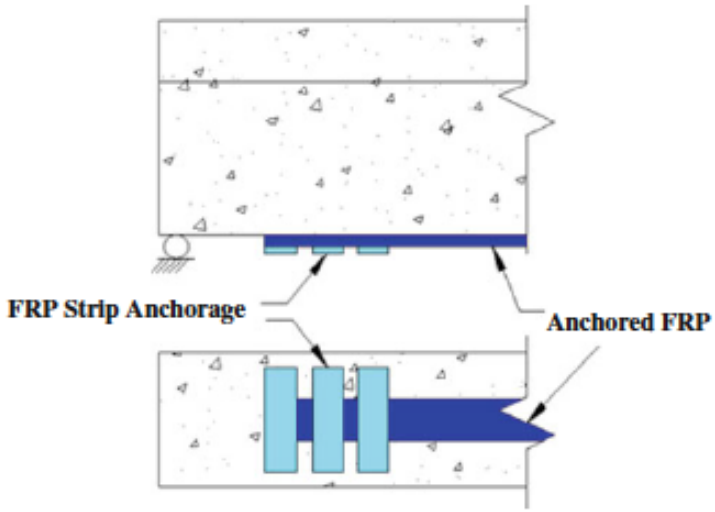

Fig. 1. 16 - Example of FRP strip anchorage (Galle and Sneed, 2013)

1.4.2..2.4 U-Anchors

U-Anchors are installed after constructing a groove in the concrete surface. Then the ends of the FRP sheet are pressed into the groove that is filled with epoxy and sometimes in combination with an FRP or steel bar, as shown in following figures. The U-Anchors system increases the bond of FRP to concrete by increasing the bonded area. This type of anchorage system improves the interfacial shear stress transfer between the FRP and the concrete.

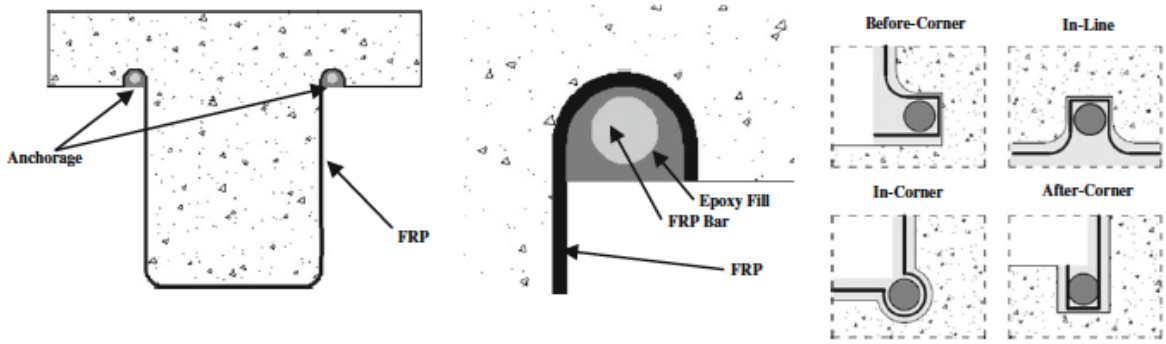

Fig. 1. 17 - Example of U-Anchors (Galle and Sneed, 2013)

1.4.2..2.5 Longitudinal Chase

First of all, a longitudinal chase is created cutting a groove along the length of the concrete in the direction of the force. Then the groove is filled with epoxy and, in some cases, with a steel or FRP bar. Finally, the FRP sheet is bonded to the concrete over the top of the groove. In this way, the interfacial shear stresses are distributed to a larger area of concrete through the mechanical properties of the epoxy. The additional bonded area is equal to the width and twice the depth of the groove, times its length. The following figure shows an example of application of longitudinal chase.

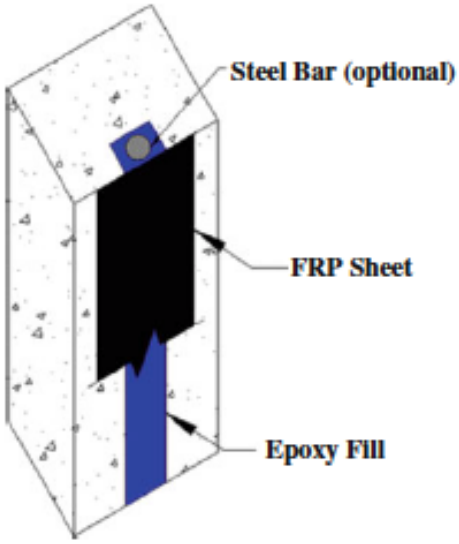

Fig. 1. 18 - Example of longitudinal chase (Galle and Sneed, 2013)

1.4.2..2.6 Plate Anchors

Metallic or composite plates have been used in the past in many studies. In this type of anchorage system, the FRP sheets are bonded to the plate and shear stresses is transferred at the FRP-plate interface. The plate then transfers the stress to the concrete substrate via its connection, which usually consist of bolts through the plate into the concrete. Moreover, the plate anchors are usually used to improved performance of U-Anchors system. The following figures illustrate two examples of plate anchors.

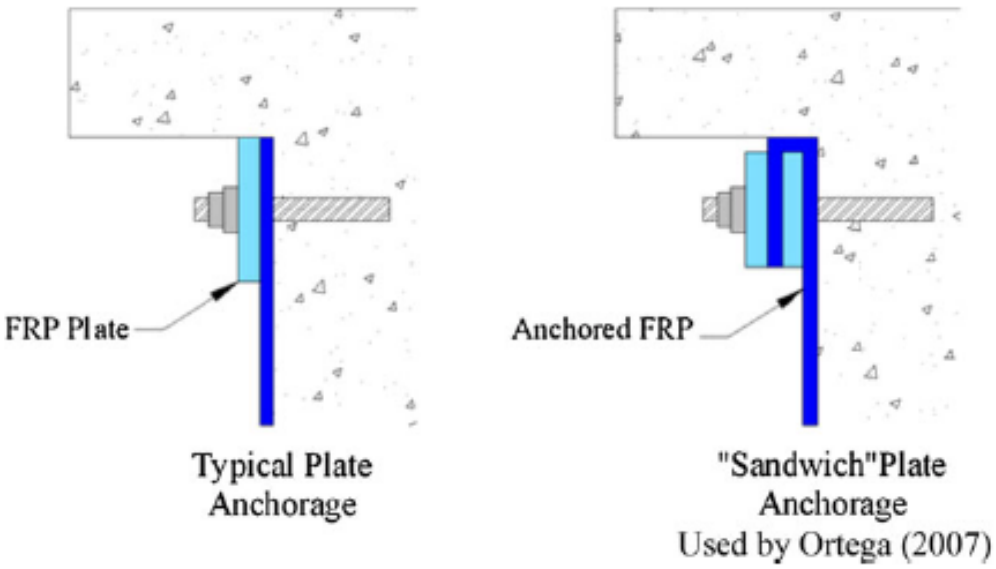

Fig. 1. 19 - Example of plated anchorage system (Galle and Sneed, 2013)

1.4.2..2.7 Bolted Angles

Other anchorage systems, which are very popular, are the bolted angles. These angles are made of aluminum or steel and they are usually used as a FRP anchorage devices at 90° joints. Typically, the FRP is laid around the joint, the angle is bonded to the FRP in the joint and is bolted to the concrete either through or around the FRP sheet.
Bolted angles were frequently used in previous researches because they are easy to obtain and require little fabrication. However, they have several limitations, as the problem of carrion due to the fact that they are made by steel or the problem of stress concentration in the FRP because of the 90° corner, which lead to a premature failure. Sometimes, to reduce the stress concentrations, an angle with a rounded corner is fabricated from steel tube and used as the anchorage, resulting noticeable improvements in strength and ductility. The following figures show some application of bolted angles.

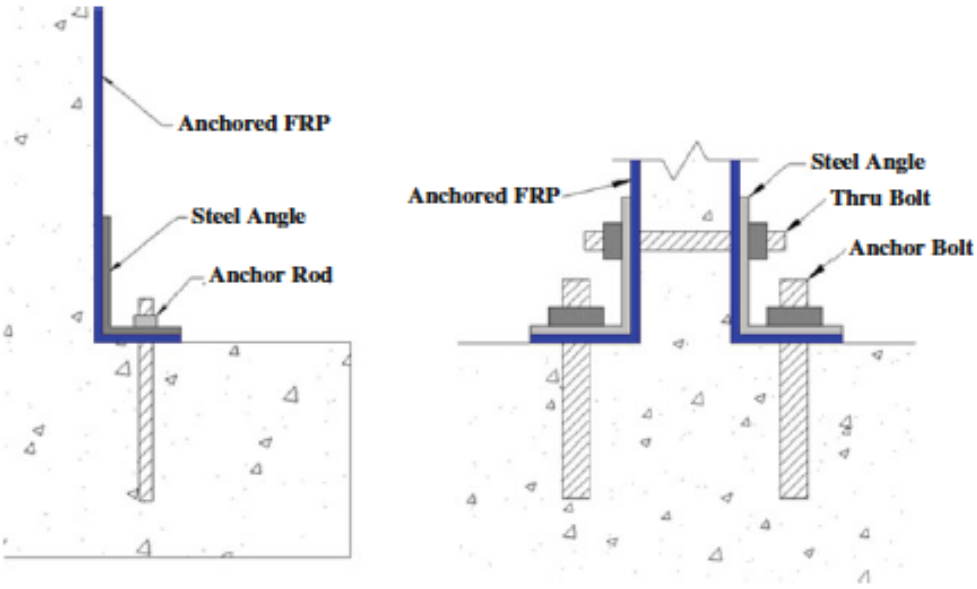

Fig. 1. 20 - Example of bolted angle anchorage system (Galle and Sneed, 2013)

1.4.2..2.8 Cylindrical Hollow Section

This type of anchorage system is usually used as FRP anchorage device at 90° joints. It is composed by a steel pipe bolted through the FRP at a 45° angle in order to eliminate the potential for local stress concentration at the 90° corner. An example of cylindrical hollow section is shown below.

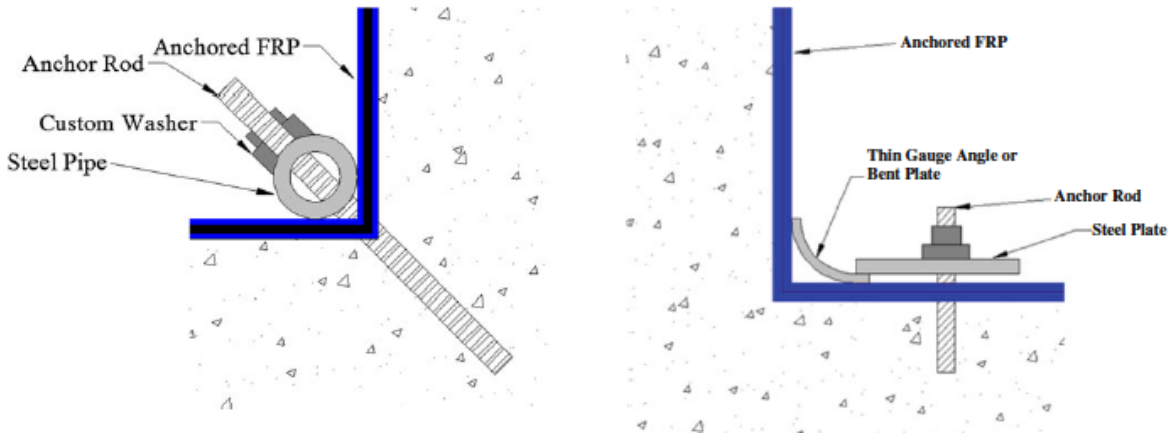

Fig.1. 21 - Example of cylindrical hollow section anchorage system (Galle and Sneed, 2013)

1.5 FRP Anchor Spikes

Above all the types of anchorage system already described, the FRP anchor spikes will be studied in depth in this research because they are currently the most common approach to prevent and delay deboning of external bonded FRP reinforcement. In general, anchors are distinguished by their load-transfer mechanism (mechanical interlock, friction, or chemical bond) and method of installation (cast-in-place, drilled in anchors, or pneumatically installed) (Eligehausen et al. 2006). In particular, FRP anchors are drilled in anchors with a chemical bond load transfer mechanism. Load is transferred from the anchor, through the adhesive, then into the concrete along the entire bond surface area (Cook at al. 1998). The bond strength of adhesive anchors is derived mostly from chemical adhesion and once the adhesive bond is broken, force transfer is provided by friction. Such force transfer is strongly affected by transverse pressure, concrete shrinkage, and roughness of the anchor surface.

The FRP anchor spikes can be fabricated in the field with the same FRP materials as the externally bonded fabric, which facilitates the construction and eliminates potential corrosion hazards from dissimilar material and makes the whole anchorage system homogenous. In addition, this type of anchorage system can be applied to wide variety of shaped FRP-strengthened RC structural elements such as beams and slabs (Zhang and Smith, 2011). The FRP anchors mainly consist in two components; the dowel, which is inserted into the concrete, and the fan, which is composed by the fibers that are fanned out and bonded onto the surface of the FRP plate. The following figure (Fig. 1.22) illustrates the typical FRP anchor.

Fig. 1. 22 - FRP anchor (ruler in inches)

However, no one design guideline exists to help designers to evaluate the enhancing given by the anchor spikes to the externally bonded FRP system and CNR-DT200 suggests to directly evaluate it with ad hoc experimental tests.

1.5.1 Past Studies on FRP Anchor Spikes

Experimental results of previous studies indicate that FRP anchors can be designed to achieve high pullout and shear capacities and hence can be used effectively to prevent or delay the debonding of externally bonded FRP sheets (Ozbakkaloglu and Saatcioglu, 2013). Diameter, length and angle of inclination of the dowel and opening angle of the fan have a significant influence on the capacities of the FRP anchors. For example, many recommendations for an effective embedment depth of FRP anchors have been presented in the past. According to tension tests conducted by Akyuz and Ozdemir (2004), an effective depth of 10 cm (approximately 3.9 inches) exists for FRP anchors, beyond which the capacity of the anchor no longer increases. The size of the anchor also determines whether the anchor has sufficient strength to allow the FRP sheet to develop its full capacity. In addition, the dimension of the embedded length of the anchors should be design to avoid interferences with the rebars of the reinforced concrete member. Orton (2007) recommends that the total cross-sectional area of FRP anchors should be two times the cross-sectional area of the FRP reinforcing sheet. Kim (2008) tested a variety of anchor sizes and found that an anchor cross-sectional area 1.33 times that of the FRP sheet was enough to develop the full capacity of the sheet. Therefore, Kim suggests a 1.50 ratio of anchor to sheet cross-sectional area as a conservative recommendation. Pham (2009) comments on Kim's 1.50 ratio after discovering anchor failures despite following Kim's. Moreover, the average bond strength of the FRP anchors decreases with increasing anchor diameter and embedded length (Ozbakkaloglu and Saatcioglu, 2013). This implies that the bond stress distribution is not uniform along the bond length of FRP dowel, and the uniformity of the distribution decreases with increasing bond length (Ozbakkaloglu and Saatcioglu, 2013). Another important aspect, which has been already analyzed in the past, is the fan configuration. The most common types are drawn below (Fig. 1.23).

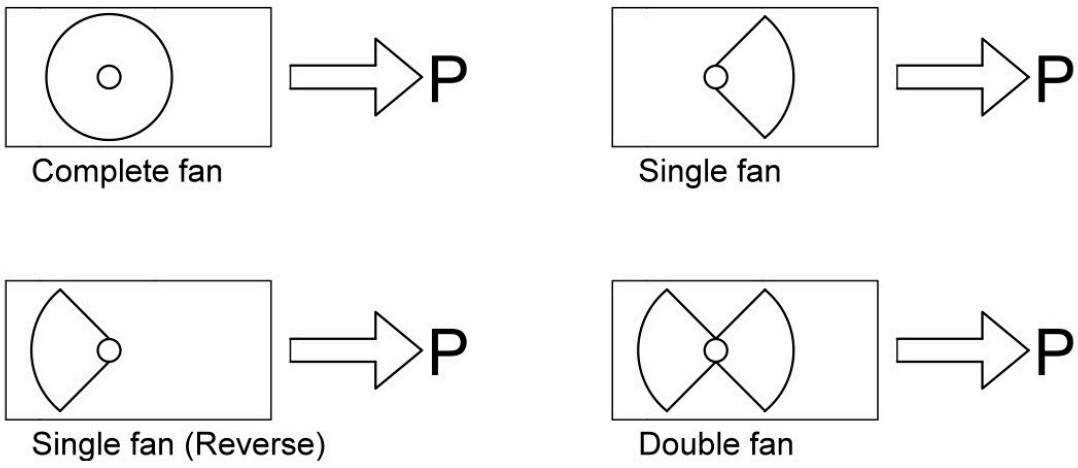

Fig. 1. 23 - Fan configurations

As illustrated in the sketches above, the anchor fan can be disposed in many ways. In the first specimen there is a complete 360° fan while in the second and third one there is a partial fan characterized by a specific fan opening angle and fibers direction. In the last specimen, the anchor fan is disposed in a symmetric way, composed by two partial fans, one in the direction of the applied tensile load and other one in the reverse direction. Based on several shear tests performed on anchored FRP sheet, it was found that the single-fan anchor configuration with the fibers of the fan oriented in the same direction of the applied load is more efficient than the one having the fibers in the reverse direction. Moreover, the single-fan FRP anchors with the fan oriented in the direction of the applied force largely perform in a similar manner to the double-fan FRP anchors although the latter cases uses twice the fibers content; for this reason if the same amount of fibers is consider, the single fan joints is much more efficient than the double-fan joints (Zhang and Smith, 2011).

Another important aspect to consider is the angle with which the anchor is inserted into the concrete because it can influence the strength and behavior of the anchored system (Zhang and Smith, 2011). Fig. 1.24 illustrates the dowel angle.

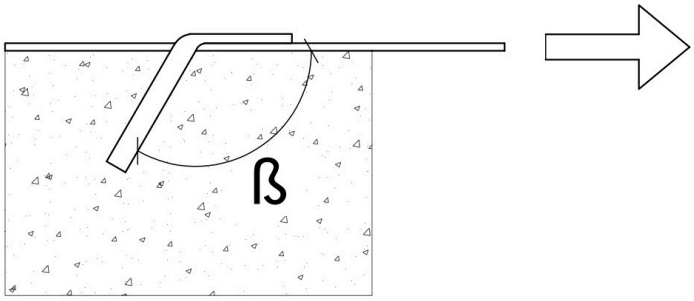

Fig. 1. 24 - Dowel angle

The different dowel angles places the FRP anchor under combination of shear and compressive force, if $\beta < 90°$, or shear and tensile (pullout) force, if $\beta > 90°$. In addition, angles smaller than 45° and larger than 157.5° were quite difficult to drill in the concrete block. For this reason, such angles were usually omitted from the studies (Zhang and Smith, 2011). Based on several pullout tests performed in the past, it was found that as the angle of the anchor dowel increases relative to the direction of the load, the strength of the joint increases and the ductility of the joint decreases (Zhang and Smith, 2011). Usually, the 90° dowel angle is adopted due to the fact that it is easy to drill in the field in most of the cases.

Another important aspect that has been already studied in the past is the layout anchor pattern; some examples are shown in following figures (Niemitz et al., 2010; McGuik and Brena, 2013)

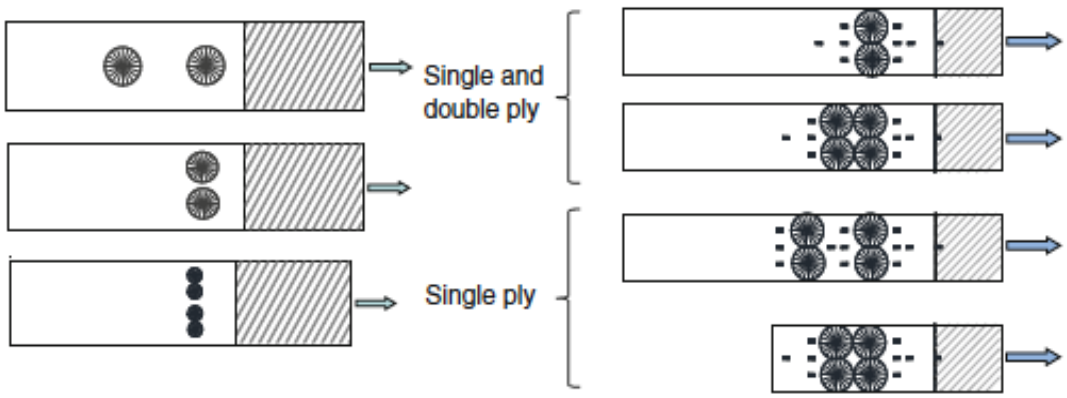

Fig. 1. 25 - Example of Anchors Patterns

Based on the results of several studies performed on anchored FRP sheets having different anchors pattern, many conclusions on the effect of the anchors pattern in terms of peak load were found. For unidirectional FRP sheets, studies conducted by Niemitz et al. found that the fan width plays an important role in development of FRP sheet force. Only regions of the FRP sheet within the width covered by the fan diameter were directly engaged. As a consequence longitudinal splitting occurs in specimens containing anchors that only partially cover the entire sheet width so the peak force developed is a fraction of the rupture force of the entire FRP sheet. Regions of the sheet in front of the location of the anchor fan reached rupture but those outside failed by debonding after longitudinal splitting of the sheet. Therefore to fully develop the rupture strength of the FRP sheet anchors fans should fully covered the width of unidirectional FRP sheets (Brenna and McGuirk, 2013).

Moreover, longitudinal spacing of anchors or anchor groups may have two effects depending on the distance between centerlines of anchors. For anchors that have a large longitudinal spacing, the strains in the sheet behind the first row of anchors dropped significantly. The second row of anchors did not contribute to force development in the FRP sheet until the debonding front had passed beyond the first row of anchors. At this point, the force in the sheet was developed by the first row of anchors and a combination of anchor and bond in the region surrounding the second row of anchors. The effect of the longitudinal anchors spaced widely apart in the longitudinal direction was to increase the ductility of the system without affecting the strength of the system significantly (Brena and McGuirk, 2013).

In contrast, anchors placed closed together in the longitudinal direction behaved as a group and led to higher force being developed in the FRP system. Anchors placed within the stress transfer zone of the bonded sheet are effective in increasing the force in the sheet, since the allowed higher stresses to develop through a combination of bond and anchorage. If multiple rows of anchors are needed to develop the strength of FRP sheets, these rows must lie within the stress transfer zone or will otherwise be relatively ineffective (Brena and McGuirk, 2013).

Another aspect, which has been already analyzed, is the variation of the peak load in the case of multiple FRP plies. Increasing the number of the FRP plies has the effect of increasing the demand on FRP anchors because of an increase in strength and stiffness of the FRP laminates. Although the strains developed in the FRP sheet were of similar magnitude, the peak force generated in the FRP sheets with two plies was

significantly larger due to the increase in thickness of the laminate. This result indicates that FRP anchors may effectively be used to anchor FRP sheets consisting of multiple plies (Brena and McGuirk, 2013).

Another important aspect about the efficient of the FRP anchors is the quality of the installation. Sometimes lower than expected pullout capacities of these anchors can be attributed to an improper hole preparation and anchor placement. The condition of the drilled hole during the installation can have a substantial influence on the bond strength of the anchors (Ozbakkaloglu and Saatcioglu, 2013).

1.5.2 Construction and Installation of FRP Anchors

FRP anchors can be either produce by hand or commercially available.

The first type of anchor is made from rolled unidirectional carbon fiber sheet, usually the same type of sheet used as an external bonded reinforcement. Commercially available FRP anchors are also available on the market and such anchors are made in an automated process. The quality control of these anchors would be expected to be higher than the hand-made FRP anchors. However, studies done by researcher have led to the conclusion that the quality of the FRP anchor manufacture is secondary to the enhancement in bond strength provided to the FRP plate (Zhang and Smith, 2011).

The following figures illustrate the procedure for the construction of the FRP anchor spike (Zhang, Smith and Kim, 2011):

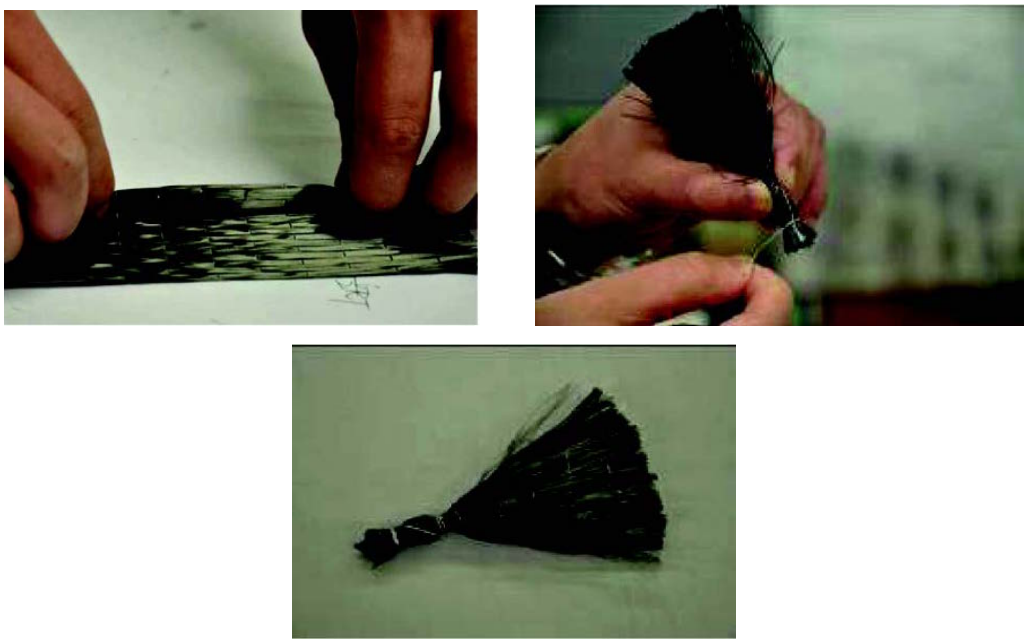

Fig. 1. 26 - FRP Anchor Spike Construction

Once the anchors are prepared, two different procedures of installation can be followed. The first one consists in two different steps: first of all, the epoxy resin is impregnated into a portion of the fibers at one end. The length of this portion is equal to the design embedded length of the anchor. After a curing period of some days into a cylindrical mold, the anchor has a solid dowel and it is ready for the installation. The second step is the saturation of the remaining fibers that composed the anchor fan and the insertion of the solid dowel into the hole, beforehand filled with epoxy resin. Then the fibers are finally spread out and epoxied onto the top of the FRP sheet. The following figures shows the procedure of application of the FRP anchor spikes just described.

Fig. 1. 27 - Installation of the FRP Anchor Spikes (Zhang And Smith, 2011)

The second procedure of installation, which is the one followed in this research, consists in just one step: the saturation of the entire anchor is followed by the insertion of it inside the hole, beforehand filled with epoxy resin, and then by the spreading out of the fan fibers on the FRP sheet. A detailed description of this type of installation is described in paragraph 2.4.5.

Moreover, the anchor can be saturated either at the same time with the external bonded FRP reinforcement or in a second moment, once the FRP sheet gets hard. In the first case the fibers of the FRP sheet are widen after the saturation in order to let the anchor get inside the hole. This procedure is followed when anchors having little diameter are used, otherwise it would be not possible to fit them between the fibers of the FRP sheet. The following figures illustrate the procedure of installation of the FRP anchor spike just described.

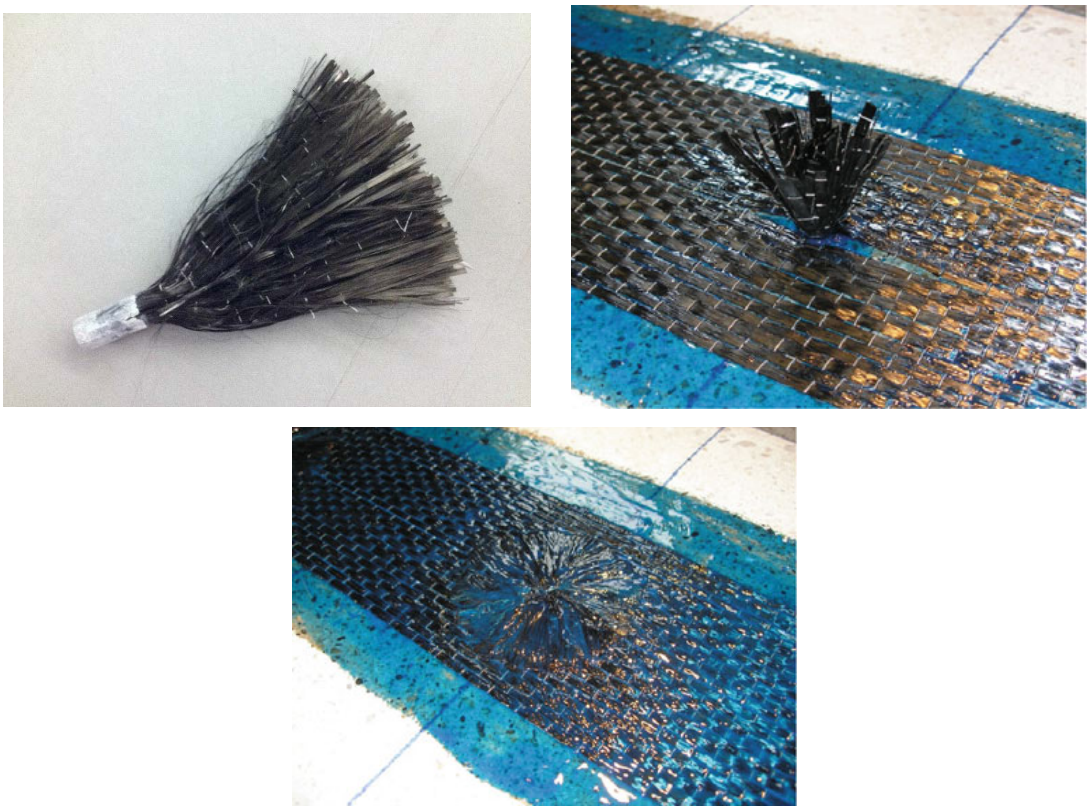

Fig. 1. 28 - Installation of the FRP Anchor Spike (Niemitz, James and Brena, 2010)

In the second case, the hard fibers of the FRP sheet are cut with a little blade just around the hole in order to allow the insertion of the FRP anchor spike. This proceed is the one followed in this research and it is described in details in paragraph 3.4.5.
One may question whether the insertion of the anchor will cause disturbance to the plate fibers and whether such disturbance will influence the tensile strength of the plate. In both the two cases, the installation of the anchor could affect the tensile strength of the FRP around the hole even if in the first case no fibers are severed to accommodate the anchor.

2. EXPERIMENTAL PROGRAM

In the previous chapter the reader was guided from the more general concepts of composite material and externally bonded FRP to the specific topic of this research, the understanding on the behavior of FRP laminates anchored using FRP anchor spikes.

Chapter 2 covers all the aspects related to the experimental campaign that was carried out to study the key parameters that govern the behavior of the FRP anchor spikes. The first section discusses the different types of tests that were performed, followed by the characterization of the materials and the preparation of the specimens. Then the test set-up and the instrumentation used during the tests are described in details in the last section

2.1 Test Program

Even if the number of studies that have focused on understanding the bond behavior of sheets to concrete is relevant, similar studies of anchored FRP sheets has not been studied in any significant details and very little information exist on the behavior of FRP anchors (Niemitz, James and Brena, 2010). Complex strain distribution exists in the plane of the FRP sheet near anchors location that avoids the usage of the bond behavior models of the FRP sheets. The objective of the research was to gain an understanding on the behavior and to identify the key parameters that govern the response of FRP laminates anchored using FRP anchor spikes for future development of design recommendations for this anchoring technique. The experimental program was composed by three different tests: two pullout tests and a pure shear test. The parameters that were analyzed are the embedded length of the anchors, the chamfer radius of the concrete at the hole surface and the different anchor configurations in terms of opening angle of the anchor fan.

The first test was a pullout test that was performed in order to measured the pure tension load capacity of the anchors used in the shear test. The diameter and the

embedded length of the anchors were kept constant during the test and respectively equal to 25,4 mm and 101 mm. The results are reported with particular attention focused on the failure mechanism, failure load and load-displacement response. The following drawing illustrates the test set-up that is described in details in the following paragraphs.

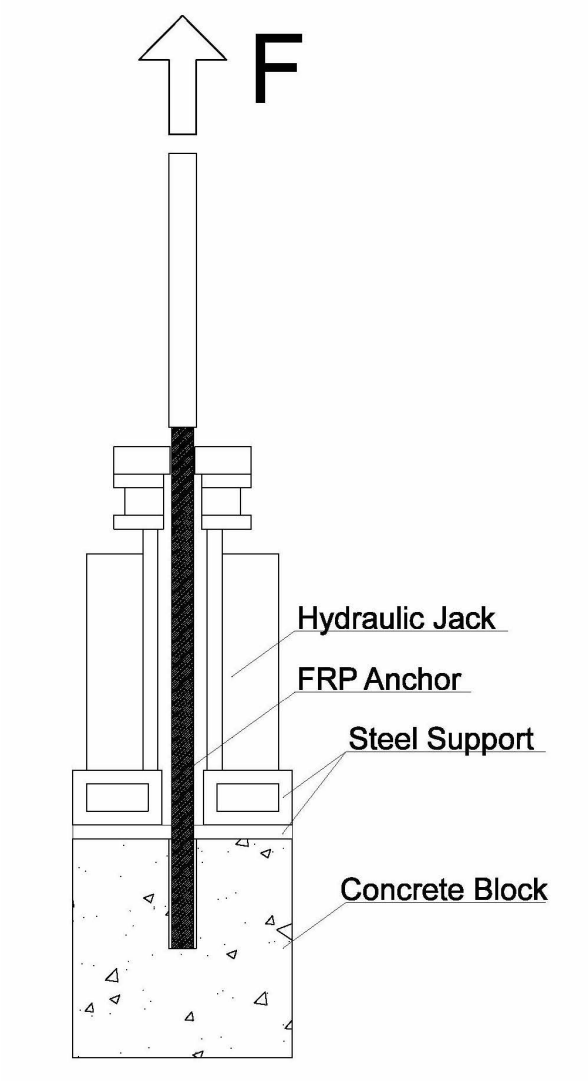

Fig. 2. 1 - Test 1 – Specimen Section

The second test was another pullout test which was performed in order to analyze the effect of the chamfer radius in the concrete at the hole surface in terms of stress concentration in the anchor fan. Three different types of chamfer radii were analyzed while the anchor diameter was kept constant and equal to the one used in previous

test. The following drawing illustrates the test set-up that is described in details in the following paragraph. As shown in the following figure, a plastic tube was used to avoid bonding between the FRP anchor and the inner surface of the hole. Thus, the only one bonded part of the anchor was the fan.

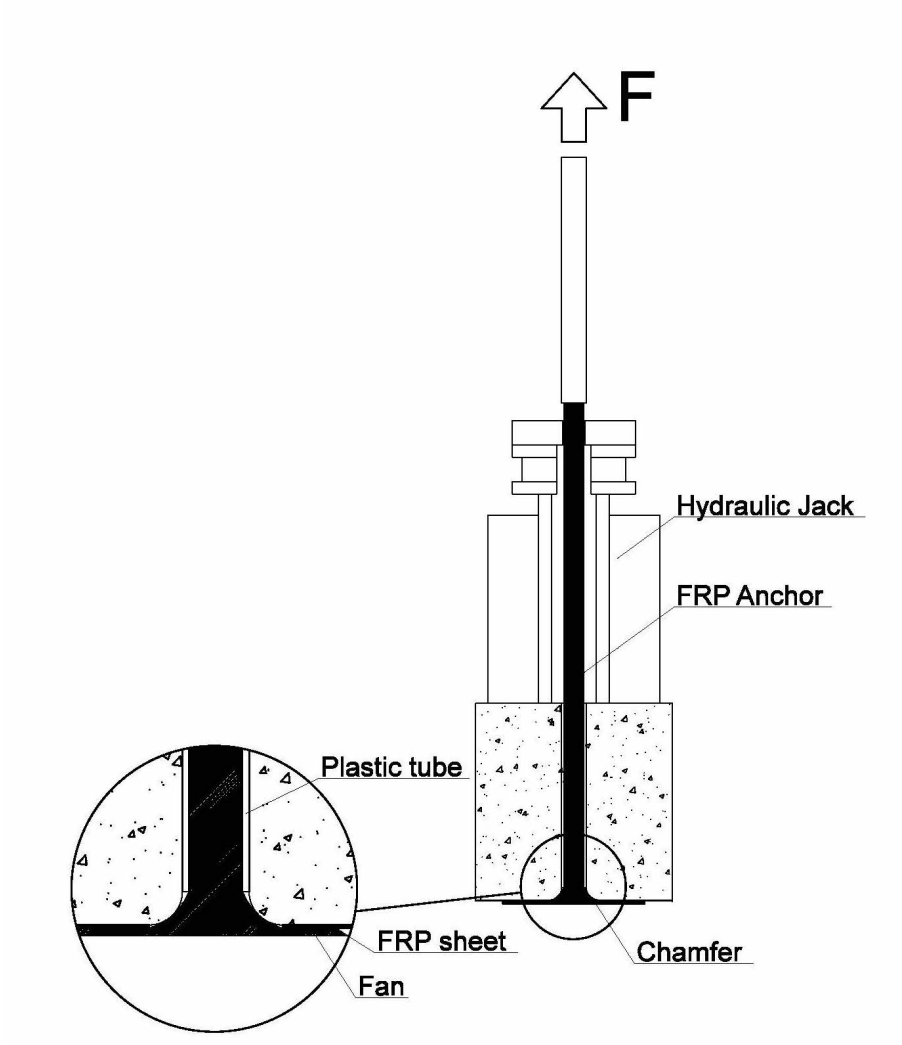

Fig. 2. 2 - Test 2 – Specimen Section

Test 3 was design as a direct double shear test in order to generate interfacial shear stresses between the surface of concrete and the FRP sheets. In general, this type of test is generally adopted for in situ quality control of bond and determination of the strength of concrete surface. Nonetheless, this test does not represent the bond-slip characteristics of real strengthening applications. Bending tests best reproduces the actual interfacial stress state in FRP strengthened RC beams, but such tests are still cumbersome to setup. The force transfer between FRP plate and concrete substrate

takes place primarily trough shear stresses and thus, shear tests are commonly adopted to determine the maximum debonding force (Sarbescu, Guadagnini, Pilakoutas, 2013). In past studies, comparisons of different set-up show that, in general, shear tests offer lower bond strength than bending tests (Miller, Nanni) and their simplicity makes them popular for laboratory investigations of FRP to concrete bond behavior.

In general, when strengthening is done with FRP laminates, tensile stress perpendicular to the interface between FRP and support (normal stress) may arise due to the significant stiffness of FRP laminate (CNR-DT200, 2013), as shown in Fig. 2.3. Normal stresses may reduce the value of interfacial shear stress as illustrated in Fig. 2.5.

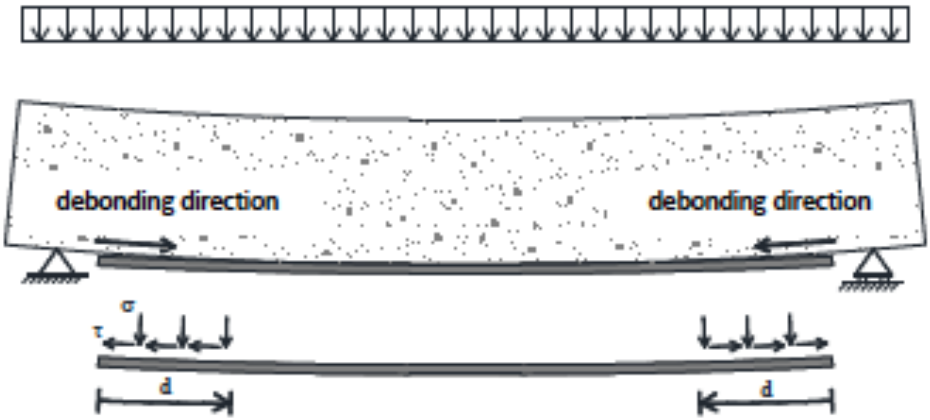

Fig. 2. 3 - Laminate end debonding (CNR-DT200, 2013)

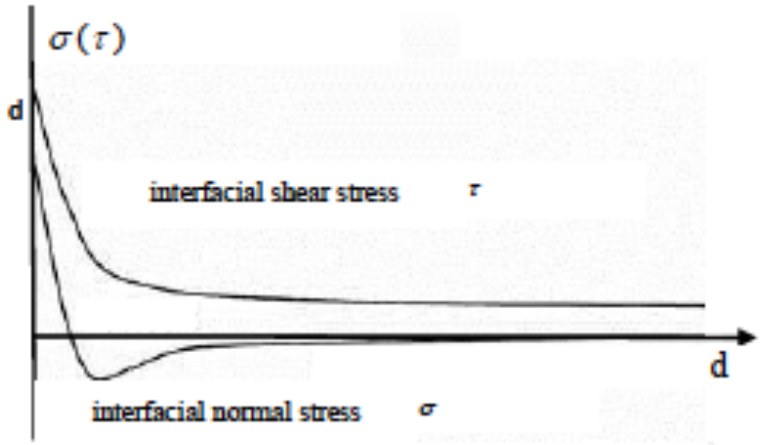

Fig. 2. 4 - Interfacial Shear and Normal Stress along the length of the bonded FRP laminate (CNR-DT200, 2013)

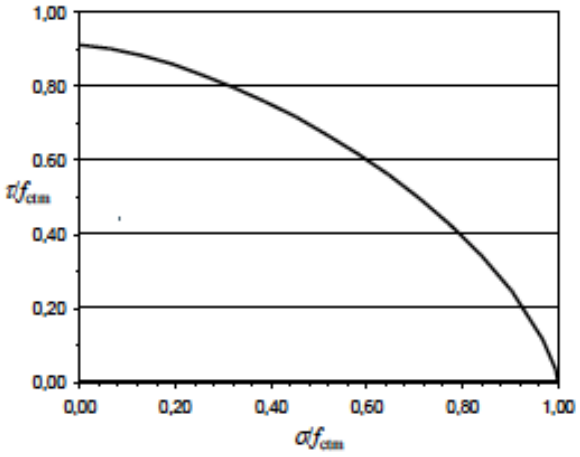

Fig. 2. 5 - Strength domain represented by interfacial shear and normal stresses (CNR-DT200, 2013)

Due to symmetry and for better control of induced normal stresses, the double shear test is generally preferred over the single shear test. However, it should be kept in mind that in flexural elements, peeling also develop along the FRP-concrete interface and their interaction with shear stresses can lead to a reduction in the bond strength of the strengthening system (Sarbescu, Guadagnini, Pilakoutas, 2013).

The specimens were arranged into four groups depending on the technique used to attach the FRP sheets to the concrete substrate. The first group, called benchmark, consisted of specimens in which the FRP sheets were attached to the concrete substrate only by bonding with epoxy resin. This group provided the baseline force that could be transferred between concrete and the FRP sheet through interface bond (control group). The second and the third group consisted of specimens where the FRP sheets were attached to the concrete blocks through a combination of epoxy bonding and FRP anchors. The differences between these two groups were on the opening angle of the anchor fan which was 60° in the second group and 90° in third group. The fourth group consisted of just one specimen in which the FRP sheet was attached to the concrete blocks through a combinations of epoxy bonding and FRP anchors having an opening angle equal to 60°. Moreover, the FRP sheets and the anchors fans were covered by rectangular FRP sheets to create a kind of sandwich configuration.

All the specimens were provided of the best chamfer radius in terms of stress concentration, based on the results of test 2.

The following figures illustrate the different types of specimens (Fig. 2.6) and the double shear test set-up (Fig. 2.7).

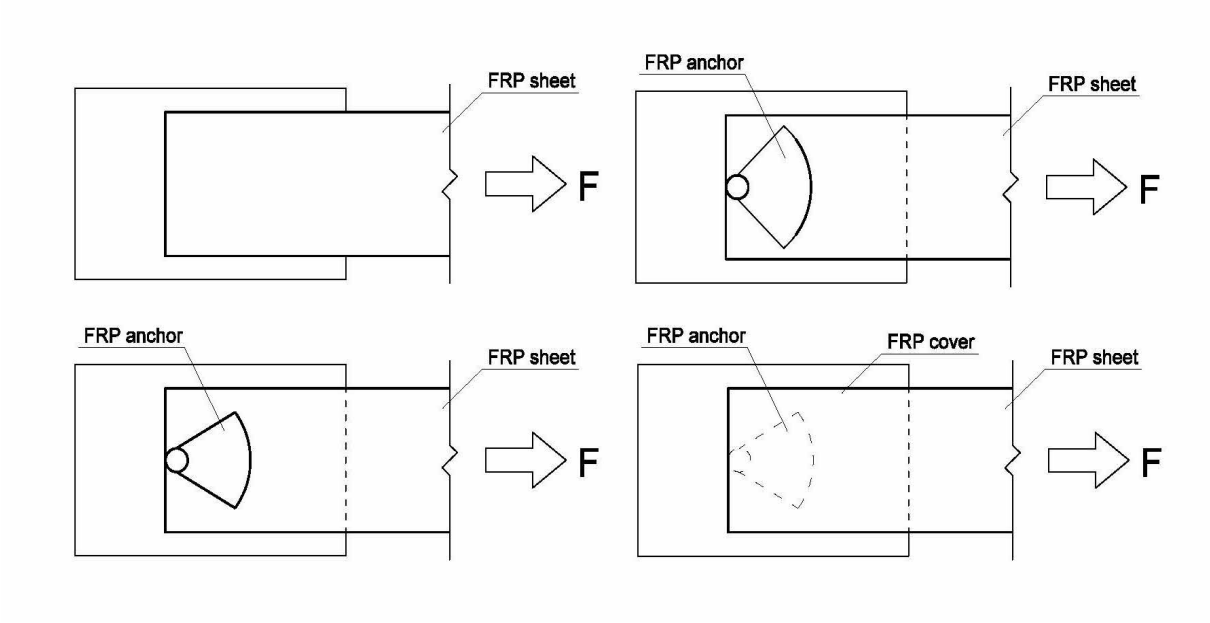

Fig. 2. 6 - Different types of specimens

Fig. 2. 7 - Test 3 set-up

2.2 Properties of Constituent Material

2.2.1 Concrete Properties

The concrete compression strength (f'_c) was calculated performing a compression test on the standardized concrete cylinders. A total of ten cylinders were obtained casting the concrete into plastic molds in accordance with ASTM C31 (2014). Plane surfaces were provided on the ends of the cylinders by following the "Standard Practice for Capping" (ASTM C617). Finally, after the curing period of 28 days, the cylinders were tested in accordance with ASTM C39 (2014).

Fig. 2.8 illustrates the test set-up for the compression test while Fig. 2.9 illustrates the cylinder before and after the compression test, respectively.

The Table 2.1 summarizes the results obtained from the test, where d is the average diameter, A is the average cross-sectional area, P_{max} is the maximum axial load and f'_c is the compressive strength of the cylindrical concrete specimens. Failure mode 3 represents the type in which there are columnar vertical cracking through both the ends and no well formed cones (as described in ASTM C39).

Based on the results in terms of compressive strength, the standard deviation (S_n) and the coefficient of variation (C.O.V.) are calculated.

Fig. 2. 8 - Concrete compressive strength set-up

Fig. 2. 9 - Cylinder before and after the Compression Test

Table 2. 1 – summary of 28 days compressive test on cylindrical concrete specimens

Specimen ID	d [mm]	A [mm^2]	P_{max} [kN]	f'_c [MPa]	Failure Mode
C1	102	8171	271	33	3
C2	102	8171	353	43	3
C3	102	8171	222	27	3
C4	102	8171	242	30	3
C5	102	8171	303	37	3
C6	102	8171	285	35	3
C7	102	8171	327	40	3
C8	102	8171	310	38	3
C9	102	8171	245	30	3
C10	102	8171	344	42	3
Average			290	36	
Sn			43	5	
C.O.V. (%)			15	15	

The concrete tensile strength (f_{ctm}) and elastic modulus (E_c) were calculated from the following formula:

$$f_{ctm} = 0.27\sqrt[3]{f'^2_c}$$

$$E_c = 5700\sqrt[3]{f'^2_c}$$

And thus:

Tensile strength f_{ctm} = 3 MPa
Elastic modulus: E_c = 62145 MPa

2.2.2 Fiber Reinforced Polymer Properties

The mechanical properties of the FRP were derived from tests on dogbone flat coupon tension specimens form in a wet lay-up manner from a layer of carbon fiber sheet.
The tensile tests were performed according to ASTM D3039 (2008). The objective of this test was to determine the in-plane tensile properties of the polymer matrix composite materials reinforced with high-modulus fibers without any aging or exposure conditioning. Average properties include experimental tensile chord modulus of elasticity, ultimate tensile stress and ultimate tensile strain.
ASTM D3039 (2008) is the corresponding test method designed to determine the tensile properties used for material specifications, research and development, quality assurance, and structural design. The procedure described in the ASTM D3039 (2008) consists of mounting a thin flat strip of material with a constant rectangular cross section in the grips of a mechanical testing machine, and monotonically loading it in tension while simultaneously recording the force.

2.2.2..1 Specimen Preparation

The materials necessary for the preparation of the tensile specimens consisted of carbon fiber sheet, epoxy (part A), and hardener (part B). The tools consisted of roller and spatula (to guarantees optimal impregnation of the fibers) and two Plexiglas panel with parchment paper having equal dimensions of the fibers sheet wrap.
The two parts were completely and thoroughly mixed together until a smooth, uniform, streak-free consistency was attained. The epoxy resin was then poured on the

fiber sheet and spread into the fibers using a spatula. Subsequently, the fiber sheet was rolled with the roller in order to obtain an ideal impregnation.

The fibers were laid down gently and then rolled in order to avoid the formation of air bubbles between the panel and the fiber sheet. The fiber sheet rested between the two Plexiglas panels and cured for 48 hours.

The specimens were cut from different panels to the prescribed dimensions using a high precision diamond blade saw. After sanding the ends of the coupon specimens, tabs were installed, as indicated in ASTM D3039 (2008), by laboratory personnel.

2.2.2..2 Tensile Test Set-up

Nominal specimen dimensions were 254 mm in length by 25.4 mm in width. The nominal thickness is 1,016 mm for the CFRP specimens. Note that the average cross sectional area was determined at the gauge range based on the average of three measurements of the width and thickness for each specimen prior to testing. Average area is reported in Table 2.3. All specimens were conditioned at room temperature 23 ± 1°C and 60 ± 5% relative humidity, for at least 24 hours prior testing, under laboratory ambient conditions.

Uniaxial tensile load was applied to all specimens. Testing was performed using a hydraulic universal test frame with a maximum capacity of 100 KN. The tensile load was measured using the internal load cell of the frame in compliance with ASTM E4 (2013), while the extension (elongation) was measured using a Class B-2 clip-on extensometer with a 50 mm gauge length, placed mid-length of the coupon specimen, in accordance with ASTM E83 (2010). The extensometer was removed half way during the test, in order to avoid potential damage to the instrument. Specimens were gripped with hydraulic wedge type grips at a pressure of 20.7 MPa. The test set up is shown in Fig. 2.10. All data was gathered using a National Instruments data acquisition system at a rate of 100 Hz.

Fig. 2. 10 – Tensile test set up

Load was applied in displacement control to induce a nearly constant strain rate in the gauge section until failure, with a constant frame head displacement of 2 mm/min, while also producing a failure within 1 to 10 minutes as for ASTM D3039 (2008) requirements.

2.2.2..3 Test Results

All products exhibited linear elastic behavior until failure. Based on the experimental tests, the average ultimate tensile strength of the material under investigation was 1339 MPa; the computed average ultimate tensile strain was 1.80%; and the average chord modulus of elasticity was equal 74,6 GPa.

The primary mode of failure is through tensile rupture of the CFRP coupons, which is equivalent to code XGM failure mode given in ASTM D3039 (2008), signifying an explosive, gauge middle failure (see Figure 2.11). Individual failure modes are reported in the tabulated results section.

The results reported below were computed following the ASTM D3039 (2008) and summarized in Table 2. 2. Note, the results are calculated using the measured cross-sectional area determined form the average of three width and thickness readings before testing.

Table 2. 2 - Definitions

Symbol	Parameter	Description
P^{max}	Maximum force at failure	Peak load recorded during test
A	Average cross-section area	Nominal or measured cross-section area. Based on three measurements.
F^{tu}	Ultimate tensile strength	$F^{tu} = P^{max} / A$
ε	Computed ultimate strain based on extensometer measurement	Strain based on the intersection of the computed chord modulus and ultimate tensile strength, equating to the ratio between the ultimate tesile strength and the tensile chord modulus
E^{chord}	Tensile chord modulus of elasticity, based on strain gauges measurement	Difference in applied tensile stress between the 1000 and 3000 με points (Δσ); divided by the difference between the two strain points, nominally 0,002 (Δε). $E^{chord} = \Delta\sigma/\Delta\varepsilon$

Every specimen behaved linear elastically until failure, which proved that the obtained results are consistent with what is presented in the literature. FRP materials are anisotropic, linear elastic until failure and are characterized by high tensile strength only in the direction of the reinforcing fibers (Wu 1990, Tamura 1993, Nanni et al. 1998).

Table 2. 3 contains the tabulated summary results. The tables include: average measured cross-sectional area of each specimen (A), maximum tensile force (P_{max}), ultimate tensile strength (F_{tu}), chord modulus of elasticity (E_{chord}), computed ultimate tensile strain (ε_u), and corresponding failure mode as per ASTM D3039 (2008). Average, standard deviation, and coefficient of variation (C.O.V.) values are also reported that are based on the respective total number of specimens under evaluation. Fig. 2.11 shows the typical failure modes given by ASTM D3039 (2008).

Table 2. 3 - Tabulated Result for ASTM D3039 (2008)

SPECIMEN ID	A [mm²]	P_{max} [kN]	F_{tu} [MPa]	E_{chord} [GPa]	ε_u [%]	Failure Mode
STe_C277_TNS_CC_00_001	26,5	37,64	1419,57	79,12	1,79	XGM
STe_C277_TNS_CC_00_002	26,5	34,35	1298,23	72,71	1,78	XGM
STe_C277_TNS_CC_00_003	26,8	34,37	1283,87	74,64	1,72	XGM
STe_C277_TNS_CC_00_004	25,1	35,17	1402,92	79,94	1,75	SGM
STe_C277_TNS_CC_00_005	26,1	32,22	1235,77	72,09	1,71	XGM
STe_C277_TNS_CC_00_006	25,8	35,05	1357,75	74,36	1,83	SGM
STe_C277_TNS_CC_00_007	26,0	33,50	1288,74	81,19	1,59	XGM
STe_C277_TNS_CC_00_008	25,6	33,53	1310,42	72,02	1,82	SGM
STe_C277_TNS_CC_00_009	25,5	33,16	1297,47	71,81	1,81	XGM
STe_C277_TNS_CC_00_010	26,3	35,59	1354,06	69,68	1,94	SGM
STe_C277_TNS_CC_00_011	25,8	37,07	1438,88	76,91	1,87	SGM
STe_C277_TNS_CC_00_012	25,9	37,45	1444,71	75,12	1,92	SGM
STe_C277_TNS_CC_00_013	25,9	35,67	1378,78	79,74	1,73	XGM
STe_C277_TNS_CC_00_014	25,9	34,27	1320,64	72,09	1,83	XGM
STe_C277_TNS_CC_00_015	25,7	31,48	1225,47	72,57	1,69	XGM
STe_C277_TNS_CC_00_016	25,8	36,72	1422,22	72,36	1,96	XGM
STe_C277_TNS_CC_00_017	25,2	33,95	1348,90	73,54	1,83	SGM
STe_C277_TNS_CC_00_018	25,0	34,18	1366,50	75,05	1,82	SGM
STe_C277_TNS_CC_00_019	25,9	32,67	1261,58	73,81	1,71	XGM
STe_C277_TNS_CC_00_020	25,9	34,49	1330,54	73,05	1,82	XGM
STe_C277_TNS_CC_00_021	27,5	31,87	1159,00	73,67	1,57	XGM
STe_C277_TNS_CC_00_022	27,3	37,67	1380,42	72,85	1,89	XGM
STe_C277_TNS_CC_00_023	26,8	40,32	1503,21	78,98	1,90	XGM
STe_C277_TNS_CC_00_024	27,2	30,93	1135,67	70,78	1,60	XGM
STe_C277_TNS_CC_00_025	25,9	28,16	1085,15	70,23	1,54	XGM
STe_C277_TNS_CC_00_026	26,3	30,95	1177,80	72,92	1,61	XGM
STe_C277_TNS_CC_00_009	26,4	39,21	1483,32	71,33	2,08	SGM
STe_C277_TNS_CC_00_013	25,1	39,90	1590,16	82,77	1,92	XGM
STe_C277_TNS_CC_00_029	25,3	35,86	1416,03	73,05	1,94	XGM
STe_C277_TNS_CC_00_030	26,0	36,35	1396,74	72,64	1,92	XGM
STe_C277_TNS_CC_00_031	25,8	36,85	1427,56	73,95	1,93	XGM
STe_C277_TNS_CC_00_019	25,6	29,72	1161,71	76,43	1,52	XGM
STe_C277_TNS_CC_00_033	26,3	38,65	1467,84	76,64	1,91	XGM
STe_C277_TNS_CC_00_034	26,7	36,41	1365,44	71,61	1,91	SGM
STe_C277_TNS_CC_00_035	26,5	37,16	1400,08	75,60	1,85	XGM
STe_C277_TNS_CC_00_036	26,8	37,22	1387,74	73,33	1,89	XGM
STe_C277_TNS_CC_00_002	26,1	27,50	1052,44	71,40	1,47	SGM
STe_C277_TNS_CC_00_038	26,2	30,41	1161,71	71,12	1,63	XGM
STe_C277_TNS_CC_00_039	27,0	33,92	1253,62	99,31	1,26	XGM
STe_C277_TNS_CC_00_003	25,2	29,17	1157,84	74,16	1,56	XGM
Average	25,8	34,63	1339,35	74,59	1,80	
S_{n-1}	0,5	1,70	65,45	3,19	0,09	
CV((%)	1,8	4,91	4,89	4,27	5,09	

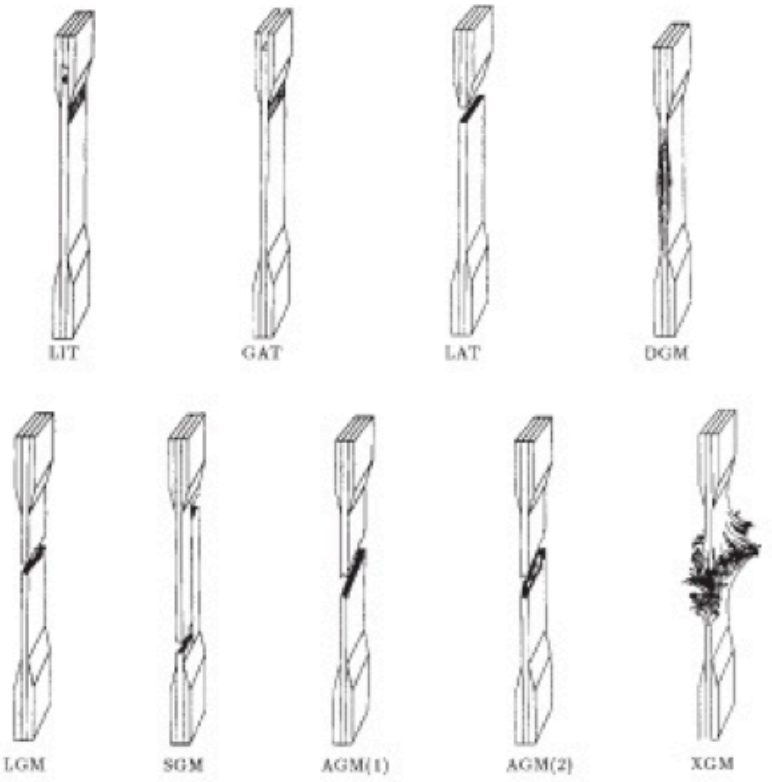

First Character

Failure Type	Code
Angled	A
edge Delamination	D
Grip/tab	G
Lateral	L
Multi-mode	M(xyz)
long. Splitting	S
eXplosive	X
Other	O

Second Character

Failure Area	Code
Inside grip/tab	I
At grip/tab	A
<1W from grip/tab	W
Gage	G
Multiple areas	M
Various	V
Unknown	U

Third Character

Failure Location	Code
Bottom	B
Top	T
Left	L
Right	R
Middle	M
Various	V
Unknown	U

Fig. 2. 11 - Typical failure modes (ASTM D3039 2008)

2.3 Specimen Preparation

The main steps of the specimen's preparation are described in the following section.

2.3.1 Casting of the Concrete Specimens

The first step of the preparation of the specimens is the casting of the concrete into the wooden molds. The molds were constructed specifically for the realization of the concrete specimens used for this research. Three types of mold were built in order to get three different types of specimens. The dimensions of them are listed in the next paragraph. Wooden panels having thickness equal to half inch were used for the construction. The Fig. 2.12 shows two moments of the fabrication.

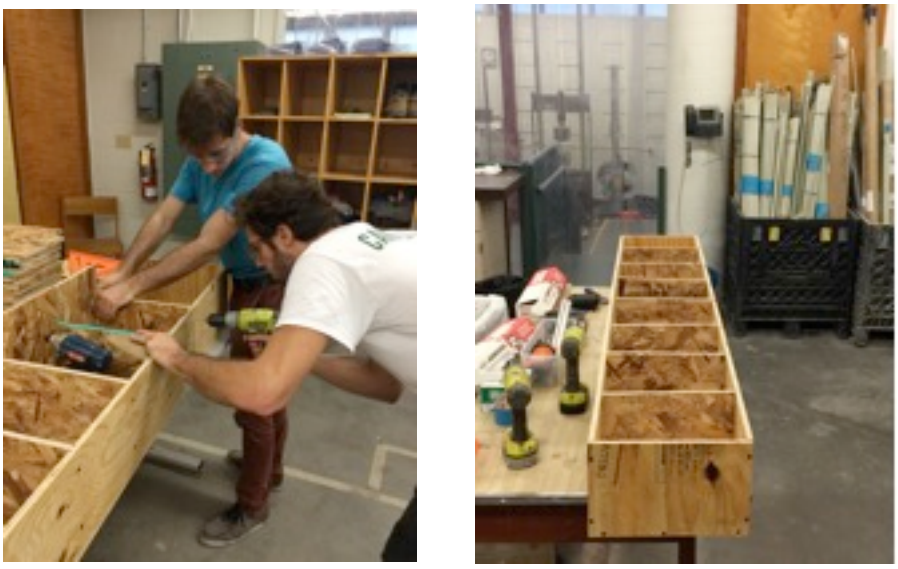

Fig. 2. 12 - Wooden mold construction

The application of the oil de-molder on the inner surfaces of the mold was done before the casting in order to have perfect separation between the concrete surface and the wooden molds during the removal of the specimens after the curing period. This operation is shown in Fig. 2.13.

Then, the Abran Cone Slump Test (ASTM C143-12) was performed during the concrete casting (Fig. 2.14). The consistency and workability of fresh concrete was measure directly through this test and the results were compared with the required one.

Fig. 2. 13 - Application of the de-molder oil

Fig. 2.14 - Abran Cone Slump Test

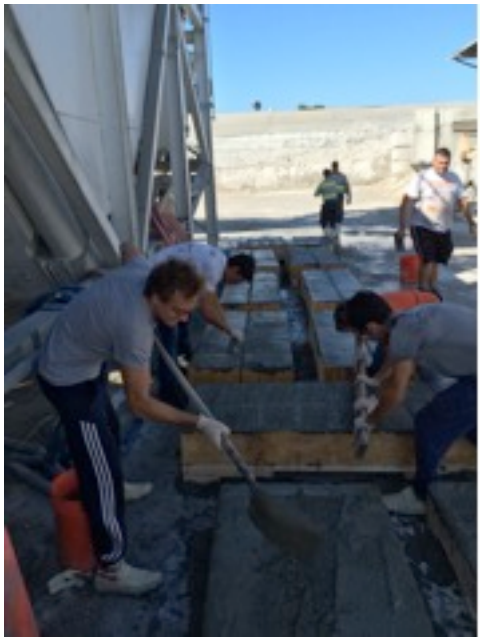

Fig. 2. 15 - Casting of the concrete

Immediately after casting, the specimens were covered with plastic sheets to avoid any loss of moisture. After seven days the specimens were uncovered and stored in the laboratory.

The concrete specimens were finally de-molded after a curing period of 28 days.

2.3.2 Substrate Preparation

With few exceptions, it is widely accepted that the surface roughness influences bond capacity. The surface of the specimens needs to be treated in order to increase the bond once the FRP sheet is applied on the concrete (Sarbescu, Guadagnini and Pilakoutas; 2013). Although most design guidelines include qualitative recommendations on the surface preparation, these recommendations are rather vague. As a consequence, before the installation of the FRP sheet, it is important to remove the cement paste from the concrete surface. On the other hand, high impact preparation, such as hammering, may potentially weaken the surface and high levels of roughness are reported by some researchers to adversely affect the concrete surface by inducing micro cracks (Sarbescu, Guadagnini and Pilakoutas; 2013). The surface preparation recommended by manufacturers guidelines are usually achieved by grinding or sand blasting and consists in the removal of the cement paste and exposure of a relative plane surface of aggregates. For design purposes, it is more reasonable to relate bond stresses to a coefficient corresponding to the type of surface preparation provided by International Concrete Repair Institute.

Fig. 2.16 illustrates the operation of sand blasting which was done to roughen the surface and remove the smooth concrete paste. The surfaces were visually inspected after the sandblasting and compared with the benchmark guidelines for the concrete surface profile (CSP) developed by the International Concrete Repair Institute. It was found a CSP level equal to 3 (Fig. 2.17).

Fig. 2. 16 - Sandblasting performed by a professional operator

Fig. 2. 17 - Sample of ICRI: CSP 3

2.3.3 TEST 1 – Specimen preparation

After grinding the surfaces, five specimens were prepared for the installation of the anchors. The dimensions of the specimens were 305 mm x 203 mm x 203 mm (12”x 8”x 8”).

- After grinding the surface, each specimen was drilled in the center of the upper surface using a Hilti hammer driller. A 25,4 mm (1 in) reinforced concrete drill bit was used in this operation in order to obtain a hole diameter 6.35 mm (1/4 in) greater than the anchor diameter. The length of the hole was 101.6 mm (4 in.). Fig. 3.18 and Fig. 3.19 show respectively the Hilti hummer drill and the operation of drilling.
- The hole was blown up with an air compressor, paying attention to clean perfectly the inner surface from the dust. Then the hole was brushed and blown up again. The drill bit used to brush the hole is shown in Fig. 2.20, while the Fig. 2.21 illustrates the operation of cleaning the hole.

Fig. 2. 18 - Hilti hammer driller

Fig. 1. 19 - Operation of drilling

Fig. 2. 20 - Brush drill bit

Fig. 2. 21 - Operation of cleaning the hole

- Each anchor was cut for a total length equal to 857.5 mm (35 in.); this length was computed based on the dimensions of the hydraulic jack, the steel support, the load cell and the plates needed for performing this test.

Once the specimens were prepared, two different types of procedure were followed to install the anchors. At the end, the second one turned up to be the more efficient.

First procedure:

- The anchors were impregnated on a table accurately covered with a plastic sheet. 101,6 mm (4 in.) of fibers were maintained dry at one end. These fibers composed the embedded length.
- After the impregnation, the anchors were picked up in a wood support in order to keep them vertically during the curing period.
- At this point of the procedure, the grip was installed; the impregnated fibers were inserted into a steel cylinder having a diameter equal to 1" and beforehand filled with epoxy resin for 1/3 of his length. The Fig. 2.22 shows the anchors and the support during the curing period.
- The holes of the specimens were primed with epoxy and then filled with thickened epoxy for 1/3 of their length. The thickened epoxy was obtained mixing epoxy resin with flumed silica with ratio 1:1 by volume.
- Once the anchors got hard, they were flipped upside down and the remaining dry fibers were impregnated. The same wood support was used even in this second case. The grips were fixed to the top of the support and the sutured fibers were inserted into the holes of the specimens, which were accurately disposed aligned with the anchors on the floor.

At this point, this procedure turned out to be wrong. First of all, there was a discontinuity between the already hard fibers and the just impregnated fiber that could have caused stress concentrations and, consequently, the premature rupture of the anchor during the test. Secondly, it was really hard to keep the fibers straight inside the hole due to the fact that it was impossible to put in tension the anchors. In addition the connector used to come out from the hole during this operation. The result is shown in Fig. 2.23.

Fig. 2. 22 - Anchors preparation

Fig. 2. 23 - Result of the first procedure

Second procedure:

- First of all, another little hole was drilled in the same point but in the opposite surface in order to get a continuous hole for all the depth of the specimen. A 9 mm diameter drill bit was used in this operation. Fig. 2.24 shows the section of the specimen.

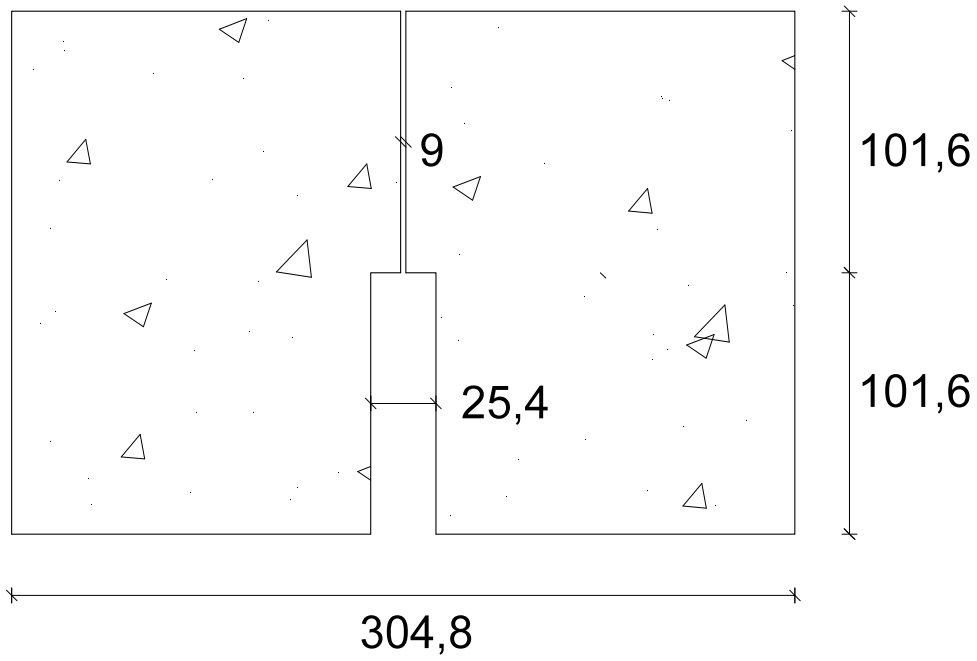

Fig. 2. 24 - Test 1 – Concrete block section

- The anchors were disposed on a table that was accurately covered with a plastic sheet. The fibers were impregnated for all their entire length paying attention to not leave any fibers dry. Once the anchors were perfectly impregnated, they were squeezed in order to take all the excessive epoxy resin off.
- A plastic lace was used to wrap one end of the anchor. Then, a long piece of fishing line was tied to the plastic lace. Fig. 2.25 shows the tip of the anchor, while Fig. 2.26 illustrates two anchors after the impregnation of the fibers.

Fig. 2. 25 - Anchor tip

Fig. 2. 26 - Anchor after the impregnation

- The hole was primed with epoxy resin and then filled with thickened epoxy resin for one third of its length. The thickened epoxy was obtained mixing epoxy resin with flumed silica with ratio 1:1 by volume.
- After this operation, the fishing line was inserted into the hole and passed throughout the entire length.
- The anchor was inserted into the hole and the fishing line was used to pull it from the other side of the specimen making the installation easy to do. Once the anchor reached the bottom of the hole, the fishing line was fixed to an external support in order to avoid any slippage of the anchor. It is important to underline how fundamental is to keep the fibers straight during the installation. In this case the anchors were kept straight by gravity maintaining the specimen upside down.
- Finally, the grips were installed into the anchors. The impregnated fibers were inserted into a steel cylinder having a diameter equal to 25.4 mm (1 in.) and beforehand filled with epoxy resin for 1/3 of its length. The following drawing, Fig. 2.27, represents the specimen section once the installation was concluded.
- Finally, the specimens were kept upside down in a steel support for 48 hours. Fig. 2.28 shows the specimens during the curing period of 48 hours.

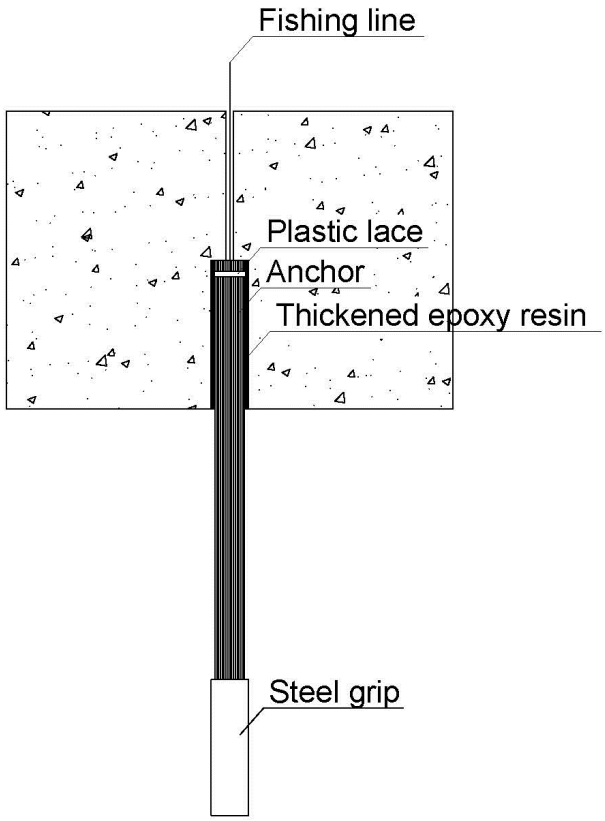

Fig. 2. 27 – Test 1 - Specimen section

Fig. 2. 28 - Specimen during the curing period

The following table summarizes the specific dimensions of the specimens described before.

Table 2. 4 - TEST 1 – Summary Table

n° specimens	Hole		Anchor	
	Length [mm]	Diameter [mm]	Dowel Lenght [mm]	Dowel Diameter [mm]
5	101,6	25,4	101,6	19

2.3.4 TEST 2 – Specimen Preparation

- After grinding the surfaces, 12 specimens were prepared for the installation of the anchors. The dimensions of the specimens were 305 mm x 203 mm x 203 mm (12”x 8”x 8”).
- Each specimen was drilled in the center of the upper surface (304.8 mm x 203,2 mm) using a Hilti hammer driller. A 25,4 mm (1 in) reinforced concrete drill bit was used in this operation in order to obtain a hole diameter 6.35 mm (1/4 in) greater than the anchor diameter. In this case the hole had to pass through all the depth of the specimen (203.2 mm). This operation was really delicate because the rupture of the concrete during the drilling must be avoided. The procedure adopted was the following: we started drilling the hole from one side, we drilled until the middle of the depth of specimen, then we flipped the specimen upside down and we started drilling on the opposite side. Going ahead in this way, a perfect hole was created without generating cracks at the bottom of the specimen.
- At this point, 3 different types of specimens were defined based on different lengths of the chamfer radius in the concrete at the hole:

1. ***Specimen T2_0***: 0 mm chamfer radius
2. ***Specimen T2_1/4***: 6,35 mm (1/4 in.) chamfer radius
3. ***Specimen T2_1/2***: 12,7 mm (1/2 in.) chamfer radius

4 specimens for each type were prepared. Fig. 2.29 (left) and Fig. 2.30 (left and right) illustrate the three different types of specimen while Fig. 2.28 (right) shows the drill tip that was used to create the chamfer.

Fig. 2. 29 - 0 chamfer radius (left), drill bit used to create the chamfer (right)

Fig. 2. 30 - 12.7 mm chamfer radius (left), 6.35 mm chamfer radius (right)

- The dust was blown up from the hole, and then the inner surface of the hole was brushed and blown up again.
- Once the surface and the hole were prepared, an FRP sheet was installed in each specimen in order to cover all the upper surfaces. The same type of sheet

chosen for Test 3 (Shear Test) was used even in this test. It had the following properties:

Average thickness: 1.016 mm
Average ultimate strain: 1.8 %
Average ultimate strength: 74.9 MPa

The procedure of installation was the following:

Specimen substrate cleaning

In order to allow a good bonding between the FRP system and the surface of application, the substrate surface have to be clean. An air compressor and a brush were used to remove all the particle of sand resulting from the sandblasting. Fig. 2.31 (left) shows the surface after the preparation of the substrate.

Primer application

A two parts thickened epoxy, also called putty, was prepared during this operation. First of all, the epoxy resin (part A) and the curing agent (part B) was added into a bucket, previously calibrated using a mixing ratio of 100:33 by weight. The two parts were mixed for 3 minutes until a smooth and uniform consistency was obtained. Then, fumed silica was added into the bucket in order to make the epoxy thicker, using a mixing ratio by volume of one of two parts epoxy resin to 0.75 of fume silica. Depending on the mixing paddle, it took several minutes to mix the putty. Once a uniform consistency was obtained, the thickened epoxy was applied using a spatula, in order to fill all the concrete cavities and pores. Finally, a two parts epoxy resin was prepared again following the same procedure of before and a thin layer of it was applied using a paintbrush over the putty. Fig. 2.31 shows the concrete surface before (left) and after (right) the application of the primer.

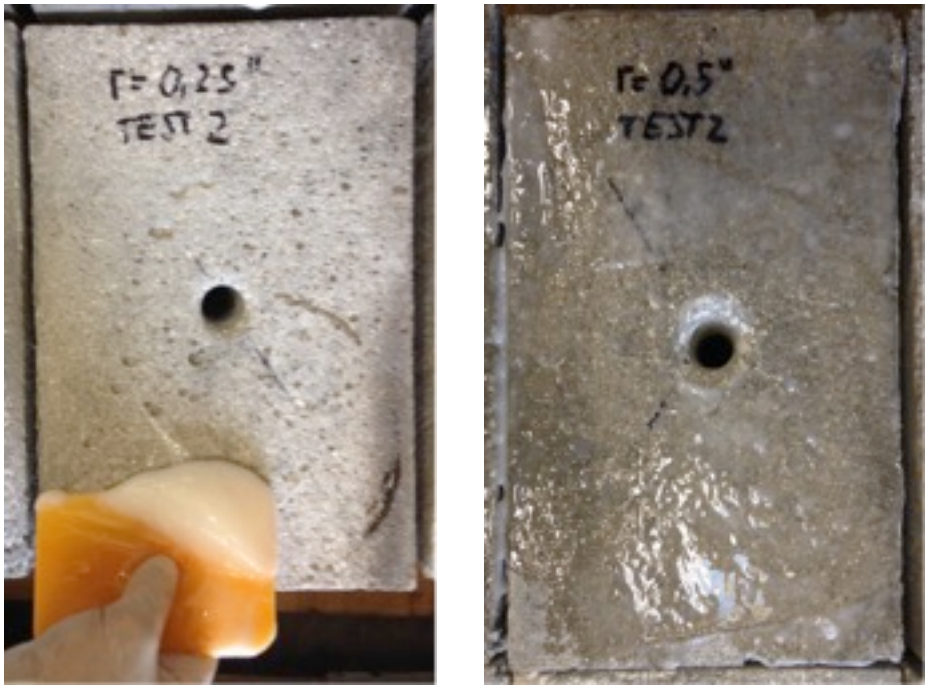

Fig. 2. 31- Substrate before (left) and after (right) the application of the primer

FRP impregnation and application

First of all, a two parts epoxy resin was prepared. The epoxy resin (part A) and the curing agent (part B) was added into a bucket, previously calibrated using a mixing ratio of 100:33 by weight. The two parts were mixed for 3 minutes until a smooth and uniform consistency was obtained. The FRP sheets, having dimensions equal to 304.8 mm x 203.2 mm, were disposed over a previously cover clean table. Secondly, the resin was gently poured on the dry fibers for their impregnation. A spatula was used to spread the epoxy out homogenously on the sheet, than the fibers were rolled in order to obtained a uniform impregnation. The procedure was followed in both the two surfaces of the FRP sheets.

The FRP system was applied to the concrete substrate within 45 minutes from the primer application and the fiber impregnation. The FRP sheet was installed with the fiber aligned with the shorter edge in order to be conservative. The fibers were laid down on the concrete surface and then rolled to avoid the formation of air bubbles in between the FRP sheet and the substrate. The specimens were left to cure in laboratory at room temperature of 23 ± 1 °C and relative humidity of 60 ± 5 %.

Fig. 2.32 (left and right) shows respectively the operation of application and rolling of the FRP sheet.

- After the installation of the FRP sheets, the specimens were left to cure in the laboratory at room temperature of 23 ± 1 °C and relative humidity of 60 ± 5 % for some hours. Once the FRP systems were starting getting hard, the holes were opened up again cutting the sheets with a little blade. Then the holes and the upper surfaces of the specimens were cleaned again blowing up the dust with an air compressor. Fig. 2.33 shows the operation of cutting the fibers.
- At this point, a plastic tube was inserted into the hole in order to avoid bonding between the anchors and the concrete surface inside the hole. The tube was fixed with some mastic at the bottom of the specimen, as shown in Fig. 2.34, in order to avoid any slippage during the installation of the anchors.

Fig. 2. 32 – Installation (left) and rolling (right) of the FRP sheet

Fig. 2. 33- Operation of cutting the FRP sheets

Fig. 2. 34 - Installation of the plastic tubes inside the holes (bottom view)

- Once the mastic got hard, the anchors were installed. As in the first test, each anchor was cut for a total length equal to 857.5 mm (35 in.); this length was computed based on the dimensions of the hydraulic jack, the load cell and the plates needed for performing this test. The diameter of the anchors was, even in this case, 3/4 inch. First of all, the anchors were disposed on a table that was accurately covered with a plastic sheet. The fibers were impregnated for all their entire length paying attention to not leave any fibers dry. Once the anchors were perfectly impregnated, they were squeezed in order to take all the excessive epoxy resin off. They were also handled to give to their cross section a round shape, paying attention to keep all fibers straight and parallel each other. Fig. 2.35 shows the operation of impregnation of the fibers.
- Once the anchors were impregnated, they were installed. The procedure was the following:

  First of all, they were pushed inside the hole from the bottom of the specimen through the entire depth. Fig. 2.36 shows the anchor inside the plastic tube at the bottom of the specimen.

  Once they got out from the upper surface they were pulled out for 3 inches.

  At this point, the fibers were fanned out homogenously in order to get a complete fan of 360° with a diameter equal to 6 inches. Then, a layer of thickened epoxy was applied over the fan. Fig. 2.37 shows the fan before and after the application of the layer of thickened epoxy.

Fig. 2. 35 – Impregnation of the fibers

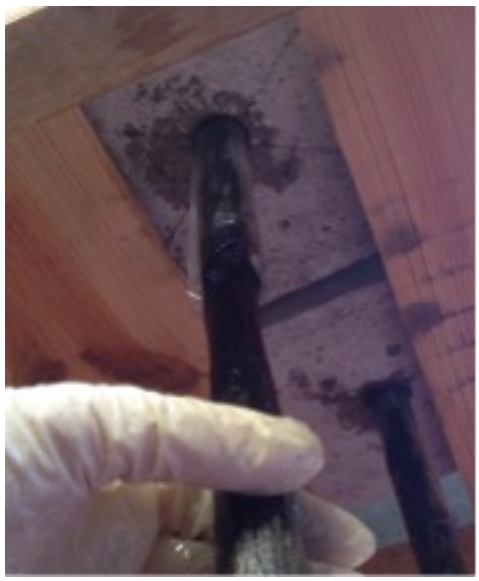

Fig. 2. 36 - Insertion of the anchor inside the tube

Fig. 2. 37 - Specimen before (left) and after (right) the application of the layer of thickened epoxy

Finally, the grips were installed in the anchors. The impregnated fibers were inserted into a steel cylinder having a diameter equal to 25.4 mm (1 in.) and beforehand filled with epoxy resin for 1/3 of its length. Fig. 2.38 illustrates the cross section of the final specimen. Once the installation was completed, the specimens were left to cure for 48 hours, as shown in Fig. 2.39.

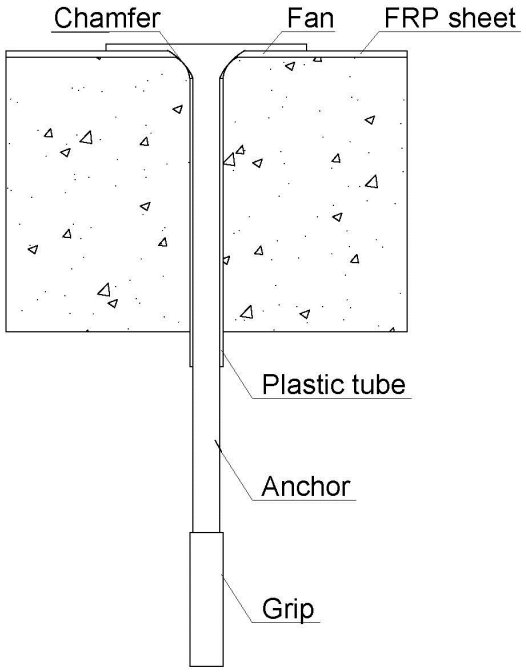

Fig. 2. 38 - Sketch of the cross section of the specimen

Fig. 2. 39 - Specimens during the curing period

The following table summarizes the specific dimensions of the specimens described before.

Table 2. 5 - TEST 2 - Summary Table

Specimen		Chamfer	Hole	Anchor	
Type	n°	Radius [mm]	Diameter [mm]	Dowel Diameter [mm]	Fan Radius [mm]
T2_0	5	0	25,4	19	76,2
T2_1/4	5	6,35	25,4	19	76,2
T2_1/2	5	12,7	25,4	19	76,2

2.3.5 TEST 3 – Specimen Preparation

In this test, 10 specimens were prepared. The dimensions of the concrete blocks were: 355.6 mm x 304.8 mm x 203.4 mm (16 in x 12 in x 8 in). The procedure adopted for the installation of the FRP system was the following:

- After grinding the surfaces of the specimens, two holes were drilled in each specimen, in particular one on each 304.8 mm x 203.4 mm surface, having a length equal to 101.6 mm (4 in). A 25,4 mm (1 in) reinforced concrete drill bit was used in this operation in order to obtain a hole diameter 6.35 mm (1/4 in) greater than the anchor diameter. The dust was blown up from the hole, and then the inner surface of the hole was brushed and blown up again. The following sketch (Fig. 2.40) illustrates the position of the hole, which was decided based on the optimal length of the externally bonded FRP sheet that was installed in a second moment (CNR-DT200).

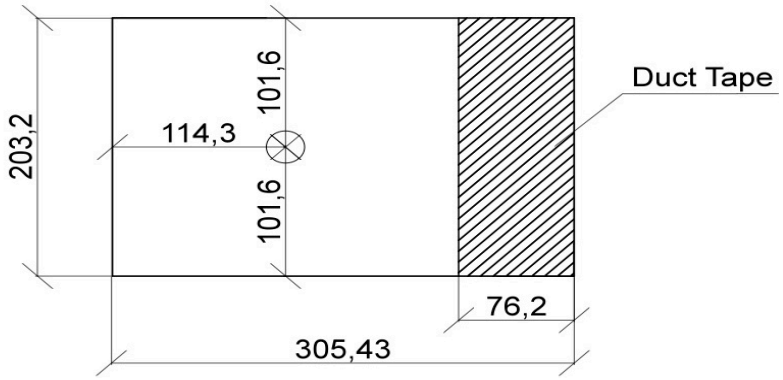

Fig. 2. 40 - Sketch of the specimen

- Based on the result of Test 2, a chamfer radius equal to 6,35 mm was created at each hole.
- As shown in the sketch above, 76.2 mm (3 in.) of duct tape were use to avoid bonding between the FRP sheet and the concrete surface. The external edge under the tape was rounded with a grinder before the application of it, in order to avoid the problem of spalling and a sudden load reduction on the FRP sheet during testing (Brena and McGuirk, 2013)

- Once the surface and the hole were prepared, an FRP sheet was cut for each specimen. The sheet had a length equal to 2540 (100 in.) and a width equal to 152.4 mm (6 in.). The length was computed based on the dimensions of the hydraulic jack, of the load cell and of the plates used to perform the test. The FRP had the following properties:

  Average thickness: 1.016 mm
  Average ultimate strain: 1.8 %
  Average ultimate strength: 74.9 MPa

  The procedure of installation was the following:

  Specimen substrate cleaning
  In order to allow a good bonding between the FRP system and the surface of application, the substrate surface had to be cleaned. An air compressor and a brush were used to remove all the particle of sand resulting from the sandblasting.

  Primer application
  A two parts thickened epoxy, also called putty, was prepared during this operation. First of all, the epoxy resin (part A) and the curing agent (part B) was added into a bucket, previously calibrated using a mixing ratio of 100:33 by weight. The two parts were mixed for 3 minutes until a smooth and uniform consistency was obtained. Then, fume silica was added into the bucket in order to make the epoxy thicker, using a mixing ratio by volume of one of two parts epoxy resin to 0.75 of fume silica. Depending on the mixing paddle, it took several minutes to mix the putty. Once a uniform consistency was obtained, the thickened epoxy was applied using a spatula, in order to fill all the concrete cavities and pores. Finally, a two parts epoxy resin was prepared again following the same procedure of before and a thin layer of it was applied using a paintbrush over the putty. Fig. 2.41 shows one of the two prepared surfaces of each specimen after the installation of the tape and the application of the primer. As we can see from the picture below, the exact

position of the FRP sheet was beforehand marked with a marker, in order to be precise during the installation.

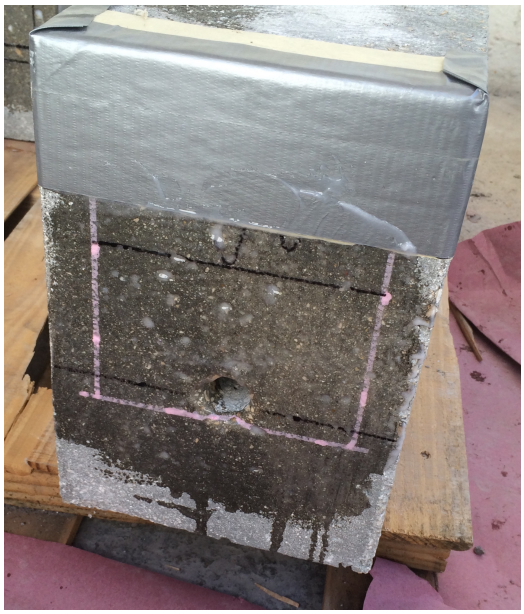

Fig. 2. 41- Prepared surface

FRP impregnation and application

First of all, a two parts epoxy resin was prepared. The epoxy resin (part A) and the curing agent (part B) was added into a bucket, previously calibrated using a mixing ratio of 100:33 by weight. The two parts were mixed for 3 minutes until a smooth and uniform consistency was obtained. The FRP sheet was disposed over a previously cover clean table and 203.2 mm (8 in.) of fibers were impregnated at each ends, while the remaining part was kept dry. The resin was gently poured on the dry fibers for their impregnation, and then a spatula was used to spread the epoxy out homogenously on the sheet. Finally, the fibers were rolled in order to obtained a uniform impregnation. The procedure was followed in both the two ends of the FRP sheets.

The lamina was applied to the concrete substrate within 45 minutes from the primer application and the fiber impregnation. The fibers were laid down on the concrete surface and then rolled again to avoid the formation of air bubbles in between the FRP sheet and the substrate. Some tape was applied over the sheet in the unbounded part in order to keep it straight and avoid any movement during the curing period.

Fig. 2.42 shows respectively the operation of rolling the FRP sheet (left) and one side of the specimen after the installation of the FRP sheet (right).

Fig. 2. 42- Impregnation of the FRP sheet (left) and specimen after the installation of the FRP sheet (right)

- After the installation of the FRP sheets, the specimens were left to cure in the laboratory at room temperature of 23 ± 1 °C and relative humidity of 60 ± 5 % for some hours.

Note: It is important to underline that the length of the bonded FRP sheet was computed based on the expression of the *Optimal Bond Length,* that is the minimum bonded length that ensures the transmission of the bonding forces (CNR-DT200). In order to compare the experimental results with those obtained from the computation of the analytical expressions given by CNR-DT200, a bonded length greater that the optimal one was taken.
The computation of the optimal bond length is presented in chapter 5.

Once the FRP laminas were installed, four different types of specimen were defined based on the characteristic of the anchors.

1. Series 1: T3_0

The first series of specimens was the benchmark, in which no anchors were installed.

2. Series 2: T3_60

An anchor was installed on each side of the specimens. The opening angle of the anchor fan was 60 degrees and the length of the bonded FRP sheet was the same as in the benchmark, in order to compare the results and compute the enhance. The procedure of installation is described below.

Once the FRP system was starting getting hard, the holes were opened up again cutting the sheets with a little blade. Then the holes and the upper surfaces of the specimen were cleaned again blowing up the dust with an air compressor.

At this point, the anchors were prepared for the installation. They had a total length equal to 7 inches; 4 inches of dowel and 3 inches of free fibers (fan radius). Fig. 3.44 shows the anchor before and after the impregnation. As we can see from the pictures, the dowel was wrapped with some rubber bends in order to keep the fibers straight during the application.

The FRP sheet was marked in order to know the precise position of the anchor fan during the installation. The opening angle of the fan was 60°. Fig. 2.43 shows one side of the specimen before the installation of the anchor.

Fig. 2. 43- Side of the specimen

Then, two parts epoxy resin was prepared. The epoxy resin (part A) and the curing agent (part B) was added into a bucket, previously calibrated using a mixing ratio of

100:33 by weight. The two parts were mixed for 3 minutes until a smooth and uniform consistency was obtained. The final compound was poured into a trough of sufficient size to fully contain an FRP anchor. Working with the epoxy into the FRP anchor, it was ensured all the rovings in the anchor were saturated. An important aspect of the impregnation is that it is better to avoid saturating too long because then working with the anchor would get harder. Another trick is to weight the anchor before and after the impregnation; the anchor needs to be about the double in weight after the saturation. Fig. 2.44 illustrates the anchor before (left) and after (right) the impregnation of the fibers.

Fig. 2. 44- Anchor before (left) and after (right) the impregnation of the fibers

In the meantime, the holes of the specimens were primed with epoxy and then filled with thickened epoxy for 1/3 of their length. The thickened epoxy was obtained mixing two parts epoxy resin with flumed silica with ratio 1:1 by volume.

Once the holes were prepared, the anchors were installed. A steel rod having a width equal to ¾ inch was used to push the anchors inside the holes. In this way, the fibers were kept straight inside the hole. Once the dowel was inside the hole, the free fibers were fanned out on the FRP sheet up to 60°. The following sketch (Fig. 2.45) illustrates the final result of the procedure. It is important to underline that the same procedure of installation was repeated for all the specimens. The quality of the

installation is fundamental for externally bonded FRP systems and it can dangerously affect the strength of the system

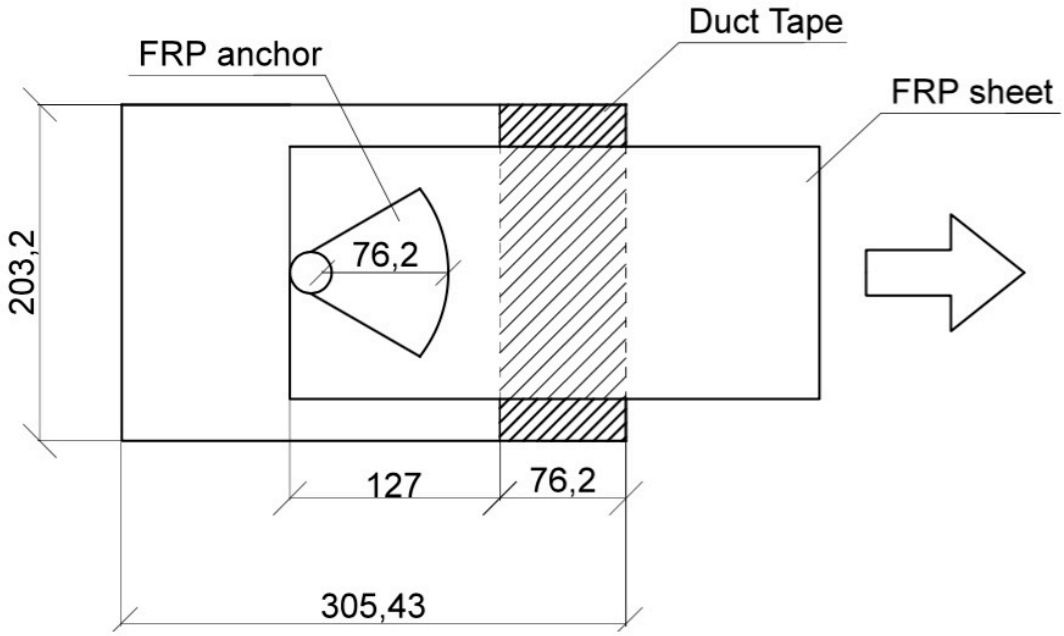

Fig. 2. 45 - Sketch of the final result of the procedure

Finally a layer of thickened epoxy was applied on the system. The thickened epoxy was obtained mixing two parts epoxy resin with flumed silica with ratio 1:1 by volume. Fig. 2.46 shows one side of the specimen after the application of the thickened epoxy

Fig. 2. 46 - Specimen after the application of the thickened epoxy

3. *Series 3:* ***T3_90***

An anchor was installed in each side of the specimen. In this case, the opening angle of the fan was 90 degrees. The procedure of installation was the same of the previous case, except for the opening angle. Fig. 2.47 illustrates the specimen before (left) and after (right) the installation of the anchor. As we can see from the picture, the opening angle of the fan was bigger than in the previous case.

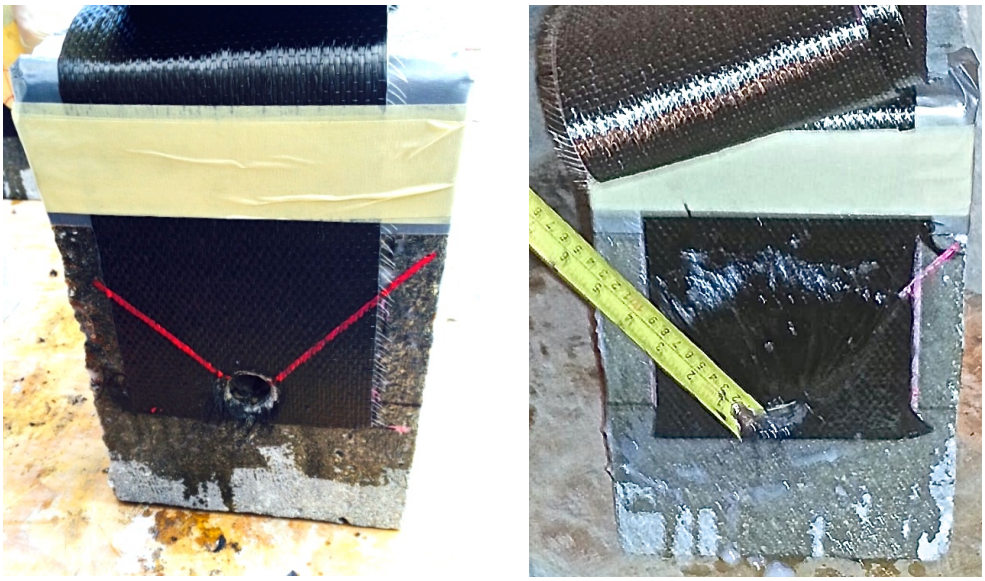

Fig. 2. 47 - Specimen before (left) and after (right) the installation of the anchor

4. *Series 4:* ***T3_60s***

The last series was composed by a sandwich type specimen. First of all, an anchor was installed on each side of the specimen, following the procedure of the previous case. The free fibers were fanned out on the FRP sheet up to 60 degrees. A layer of thickened epoxy was applied over the fan in order to prepare the surface filling out all the groves and irregularities. Secondly, two FRP sheets were cut and saturated following the standard procedure. The dimensions of them were 203.2 mm x 152.4 mm (8 in x 6 in) and they were installed in order to cover the anchors and all the bonded part of the previously installed FRP sheet. The fibers were rolled to avoid the formation of air bubbles in between the two layer of FRP sheet. Fig. 2.48 shows the specimen at the end of the procedure.

Fig.2. 48 – T3_60s: Sandwich type specimen

The following table summarizes the characteristics of the specimens described before while Fig. 2.49 shows the specimen at the end of the preparation.

Table 2. 6 - TEST 3 - Summary Table

Specimen		**Anchor**				**Chamfer**	**Hole**	
Type	n°	Fan Opening Angle [Deg]	Fan Radius [mm]	Dowel Diameter [mm]	Dowel Length [mm]	Radius [mm]	Diameter [mm]	Length [mm]
T3_0	3	-	-	-	-	-	-	-
T3_60	3	60°	76,2	19	101,6	6,35	25,4	101,6
T3_90	3	90°	76,2	19	101,6	6,35	25,4	101,6
T3_60s	1	60° + cover	76,2	19	101,6	6,35	25,4	101,6

Fig. 2. 49- Specimen Test 3

A fully description of the instrumentation used during test 3 is provided in paragraph 2.4.3. A set of strain gauges were installed in one side of each specimen in order to measured the strain in the FRP sheet. In order to make the specimens fail in the side provided with the instrumentation, the other side was reinforced with another FRP sheet, as shown in figure 2.50 a 2.51.

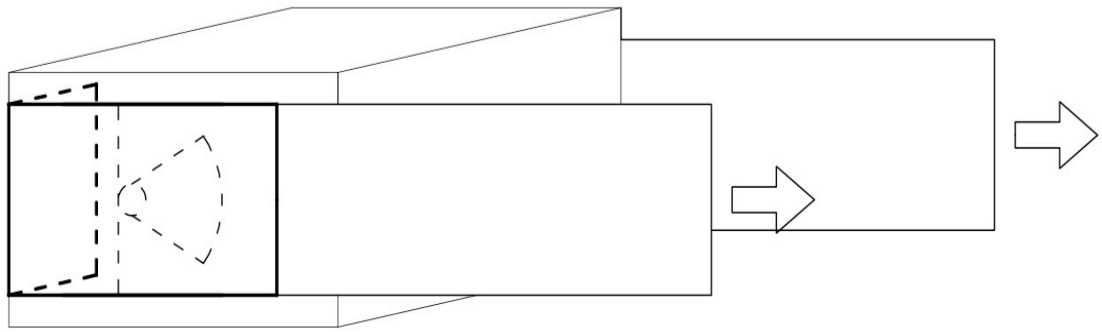

Fig. 2. 50 - Reinforced side of the specimen

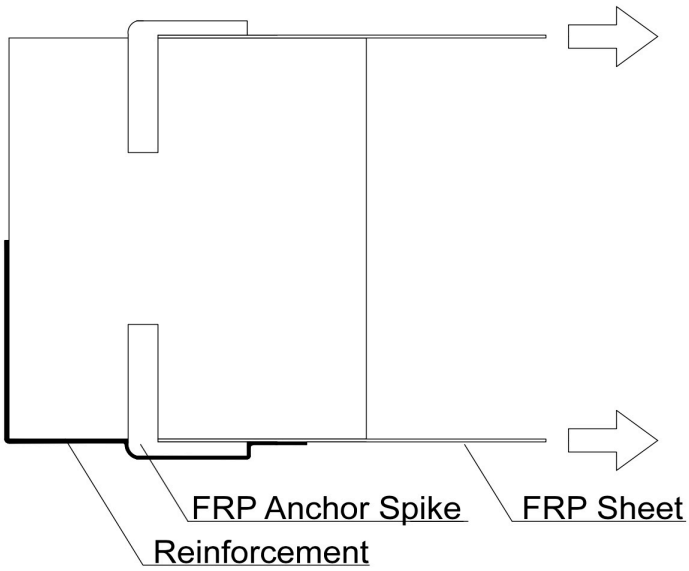

Fig. 2. 51 - Section of the specimen

2.3.6 Final Tests Matrix

The following table summarizes the entire experimental program.

As written before, it is composed by three different tests in which some parameters are analyzed in order to fully understand the behavior of the FRP anchor spikes.

Table 2. 7 – Final Test Matrix

Test	Specimen		Anchor				Hole		Chamfer
	Type	n°	Dowel Diameter [mm]	Dowel Length [mm]	Fan Opening Angle [mm]	Fan Radius [mm]	Depth [mm]	Diameter [mm]	Radius [mm]
Test 1	T1	5	19	101,6	-	-	101,6	25,4	-
Test 2	T2_0	5	19	-	360°	76,2	-	25,4	0
	T2_1/4	5	19	-	360°	76,2	-	25,4	6,35
	T2_1/2	5	19	-	360°	76,2	-	25,4	12,7
Test 3	T3_0	3	-	-	-	-	-	-	-
	T3_60	3	19	101,6	60°	76,2	101,6	25,4	6,35
	T3_90	3	19	101,6	90°	76,2	101,6	25,4	6,35
	T3_60S	1	19	101,6	60° + cover	76,2	101,6	25,4	6,35

2.4 Test Set-up and Procedure

While the previous sections fully describes the preparation of the specimens, from the casting of the concrete to the installation of the FRP laminas and anchors, the purpose of this paragraph is to describe the set-up and the instrumentation used during the tests.

2.4.1 Test 1 – Set-up

The Test 1 was a pullout test on the anchors performed by using a double action 222KN hollow-core hydraulic jack. The anchors had an embedded length equal to 4 inches and they were installed following the procedure described before. Because loading was applied using a hand controlled hydraulic pump, the loading rate was not constant and varied between 200-400 N/s. Within this loading rate range, rate effects on the behavior of the specimens were believed to be negligible. Applied load was measure by a 111 KN (25 Kips) load cell, carefully aligned with the anchor and disposed between two plates. A potentiometer (Fig. 3.52) was installed in each specimen in order to measure the slippage of the anchor inside the hole. It was installed next to the specimen and it was fixed to the anchor with two plastic bands, as shown in Fig. 3.53. Both the load and the displacement data were acquired and recorded every 0.1 seconds during the loading. The hydraulic jack, the load cell and the plates were disposed over a steel support in order to not constrain the concrete surface around the anchor during the test. In this way, it was also possible to install the potentiometer without having problem of room. Finally an element of contrast was inserted between the last plate and the grip. The load was applied continuously at a slow rate until failure of the specimens to avoid effect of stress redistribution on the measurements once the FRP debonding initiated.

The test procedure was the following:

1. Each specimen was place on a plane floor
2. The steel support was disposed over the specimen
3. The hollow-core hydraulic jack was place over the specimen.

4. The plates, the load cell and the element of contrast were place over the specimen, paying attention to align them with the anchor.
5. The instrumentation (potentiometer and load cell) were connected to the data acquisition system and calibrated.
6. The data acquisition system was started prior the loading to ensure data was being recorded before loading began.
7. Each specimen was pre-loaded to a load of 1-2 KN.
8. The load was increased by load control at a rate of 0.2-0.4 N/s.
9. The load was applied until failure and the test was stopped when the load dropped after reaching the peak.

Fig. 2.54 illustrates the cross section of the final set-up while Fig 2.55 shows the specimen during the test.

Fig. 2. 52 - Potentiometer

Fig. 2. 53 - Installation of the potentiometer

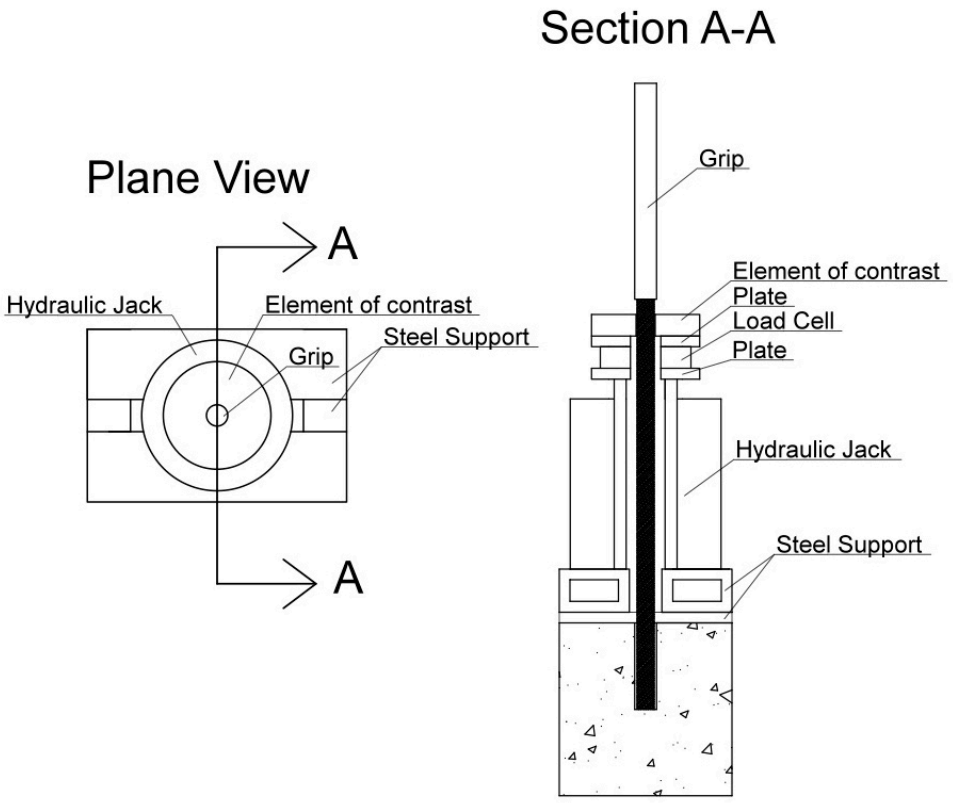

Fig. 2. 54 - Cross section of the final set-up

Fig. 2. 55 – Final set-up (Test 1)

2.4.2 Test 2 – Set-up

The Test 2 is another pullout test on the anchors performed by using a double action 222KN hollow-core hydraulic jack. As explained in the previous sections, the anchor was bonded to the concrete just under the fan. The anchor dowel passed trough the specimen inside a plastic tube, so that the only one bonded part was the fan. The procedure of installation that was followed is described in the previous chapter. Because loading was applied using a hand controlled hydraulic pump, the loading rate was not constant and varied between 200-400 N/s. Within this loading rate range, rate effects on the behavior of the specimens were believed to be negligible. Applied load was measure by a 111 KN (25 Kips) load cell, carefully aligned with the anchor and disposed between two plates. In order to measure the slippage of the fan two LVTD were use in each specimen (Fig. 2.56). Two little squares were glued to the fan, paying attention to keep them parallel to the fibers of the fan, as shown in Fig. 2.57. These squares were used in order to give to the LVTDs two supports to measure the slippage of the fibers of the fan. Both the load and the displacement data were acquired and recorded every 0.1 seconds during the loading. The set-up was the same in all the three types of specimens and it is show in Fig. 2.58.
Fig. 2.59 illustrates the final set-up.

The test procedure was the following:

1. Each specimen was place over 4 bricks in order to have room to use the LVTDs.
2. The hollow-core hydraulic jack was place over the specimen.
3. The plates, the load cell and the element of contrast were place over the specimen, paying attention to align them with the anchor.
4. The LVDTs were clamped to a support and disposed on the floor, pointing the two squares.
5. The instrumentation (LVTDs and load cell) were connected to the data acquisition system and calibrated.
6. The data acquisition system was started prior the loading to ensure data was being recorded before loading began.
7. Each specimen was pre-loaded to a load of 1-2 KN.

8. The load was increased by load control at a rate of 0.2-0.4 N/s.
9. The load was applied until failure and the test was stopped when the load dropped after reaching the peak.

Fig.2. 56 - LVDT

Fig. 2. 57 - Installation of the two squares

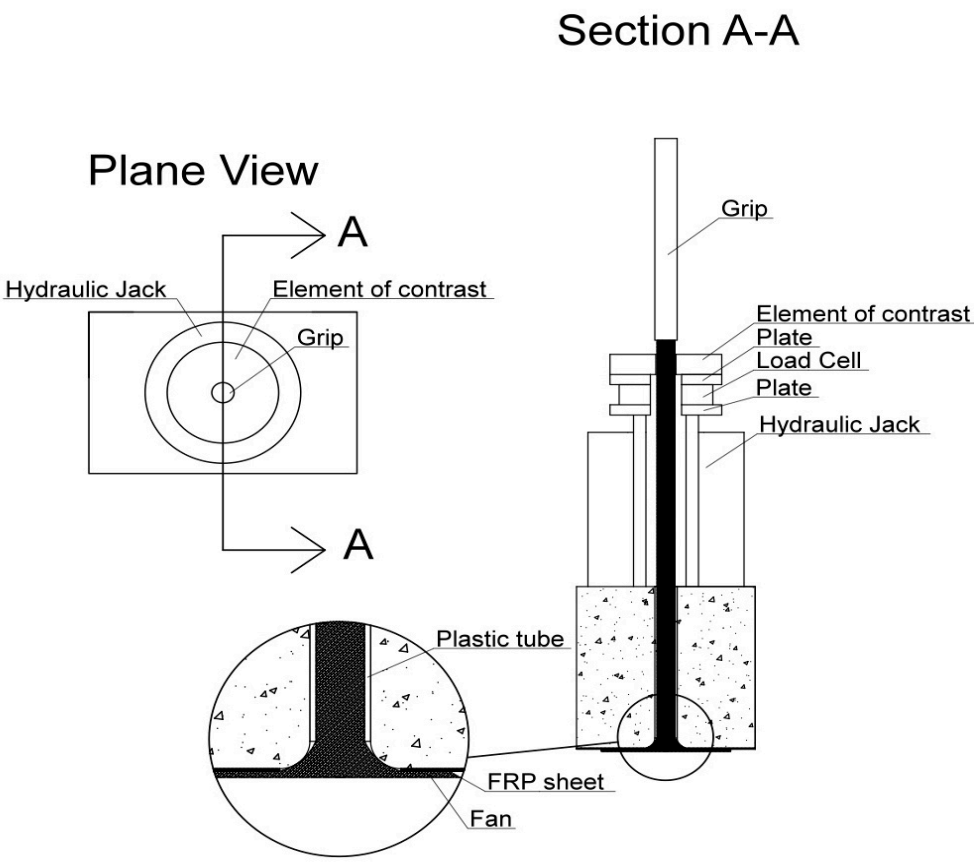

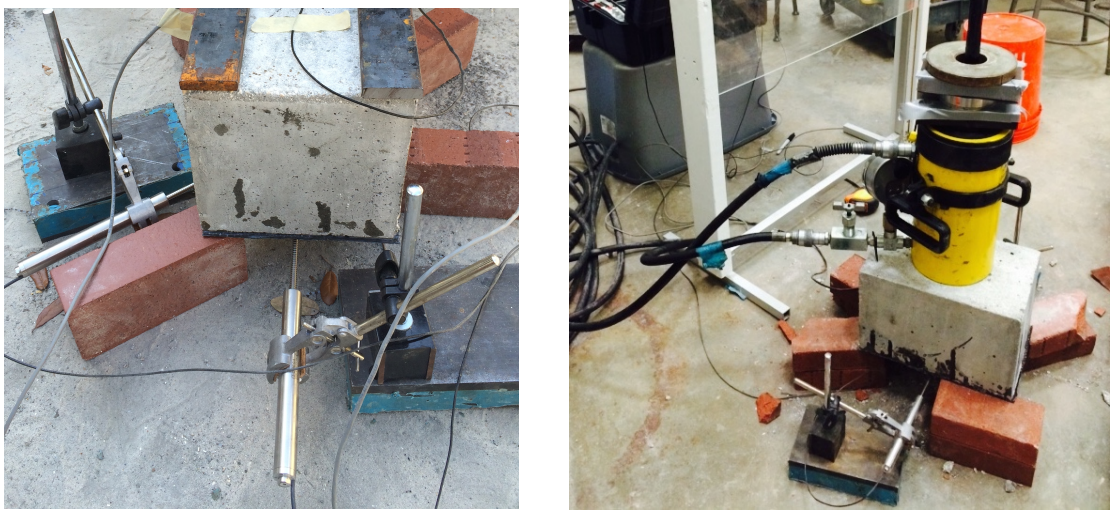

Fig. 2. 59 - Final set-up Test 2

2.4.3 Test 3 – Set-Up

The Test 3 was a direct double shear test on the specimens described in the previous sections. Four types of specimen were tested, depending on the configuration of the anchor fan, but the set-up was the same for all of them. The test was performed by using a double action 222 KN hollow-core hydraulic jack. Because loading was applied using a hand controlled hydraulic pump, the loading rate was not constant and varied between 200-400 N/s. Within this loading rate range, rate effects on the behavior of the specimens were believed to be negligible. A steel support was specifically designed for the test, as described in Appendix B. Applied load was measure by a 111 KN (25 Kips) load cell, carefully disposed between two plates.

The set-up procedure was the following:

1. Each specimen was place over some cylindrical rollers to allow it to move backyard during the test.

Fig. 2. 58 - Cross section of the final set-up

2. Some bricks were used to raise the specimen up and maintain the FRP sheet straight during the test.
3. The steel support was disposed in front of the specimen. The external surface of the cylinder was cover with a plastic sheet in order to minimize the friction.
4. The hollow-core hydraulic jack was place in between the concrete block and the steel support.
5. The plates and the load cell were disposed between the hydraulic jack and the concrete block, paying attention to their alignment. They were put over some bricks to make it easier.
6. A steel plate, having thickness equal to 50.8 mm and a surface equal 203.2 mm x 304.8 mm, was used in order to let the load diffuse all over the surface of the concrete block, avoiding stress concentration.
7. A thin wood plate, having thickness equal to 6.35 mm, was used to compensate the problem related to the irregularity of the concrete surface.

Fig. 2.60 and Fig. 2.61 represent two sketches of the system, while Fig. 2.62 and 2.63 show the specimen after the first part of the set-up.

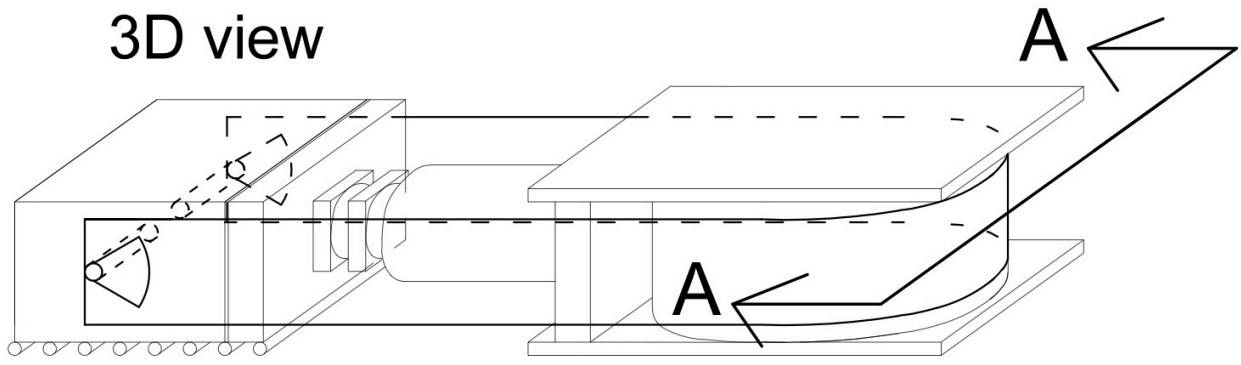

Fig. 2. 60 - 3D view of the system

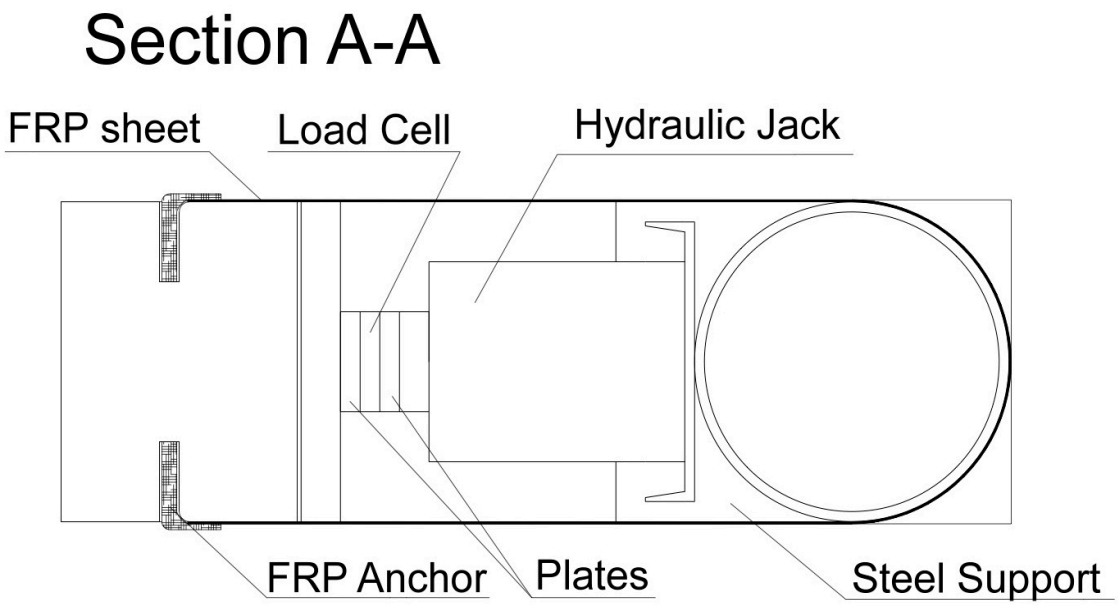

Fig. 2. 61- Section A-A

Fig. 2. 62 - Front view of the initial set-up

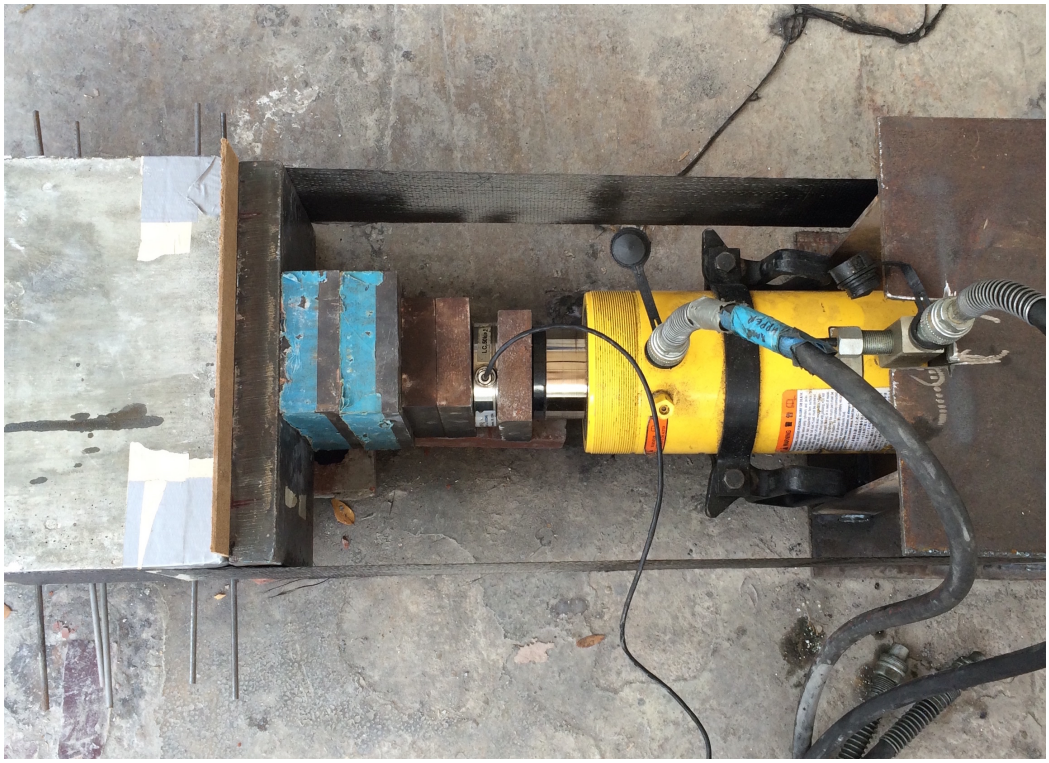

Fig. 2. 63 - Plane view of the initial set-up

The specimens were instrumented using 6 mm electrical strain gauges (Fig. 2.64) array placed on the surface of the FRP sheets. They were used to investigate the transversal strain distribution in the FRP sheet and the variation in the strain field as a consequence of the FRP anchor placement. The strain gauges were selected for their compatibility with the composite material and they were attached using specified adhesive. Most of them were place along the centerline of the FRP sheets while some others were disposed next or behind the anchor. The position varied depending on the type of specimen and the repetition.

Fig. 2. 64 - Electrical Strain Gauges

Both the load and the displacement data were acquired and recorded every 0.1 seconds during the loading. The following sketches represent the strain gauges layouts on the different types of specimen. SG means “Strain Gauges” and, as we can see from the drawings below, most of them are placed along the centerline of the specimen (SG1, SG2, SG3, SG6).
A complete list with the strain gauges positions is presented below, followed by some sketches that illustrate the final layouts of each specimen:

- SG1 was placed on the unbounded part of the FRP sheet, next to the boundary between the bonded and unbounded part. It was installed in all the types of specimens, as illustrated in the drawing above.
- SG2 was placed on the bonded part of the FRP sheet, in front of the anchor. In order to compare the results, SG2 was placed in the same position even in the benchmark type specimen, in which no anchors were installed. The exact position of these strain gauges may be seen in the sketches below.
- SG3 was placed over the anchor, 55 mm from the center of the hole. This distance represents 2/3 of the fan radius. This strain gauge was installed just on the 60° and 90° configuration types.
- SG4 was placed between the hole and the lateral edge and it was installed just on the 60° and 90° configuration types. The exact position may be seen below in Fig 2.66.
- SG5 was placed between the end of the most external fiber of the fan and the lateral edge of the FRP sheet. It was installed on the 60° and 90° configuration types and on the sandwich type. The exact position of the strain gauges may be seen in the sketches below.
- SG6 was installed just on the benchmark and it was placed in the same position of the hole center.

After a briefly description of the different strain gauges used during the test, the following drawing illustrates their position on the specimens.

- ***Benchmark Strain Gauges layout***

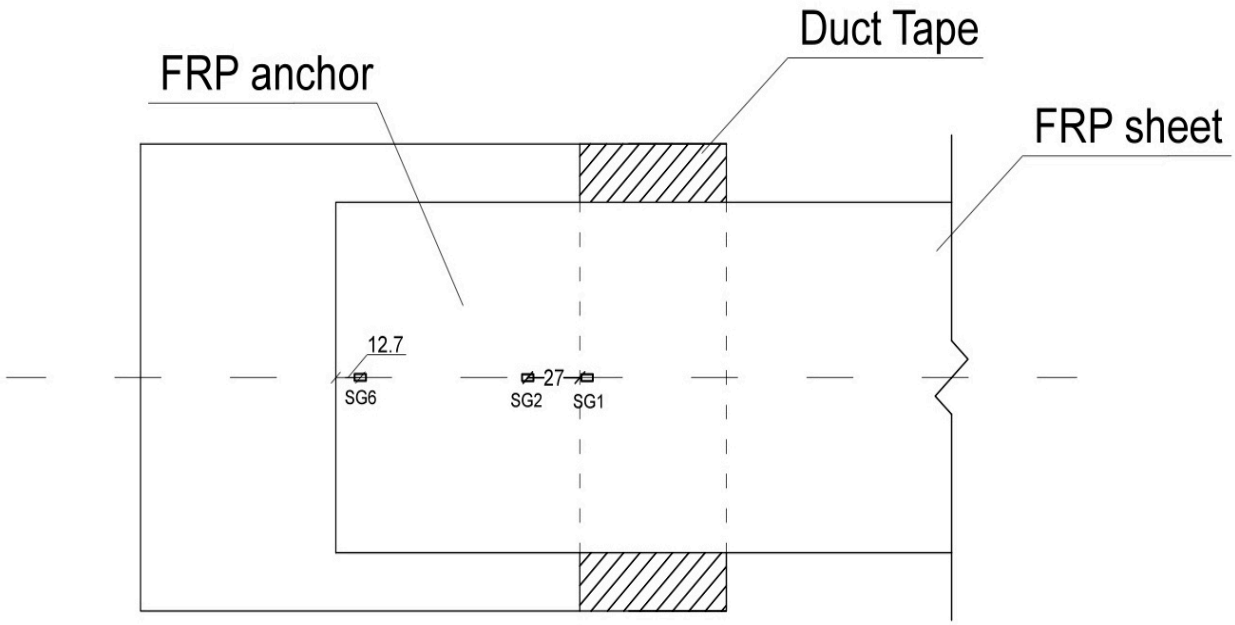

Fig. 2. 65 - Benchmark specimen

- ***60° and 90° Strain Gauges Layout***

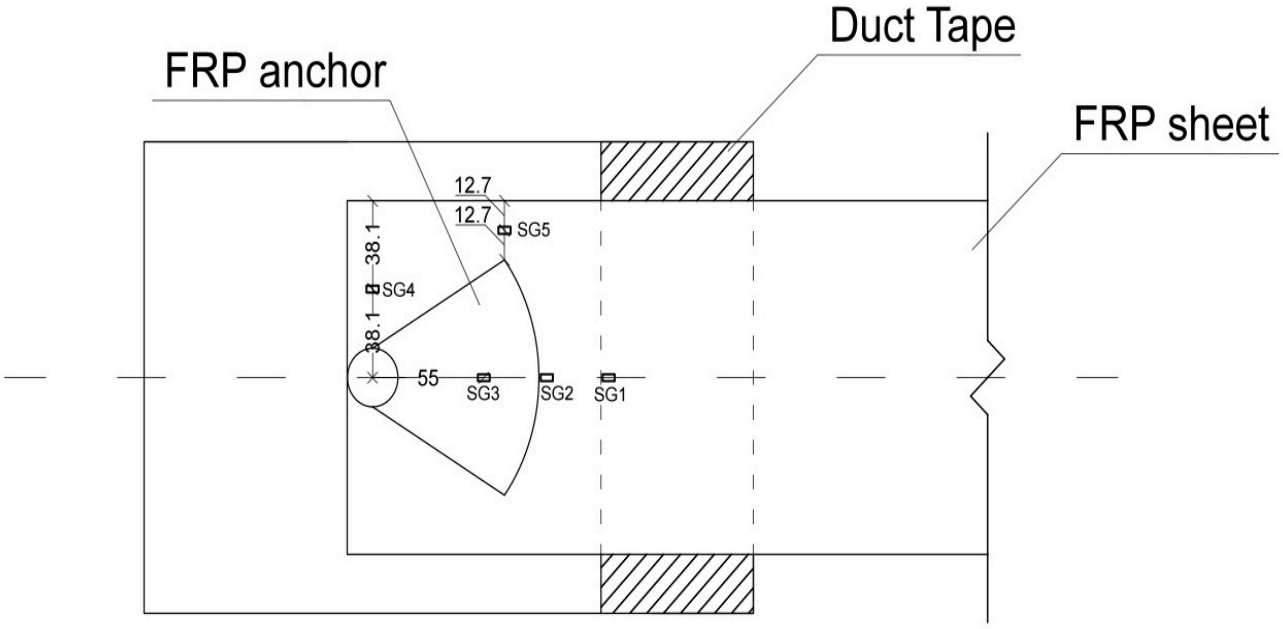

Fig. 2. 66 - 60° and 90° configuration specimen

- ***60°S (Sandwich) Strain Gauges Layout***

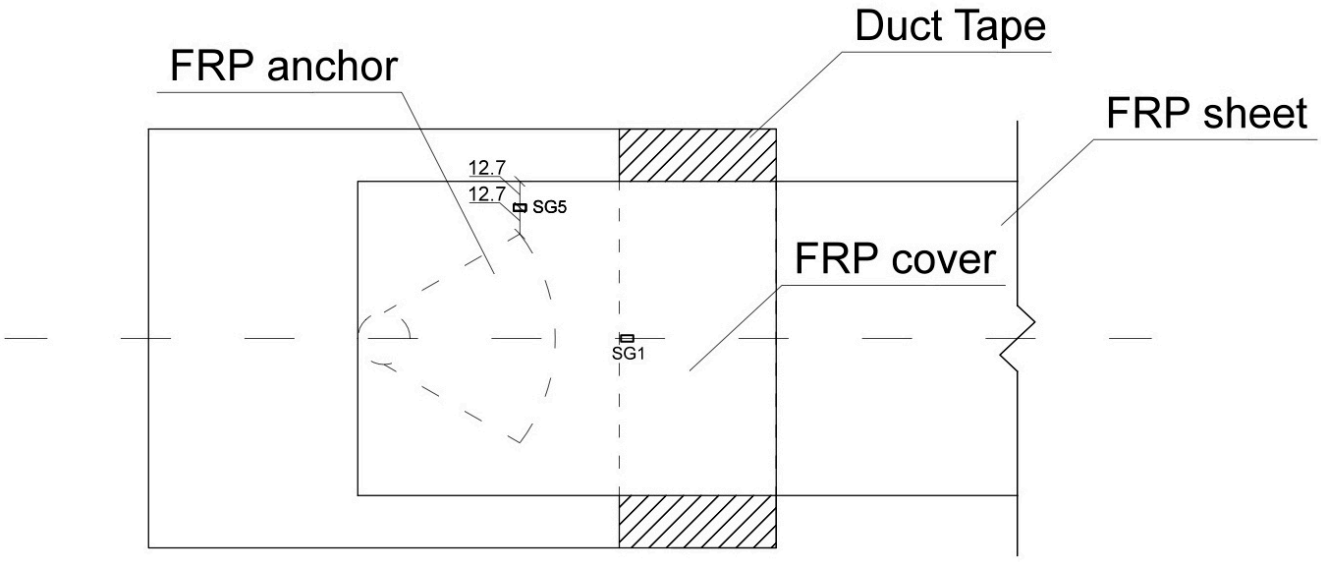

Fig. 2. 67 - 60°S configuration specimen

Not all the specimens were instrumented with strain gauges during the experimental program. For example, the first repetition of T3_0, T3_60 and T3_90 were tested without any strain gauges in order to measure just the peak load. The following table explains how many strain gauges were used in each specimen.

Table 2. 8 - Strain Gauges Position Table

Specimen ID	Fan Opening	Strain Gauges position					
	[Deg]	SG1	SG2	SG3	SG4	SG5	SG6
T3_0_001							
T3_0_002	0	x	x				x
T3_0_003		x	x				x
T3_60_001							
T3_60_002	60	x	x	x	x		
T3_60_003		x	x			x	
T3_90_001							
T3_90_002	90	x	x	x	x		
T3_90_003		x	x			x	
T3_60S_001	60s	x				x	

As shown in the table above, except for the first repetition, the benchmark type was always instrumented with the strain gauges SG1, SG2 and SG6.

The second repetition of T3_60 and T3_90 were provided with SG1, SG2, SG3 and SG4. Based on the result obtained from this repetition, it was decided to not install

SG3 and SG4 in the third repetition and to place another strain gauges next to the anchor in position 5 (SG5).

The sandwich type was provided with SG1 and SG5 but unfortunately the presence of the cover avoids the recording of the deformation of the FRP reinforcement.

Fig. 2.68 and Fig. 2.69 illustrate respectively the benchmark and the sandwich type after the installation of the strain gauges.

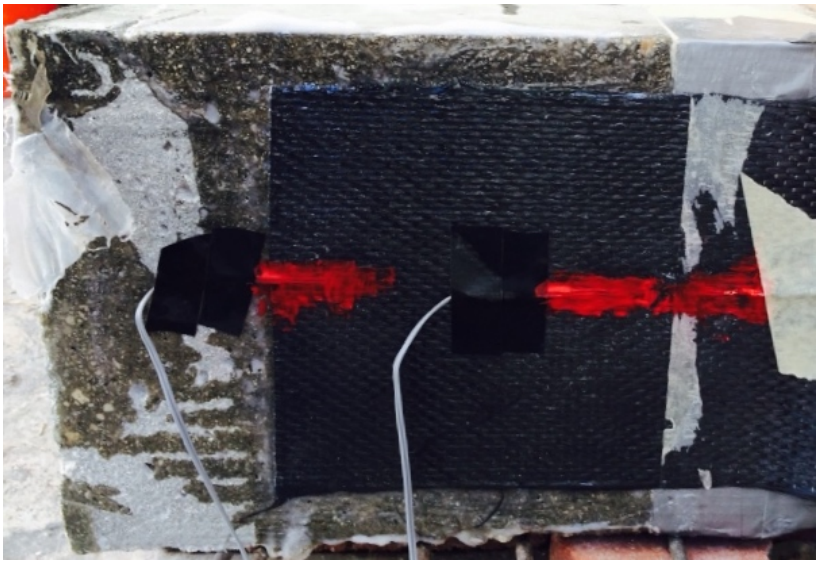

Fig. 2. 68 - Benchmark Specimen Type

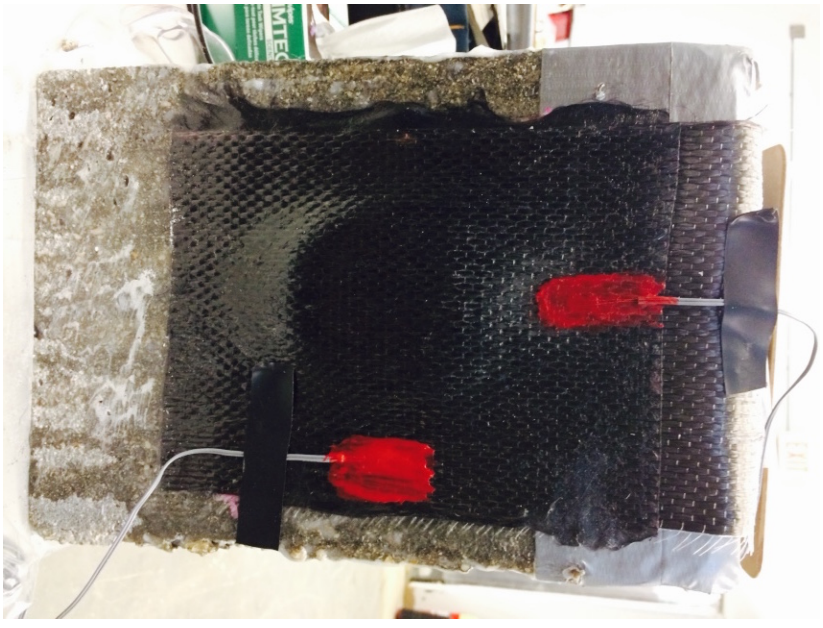

Fig. 2. 69 Sandwich Specimen Type

Once decided the position of the strain gauges in each specimen, the set-up procedure continued with the following steps:

8. The strain gauges were installed
9. The instrumentation (Strain Gauges and Load Cell) were connected to the data acquisition system and calibrated.
10. The data acquisition system was started prior the loading to ensure data was being recorded before loading began.
11. Each specimen was pre-loaded to a load of 1-2 KN.
12. The load was increased by load control at a rate of 0.2-0.4 KN/s.
13. The load was applied until failure and the test was stopped when the load dropped after reaching the peak.

Fig. 2.70, Fig. 2.71 and 2.72 show the final set-up of the Test 3.

Fig. 2. 70- Final set-up of Test 3

Fig. 2. 71- Performing of Test 3

Fig. 2. 72 - Setting up the hydraulic jack

3. EXPERIMENTAL RESULTS

First of all, a detailed description of the failure modes observed during the experimental campaign is given, followed by the results obtained during the tests.
The previous chapter covers all the aspects of the experimental campaign that was carried out, from the mold construction to the FRP installation. This chapter is divided into two main sections according with the main studies developed in this research.
The first section presents a fully description of the failure modes observed in each single test while the second one provides the analysis of the results.

3.1 Failure Modes

Different types of failure modes were observed in the three tests. Each test is analyzed in the following paragraphs in order to give a fully description of each single specimen.

3.1.1 Test 1 - Observed Failure Modes

In the case of Test 1, three different types of failure modes were observed during the pullout tests. In general, all the failures were sudden and the splitting of the concrete block was observed in most of the cases.

3.1.1..1 Failure mode A

In the case of failure mode 1, a combined failure mode was observed, composed by an anchor rupture 25 mm far from the bottom of the hole and a bond failure mode in the remaining portion. The rupture of the anchor was in correspondence of the plastic bend used to wrap the tip of the anchor during the installation. Some dry fibers were noticed in that section. The bond failure was at the adhesive-to-concrete interface. In addition, the global failure of the system was premature and the load obtained was lower than the average of the other repetitions. For these reasons, the test was not considered valid.
Fig. 3.1 is a representative picture of the failure mode 1 taken during the testing.

Fig. 3. 1 – Failure mode A

3.1.1..2 Failure mode B

The failure mode 2 was a combined failure mode in which was observed a concrete cone and bond failure. The cone failure mode was observed near the face of the concrete block with which the anchor was cast into while the bond failure in the remaining portion at the adhesive-to-concrete interface. The angle between the two sides of the cone and the upper surface of the block was 35°. The splitting of the concrete was observed during the failure.

Fig. 3.2 is a representative picture of the failure mode 2 taken during the testing.

Fig.3. 2 - Failure mode B

3.1.1..3 Failure mode C

A pure splitting of the concrete block was observed in the failure mode 3. In the following pictures, two different cases are shown; in the first one the anchor was still attached to one side of the splitted concrete block after the failure of the system while in the second case it completely came out from the hole. In general, the concrete splitting indicates that the tension stresses in concrete caused by the transfer of axial stresses from the anchor were higher than the splitting tensile strength of concrete. This means that the dimensions of the concrete test specimens are not sufficiently large. Fig. 3.3 are representative pictures of the failure mode 3 taken during the testing.

Fig. 3. 3 - Failure Mode C

The following table (Table 3.1) summarizes the failure modes observed in the specimens.

Table 3. 1 – Observed Failure Modes

Failure mode	Description
A	Combined failure: rupture of the anchor and bond failure.
B	Combined failure: concrete cone and bond failure followed by the plitting of the concrete specimen.
C	Splitting of the concrete specimen.

3.1.2 Test 2 – Observed Failure Modes

In the case of Test 2, two different types of failure modes were observed. In both the two cases the fan was still bonded to the FRP sheet after the failure of the system. The first failure mode was due to debonding and rupture of the FRP lamina installed under the fan while in the second failure mode the debondig was followed by the sudden rupture of the anchor dowel at the chamfer. Due to the fact that the anchors were installed by hand, the fans were not homogeneous in the disposition of the fibers. As a consequence, some parts of the sheets were still bonded to the concrete substrate at the end of the test while some others were completely debonded.

3.1.2..1 Failure Mode A

This type of failure was composed by an initial debonding of the FRP sheet at the adhesive to concrete substrate interface, followed by the final rupture of the lamina. The debonding occurred just in some parts of the sheet/fan system due to the fact that anchor was installed by hand and the distribution of fibers in the fan was not homogeneous. The anchor dowel was still attached to the fan after the failure of the system. Fig. 3.4 are representative pictures of the failure mode A.

Fig. 3. 4 - Failure Mode A

3.1.2..2 Failure Mode B

This type of failure was composed by an initial debonding of the FRP sheet at the adhesive to concrete substrate interface followed by the rupture of the FRP system. In this case, the global failure of the system was determined by the sudden tensile rupture of the anchor dowel at the chamfer. Even during this failure mode, the initial debonding occurred in just some part of the FRP sheet/fan due the non-homogeneity of the system.

Fig. 3.5 (left) shows the surface of the specimen, in which the debonding and rupture of the FRP sheet are observed while the figure on the right illustrates the anchor dowel after the failure.

Fig. 3. 5 - FRP System (left) and Anchor Dowel (right) after the failure (Failure mode B)

The following table (Table 3.2) summarizes the failure modes observed during Test 2.

Table 3. 2 – Observed Failure Modes

Failure mode	Description
A	Debonding and rupture of the FRP sheet.
B	Initial debonding of the FRP sheet followed by the tensile rupture of the anchor at initial chamfer radius.

Note Fan still bonded to the FRP sheet in all the failure modes

3.1.3 Test 3 - Observed Failure Modes

In general, all the unanchored specimens (benchmark) failed by debonding of the FRP sheet at the adhesive-to-concrete interface. Debonding initiated at the loaded end of the sheet and propagated to the unloaded end. This is the typical failure mode of an unanchored external bonded FRP reinforcement. The anchored specimens essentially behaved in a similar manner to the benchmark. Debonding initiates at approximately the same load in both the unanchored and anchored specimens. In last case, after the propagation of the debonding cracks toward the fan region, the enhanced strength of the anchored system was achieved due to the remaining length of the bonded FRP sheet and the restraint provided by the FRP anchor (Zhang and Smith). When the sheet completely debonded the FRP anchor was still found to be largely intact in each specimens. In general, the test was stop after the sudden drop of the load.

In the case of the sandwich-type specimen, it was not possible to observe the steps of the failure due to the presence of the cover over the FRP system.

Four types of failure modes were observed during the test and a fully description is provided below. They were mainly due to the reinforcement debonding from the substrate with a very thin concrete layer attached to the FRP sheet.

3.1.3..1 Failure Mode A

The failure mode A was observed in the benchmark due to the absence of the FRP anchors. It was composed by an initial debonding of the FRP sheet from the concrete

substrate, followed by its rupture. Debonding initiated at the loaded end of the sheet and propagated to the unloaded one. As illustrated in the pictures below (Fig. 3.6), the failure was in the adhesive-to-concrete interface. The layer of primer was completely removed from the substrate and a very thin concrete layer was attached to the FRP sheet. Fig. 3.6 are representative pictures of the failure mode A.

Fig. 3. 6 – Failure Mode A

3.1.3..2 Failure Mode B

The failure mode B was observed in the anchored specimens. It was composed by an initial debonding of the FRP sheet from the concrete substrate, followed by its rupture. The rupture of the fibers took place around the fan that appeared still bonded to the FRP sheet after the failure, as shown in Fig. 4.7. Even in this case, debonding initiates at approximately the same load as in the unanchored specimens. After the propagation of the debonding cracks toward the fan region, the enhanced strength of the anchored system was achieved due to the remaining length of the bonded FRP sheet and the restraint provided by the FRP anchor. The initial debonding was in the adhesive-to-concrete interface and the layer of primer was completely removed from the concrete surface at the end of the test. Fig. 3.7 are representative pictures of the failure mode A.

Fig. 3. 7 - Failure Mode B

3.1.3..3 Failure mode C

The failure mode C was observed in the anchored specimens. Even in this case, the initial debonding was in the adhesive-to-concrete interface and the primer was completely removed from the concrete surface. A very thin concrete layer was attached to the FRP sheet at the end of the test.

The final failure of the system was due to the slippage of the FRP sheet under the anchor. In this case, delamination between the fan and the FRP sheet was observed. Fig. 3.8 shows the specimen (left) and the FRP sheet (right) after the failure of the system.

Fig. 3. 8 - Specimen (left) and FRP sheet (right) after the failure of the system (Failure Mode C)

3.1.3..4 Failure Mode D

The failure mode D was observed in the anchored specimens. In this case, the failure was due to rupture of the concrete substrate, as shown in the following pictures (Fig. 4.9). The system was considered failed when the load drop suddenly to a load lower than the 40% of the peak load. Fig. 3.9 are representative pictures of the failure mode D.

Fig. 3. 9 – Observed Failure Mode D

The following table (Table 3.3) summarizes the failure modes observed in the specimens.

Table 3. 3 - Observed failure modes

Failure mode	Description
A	Adhesive-to-concrete interface debonding followed by rupture of the FRP sheet (unanchored system)
B	Adhesive-to-concrete interface debonding followed by rupture of the FRP sheet around the anchor
C	Adhesive-to-concrete interface debonding followed by slippage of the FRP sheet under the anchor
D	Failure at the concrete substrate

3.2 Tests Results

The following paragraphs provide the experimental results obtained in each test. The next chapter gives a comparison with the analytical models present in literature while chapter 5 provides comments and guidelines about the use of FRP anchor spikes.

3.2.1 Test 1 – Results

As described before, Test 1 was a pullout test on the anchors. The anchors were embedded into the concrete blocks for a total length equal to 101 mm. The following table (Table 3.4) shows the results in terms of applied peak load, slippage of the anchor dowel inside the hole and failure mode.

Table 3. 4 - Summary of the first series

Specimen ID	Embedded length	Peak load	Slippage at Peak	Failure mode	Comments
	[mm]	[kN]	[mm]		
T1_001	101,6	24,0	0,143	A	Premature failure
T1_002	101,6	33,5	0,150	B	
T1_003	101,6	39,6	0,160	C	
T1_004	101,6	34,7	0,142	C	
T1_005	101,6	35,9	0,073	C	
Average		33,5	0,134		
Standard deviation		5,8	0,035		
C.O.V (%)		17,3	26,1		

The average pullout load was 33,5 KN with a coefficient of variation of 17,3%. A low value of peak load was obtained in the first specimen (T1_001) due to a premature failure of the system. In fact, the anchor broke at the tip in correspondence to the plastic bend due to a problem of dry fibers and discontinuity. If this value was not considered, the coefficient of variation would be lower and equal to 7,3%. Moreover, the first specimen was the only one in which a combine cone-bond failure mode was observed, even if it was premature. All the remaining specimens presented a splitting failure mode.

As shown in Table 3.4, the average anchors slippage at peak load was equal to 0,134 mm with a quite big coefficient of variation. Fig. 3.10 illustrates the slippage of the anchors inside the holes versus the applied pullout load.

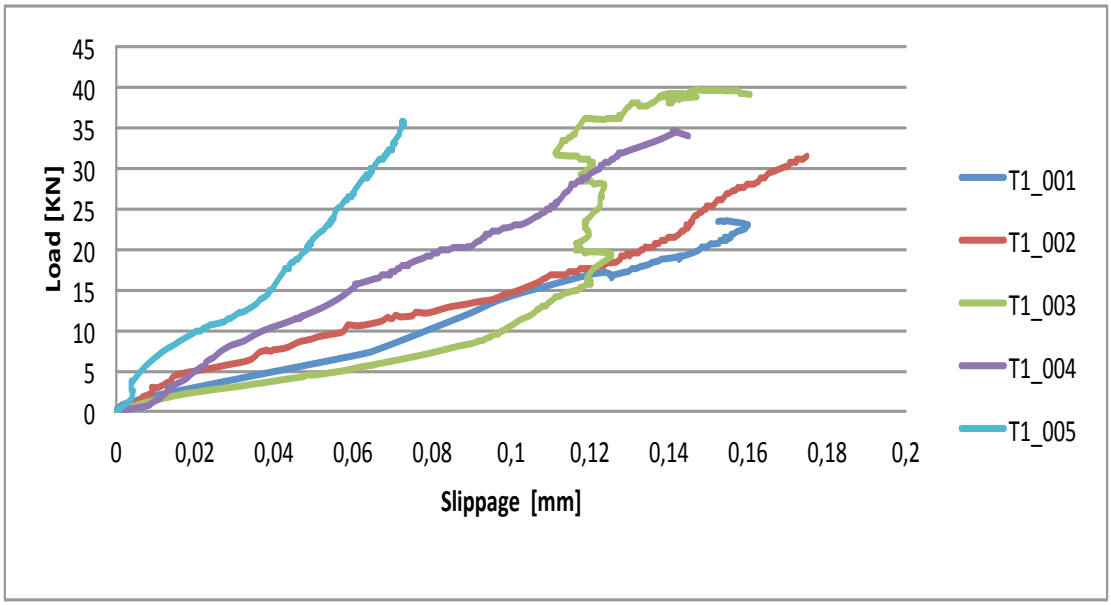

Fig. 3. 10 - Slippage vs. Applied Load

Even if the dimensions of the concrete test specimens were considered sufficiently large to ensure that the failure was not due to the splitting tensile cracking of concrete, this failure mode was observed in the 80% of the specimens. It means that the tension stresses in the concrete caused by the transfer of axial stresses from the anchor were higher than the splitting tensile strength of concrete (Ozbakkalogu and Saatciogli, 2013).

The experimental results in terms of average peak load are compared with those obtained from existing analytical models in the next chapter.

3.2.2 Test 2 – Results

As described before, this test was another pullout test on the anchors. In this case, the anchors were bonded to the concrete blocks just under the fan. The test was instrumented with a load cell and two LVDTs in order to measure the applied pullout load and the slippage of the fan. In the following table (Table 3.5), the peak loads and the failure modes observed in each specimen are listed. Moreover, the average increase in terms of peak load with respect to the specimens without chamfer is calculated.

Table 3. 5 - Summary of Test 2

Specimen	Chamfer Radius [mm]	Peak Load [kN]	Increase [%]	Failure Mode	Comments
T2_0_001	0	140,2	0,0	B	
T2_0_002		117,0		A	
T2_0_003		137,2		A	
T2_0_004		122,6		A	
Average Peak		129,3			
Standard deviation		11,2			
C.O.V (%)		8,7			
T2_1/4_001	6,4	158,8	27,0	A	
T2_1/4_002		185,5		A	
T2_1/4_003		165,5		A	
T2_1/4_004		146,9		B	
Average Peak		164,2			
Standard deviation		16,2			
C.O.V (%)		9,8			
T2_1/2_001	12,7	26,8	38,2	A	Premature failure
T2_1/2_002		159,3		A	
T2_1/2_003		198,1		B	
T2_1/2_004		178,5		B	
Average Peak		178,7			
Standard deviation		19,4			
C.O.V (%)		10,9			

In the case of T2_1/2 specimens, the first one (T2_1/2_001) was not taken into account in the calculation of the average pullout peak load and the coefficient of variation. In this case in fact, the failure was premature due to a bad installation of the system and the peak load was largely lower than those obtained from the other specimens. Except for this specimen, the values of the coefficients of variation obtained from the other repetitions were always lower or equal to the 10%.

As shown in Table 3.5, the peak load gradually increased with the chamfer radius and no relationships with the failure modes were observed.

The following graph (Fig. 3.11) shows the average pullout peak load measured during the test versus the dimension of chamfer radius.

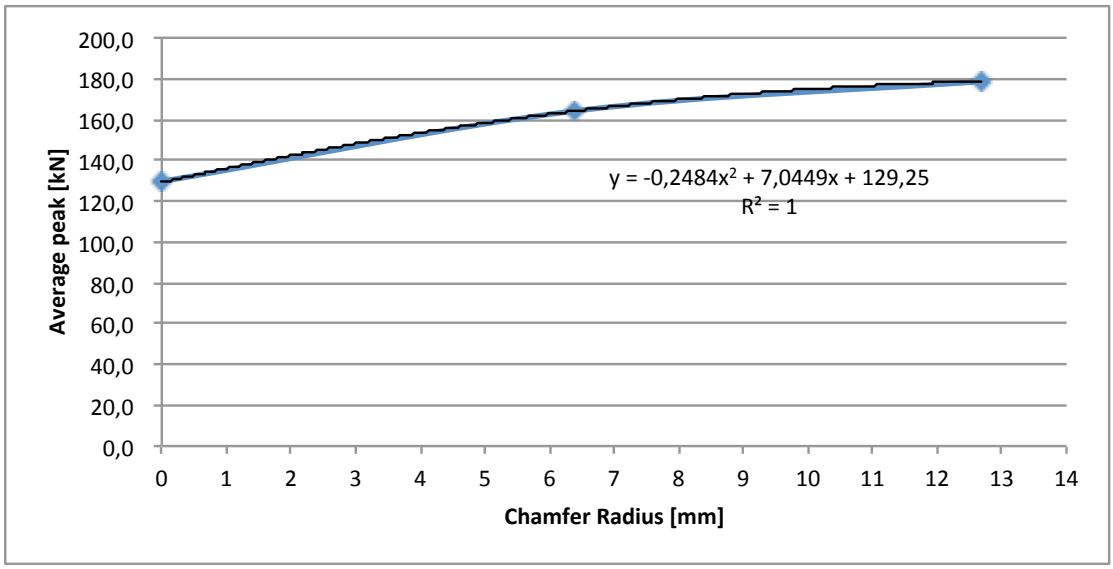

Fig. 3. 11 - Average Pullout Peak Load vs. Chamfer

The following graph (Fig. 3.12) shows the increase in terms of pullout peak load versus the dimension of chamfer radius.

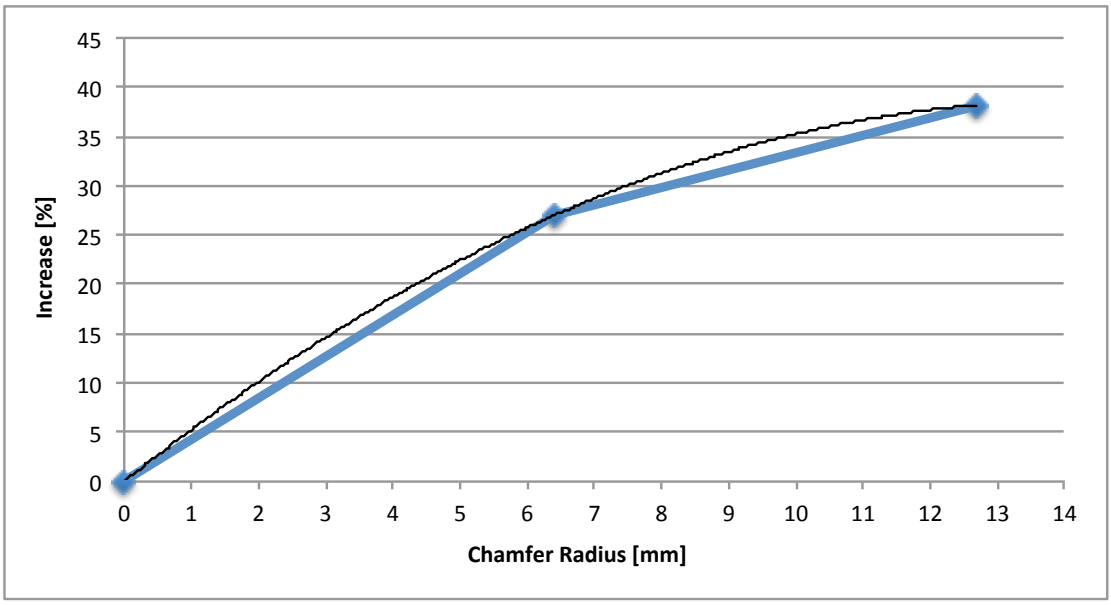

Fig. 3. 12 - Increase vs. Chamfer Radius

As observed in the two graphs above, there is a parabolic increase of the average peak load with respect to the specimens without chamfer. Thus, the effect of the chamfer radius on the anchor capacity may not increase substantially more beyond a certain radius.

The following graph (Fig. 3.13) is representative of the slippage of the anchor fans during Test 2. The absence of some specimens is due the fact that the LVDTs did not record any movements in some cases. Because of the anchors were installed by hand, the fans were not homogeneous in the disposition of the fibers. As a consequence, the part of the fans that failed firstly was random and sometimes not in correspondence of the LVTDs. The range of values of the measured slippage of the anchor fan was between 0.001 and 0.13 mm and no relation between the order of magnitude of the slippage, the dimension of the chamfer radius and the applied pullout load was found.

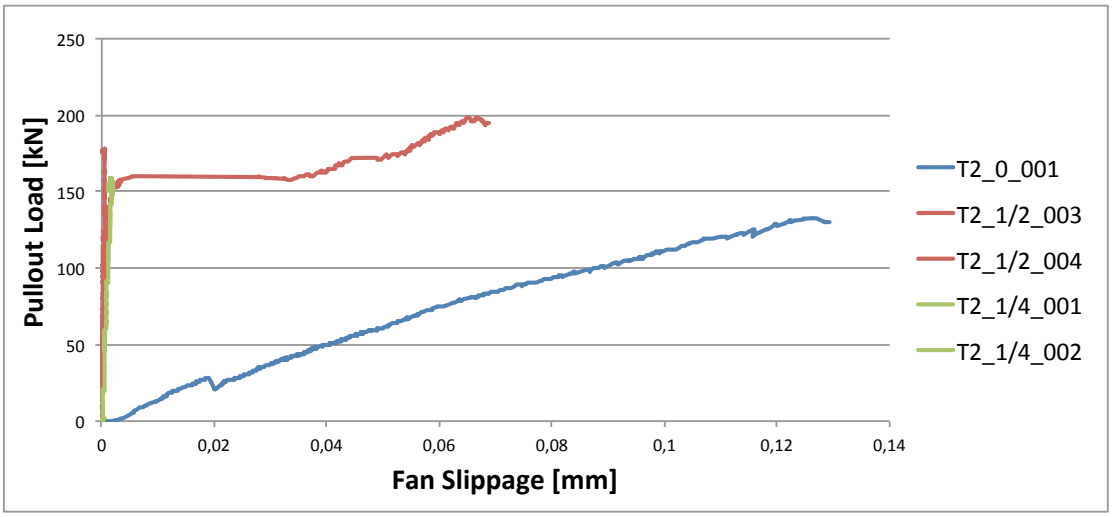

Fig. 3. 13 - Fan Slippage vs. Applied Load

Based on the results of the test, the maximum average pullout force was measured in the specimen provided with the biggest chamfer radius (12.7 mm). In this case, the increment with respect to the specimen with no chamfer radius was of the 38%. Without considering the time spent to prepare the chamfer, the bigger is the chamfer radius the better is the stress distribution of the anchor fibers at the hole. On the other hand, the bigger is chamfer radius the more labor is required for the preparation. Moreover, as shown in fig. 3.12, the effect of the chamfer radius on anchor capacity may not increase substantially more beyond a certain radius. Based on these

considerations, 6.35 mm chamfer radius is considered the best solution in the field. The increment of the average pullout load with respect to the specimen without chamfer was of the 27%, in addition the time spent to prepare the chamfer was half of the time needed for the 12.7 mm chamfer radius. This means less time and cost for the preparation.

Based on the considerations written above, the shear test specimens (Test 3) were provided with a chamfer radius equal to 6.35 mm.

3.2.3 Test 3 – Results

As described in the previous chapters, the Test 3 was a direct double shear test in which 4 types of specimens were tested: benchmark, 60° configuration, 90° configuration and 60°s (sandwich) configuration. The following table (Table 3.6) summarizes the results in terms of peak loads, increases of the load with respect to the benchmark, nominal stress, measured strain in the FRP sheets and failure modes.

The *Peak Load P* represents the maximum load applied by the hydraulic jack during tests. It is very important to remind that the side without strain gauges was strengthened with another FRP sheet in order to make each specimen fail in the other one provided with instrumentation. In particular, debonding initiated at the same load in both the two sides and the enhance strength of the anchored system was achieved once the cracks propagate toward the fan regions. At this point, the distribution of load was no more perfectly symmetric until the failure of the system due to the presence of the reinforcement in just one side.

In the case of benchmark specimens, the debonding load was exactly half of the peak load because P did not increase until the failure of the system once debonding initiated at the loaded ends of the FRP sheet. In order to compare the results with those obtained from the benchmark specimens, an approximated symmetric distribution of force was considered even in the case of the anchored FRP specimens. The debonding force was evaluated as half of the applied peak load P.

The following figure (Fig. 3.14) illustrates the approximated distribution of load in the anchored FRP system.

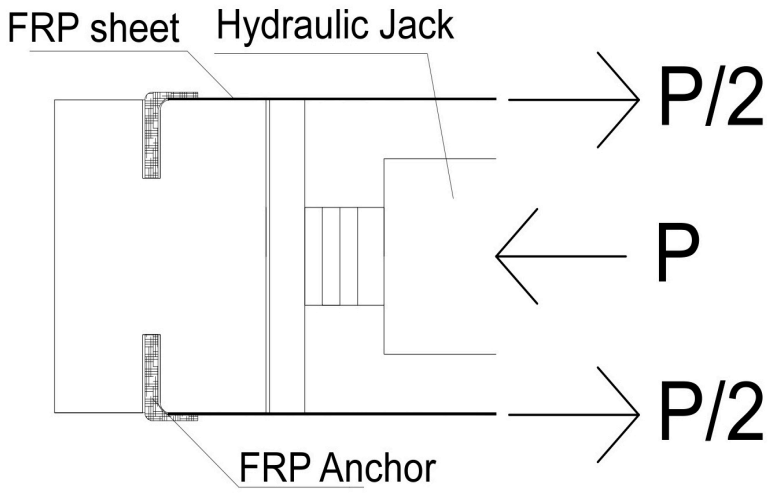

Fig. 3. 14 – Sketch of the approximated symmetric distribution of load

Table 3. 6 - Summary Test 3

Specimen ID	Fan Opening	Peak Load P	P/2	Average Increase in peak load	Nominal Stress	Corresponsing Strain at Peak Load						Failure mode
						SG1	SG2	SG3	SG4	SG5	SG6	
	[Deg]	[kN]	[kN]	[%]	[MPa]	[%]	[%]	[%]	[%]	[%]	[%]	
T3_0_001		73,02	36,51		235,79	-	-	-	-	-		A
T3_0_002	0	91,12	45,56	0,00	294,25	0,41	0,40	-	-	-	0,01	A
T3_0_003		89,27	44,64		288,28	0,56	0,48	-	-	-	0,03	A
Average		84,47	42,24		272,77	0,49	0,44				0,02	
Standard deviation		9,96	4,98		32,17	0,11	0,05				0,02	
C.O.V (%)		11,79	11,79		11,79	21,79	12,00				95,36	
T3_60_001		114,06	57,03		371,24	-	-	-	-	-	-	B
T3_60_002	60	117,16	58,58	36,86	384,35	0,51	0,92	-	-	0,06	-	B
T_60_003		110,2	55,1		355,85	0,87	0,86	0,12	0,05	-	-	B
Average		115,61	57,80		377,80	0,74	0,86					
Standard deviation		2,19	1,10		9,27							
C.O.V (%)		1,89	1,89		2,45							
T3_90_001		137,00	68,50		449,45	-	-	-	-	-	-	C
T3_90_002	90	132,84	66,42	57,18	435,81	0,60	0,78	-	-	0,05	-	D
T3_90_003		128,47	64,23		421,45	0,69	0,63	0,12	0,07	-	-	D
Average		132,77	66,38		435,57	0,65	0,70					
Standard deviation		4,27	2,13		14,00							
C.O.V (%)		3,22	3,22		3,22							
T3_60S_001	60s	173,24	86,62	105,09	-	0,30	0,10	-	-	0,00	-	-

As shown in the table above (Table 3.6), the average peak load gradually increased from the specimens without anchors (T_0) to the specimens with anchors, depending on the type of anchor fan configuration adopted. The following graph (Fig. 3.15) shows the average peak load $\frac{P}{2}$ in different types of specimen.

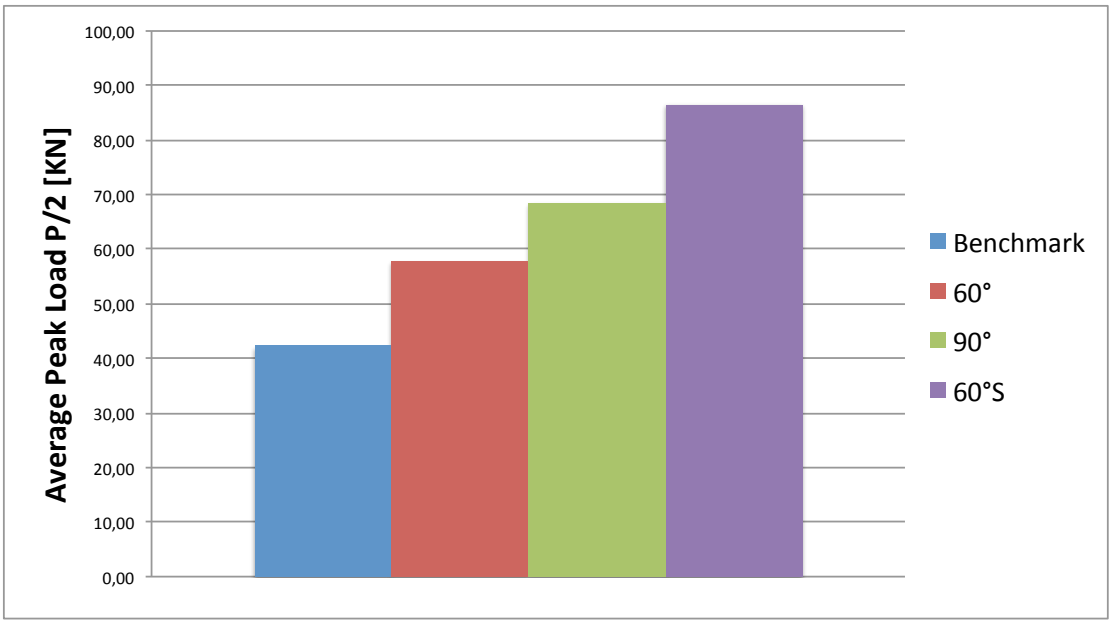

Fig. 3. 15 - Average Peak Load P/2 in the different types of specimen

The following graph (Fig. 3.16) illustrates the increase in term of average peak load $\frac{P}{2}$ with respect to the benchmark.

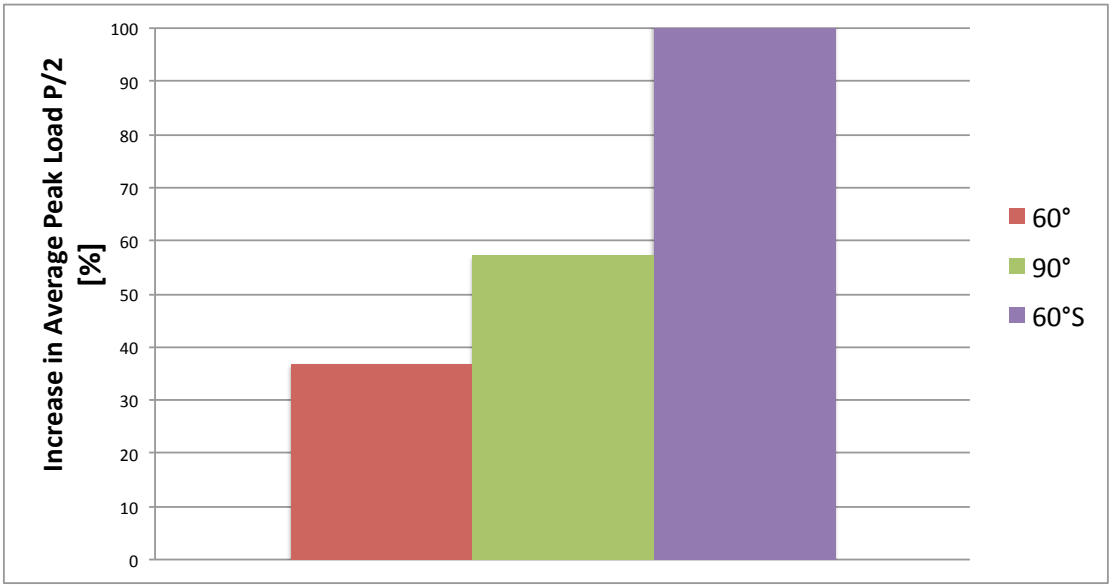

Fig. 3. 16 –Increase of the Average Peak Load P/2 in different types of specimen

In the legend, "90°" represents the specimen provided with an anchor having fan opening angle equal to 90°, "60°" represents the specimens provided with an anchor having fan opening angle equal to 60° and 60°S represents the sandwich type

specimen. As illustrated in Fig. 3.16, the 60° configuration increased the shear capacity of the system of the 36%, the 90° configuration of the 57% and the sandwich configuration of the 105%.

In addition, the difference between the theoretical tensile rupture load of the FRP sheet ($P_{ultimate}$), calculated using the measured FRP material properties, and the average peak load P/2 is listed in Table 3.7. The theoretical tensile rupture was calculated based on the strength and on the nominal section of the FRP sheet, assuming linear elasticity.

FRP Strength = 1339 MPa

Nominal Area = 152,4 mm^2

$P_{ultimate} = 1339\ Mpa \times 152{,}4\ mm^2 = 204064\ N = 204{,}1\ KN$

Table 3. 7 – Comparison between the theoretical rupture load and the average peak load

	P/2 [kN]	**ΔP** [%]
$P_{benchmark}$	42,24	79
$P_{60°}$	57,8	72
$P_{90°}$	66,38	67
$P_{60°S}$	86,62	58

As observed, ΔP values range between 58% and 79%, with lower values in the case of sandwich specimens in which the FRP sheets were attached using a combination of bond and FRP anchors and cover by another FRP lamina. Specimens relying solely on bond (benchmark type) developed the highest difference in peak load (ΔP equal to 58%). These results highlight the importance of relying on various load transfer mechanisms (bond and anchorage) to improve efficiency of the system.

Moreover, the *Nominal Stress* in the FRP sheets was calculated, as shown in Table 3.6. It was computed dividing the peak load applied on each FRP sheet (P/2) by its nominal section, assuming constant stress along the width of the laminas. The nominal section of the FRP sheet was the following:

A = 1.02 mm x 152.4 mm = 155,5 mm^2

As described in the previous chapter, four different types of failure were observed. The benchmark specimens were characterized by failure mode A, which is the typical one of unanchored FRP reinforcements. The anchored specimens had three different types of failure modes. Those having anchors provided with a fan opening angle of 60° were characterized by failure mode B while those having anchors provided with a fan opening angle of 90° by failure mode C and D. As described in paragraph 3.1.3, failure mode B was characterized by the rupture of the FRP sheet fibers around the anchor fan, failure mode C was characterized by the slippage of the FRP sheet under the anchor fan while failure mode D was characterized by the concrete substrate rupture.

Finally, the data obtained from the *Strain Gauges* were analyzed. The gauges layout on the FRP sheet has been already described in chapter 2 and the results in terms of strain are listed in the table above (Table 3.6). As explained before, debonding initiated at the loaded end and rapidly propagated towards the free end. The response recorded by the strain gauges near the free end and on the anchor (SG3, SG4 and SG5) show that there was a very little bond damage at this location during test. In fact, the strain measured by these gauges was always lower than 0,1%

The following graph (Fig. 3.17) illustrates the average strain of the FRP sheet at each average peak load recorded by SG2. This strain gauge was considered the most important due to the fact that was placed in the midline in front of the anchor fan. This region was of particular interest being the sheet fibers directly engaged by the anchor fan. For this reason, SG2 recorded the greatest value of deformation and it may be considered as the bond capacity of the system.

Fig. 3.18 and Fig. 3.19 show again the position of SG2. As explained before, the sandwich specimen was not analyzed due to the problem related with the cover and the measurement of the strain.

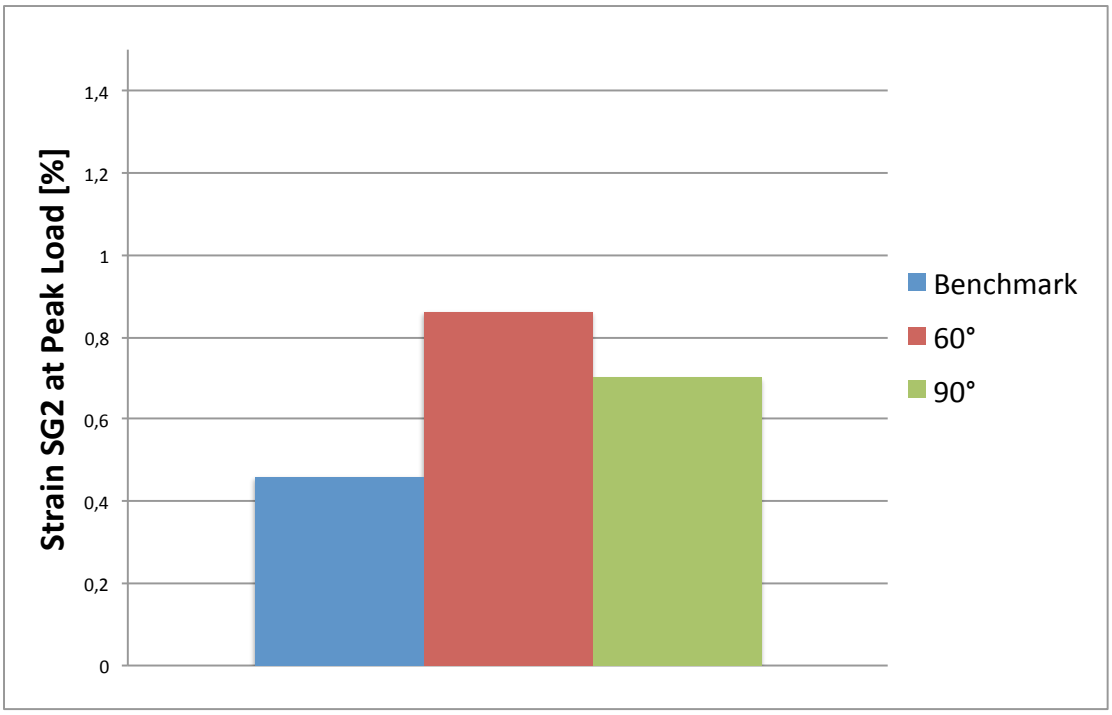

Fig. 3. 17 – Average Strain at Peak Load P/2 in different types of specimen

- *Benchmark specimen*

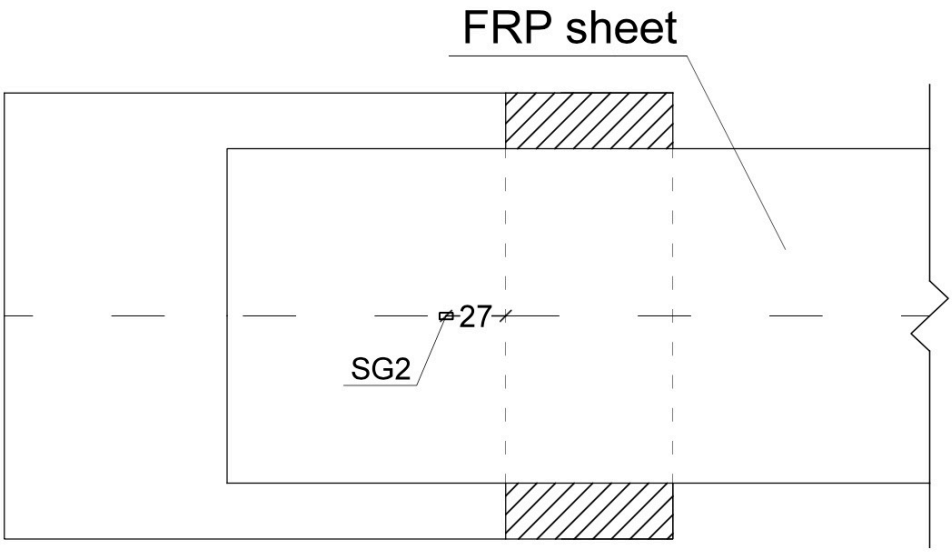

Fig. 3. 18 – SG2 Position - Benchmark

- *60° and 90° configuration specimen*

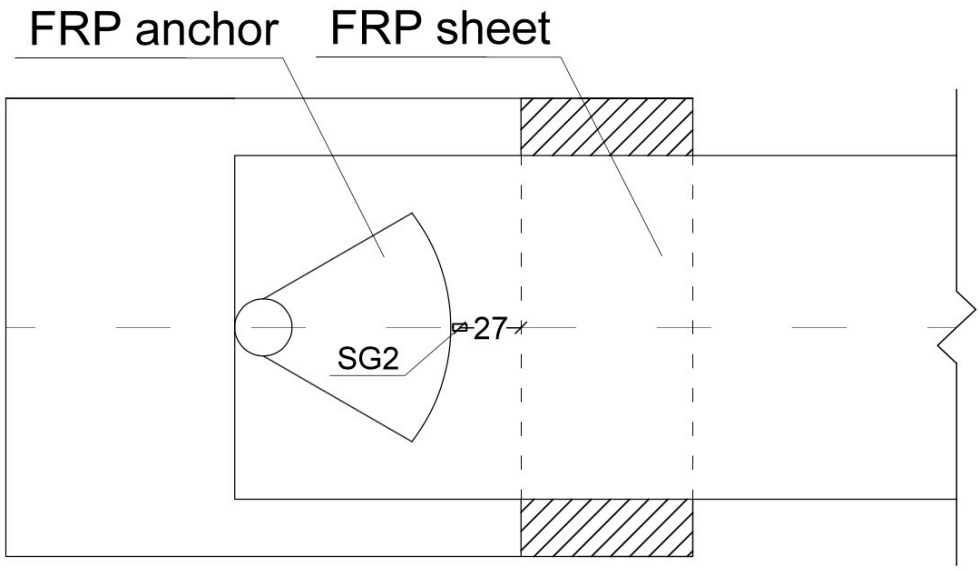

Fig. 3. 19 – SG2 Position – 60° and 90° configuration specimens

In general, because of local stress concentration generated from the anchor placement, peak strain values and their corresponding location on the sheet vary considerably.
The strain measured across the FRP sheet varied depending on how the debonding propagates toward the unloaded end of the sheet. The strain values were used to get an estimation of the load carried by the FRP sheet for comparison with the value measured using the load cell. Some strictly assumptions were made in order to simplify the computation and get an estimation of the load, such as:

- Stepwise distribution of strain in the FRP sheet instead of consider a more realist Gaussian distribution
- Pure tension applied to the FRP sheet
- Normal (peeling) stress in the adhesive layer not taken into account
- Adhesive layer subjected to constant shear stress across the thickness
- Interfacial linear ascending with sudden drop bond-slip relationship
- Substrate and reinforcement are homogenous and linear elastic untile failure

For strain gauges located in front of the FRP anchors, strains were assumed constant within the sheet covered by the anchor fans and equal to the value measured by SG2. The sheet parts outside this area were considered to be at strain equal to the value measured by strain gauges placed near the edge of the sheet (SG5).

Fig. 3.20, Fig. 3. 21 and Fig. 3.22 illustrate the assumed strain distribution in the specimens. The following table (Table 3.8) shows the estimated force on the FRP sheet (P_{theor}), the average applied peak load P/2 and the differences between them.

Table 3. 8 – Estimation of the Peak Load

	E [MPa]	ε_1 [%]	L_1 [mm]	ε_2 [%]	L_2 [mm]	P_{theor} [kN]	P_{exp} [kN]	**ΔP** [%]
Benchmark	74,6	0,44	152,4	-	-	50	42,24	16
60°	74,6	0,86	101,6	0,06	50,8	63,2	57,8	9
90°	74,6	0,7	132,1	0,05	20,3	69,7	68,5	2

As shown in the table above, the force on the FRP sheet, computed based on the assumed strain distributions written before, exhibited good agreement with the applied load P/2 in the case of anchored FRP reinforcements and poor agreement in the unanchored one. P_{theor} was computed simply multiplying the area under the strain distribution by the elastic modulus and the thickness of the FRP sheet.

Based on the results, the strain distribution across the width of the FRP sheet varies in a more complex manner than the stepwise distribution assumed in these calculations. Strain measured at a particular point in the sheet should not be used to estimate the maximum force being carried by the system even if good agreement were found in the case of anchored FRP reinforcement system.

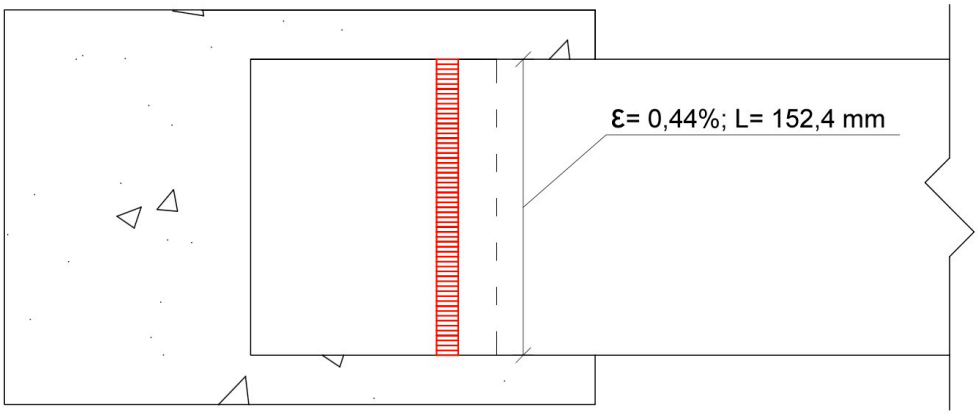

Fig. 3. 20 – Strain distribution (Benchmark)

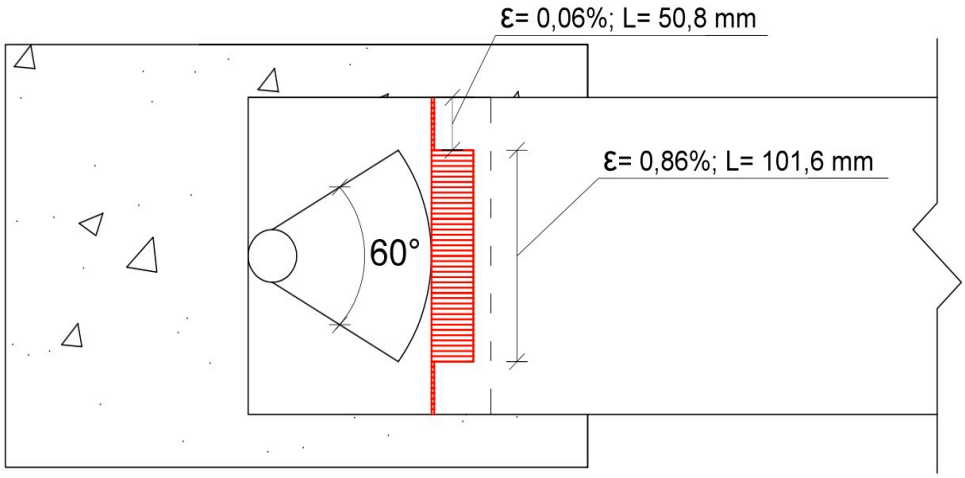

Fig. 3. 21 – Strain distribution (60° configuration)

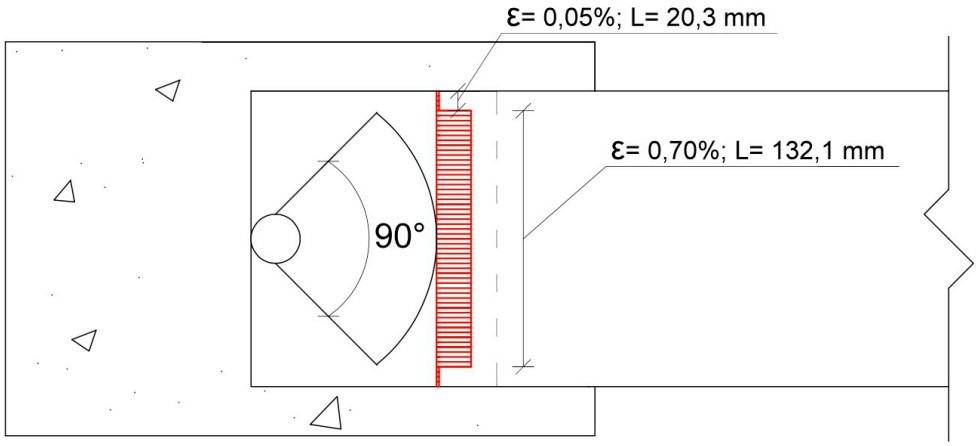

Fig. 3. 22 – Strain distribution (90° configuration)

Another important aspect about the double shear test (Test 3) that has to be underlined is related with its set up. The results obtained from the test were found to be highly dependent on the alignment of the system. Perfect alignment was very difficult to ensure and different degrees of load eccentricity were observed. Moreover, the specimens were found to be very sensitive to the handling operations.

The experimental results which have been just presented are compared with those obtained from analytical models in chapter 4. Comments and guidelines about the use of FRP anchor spikes are finally given in chapter 5.

4. ANALYTICAL MODELS

The results obtained from the experimental research were compared with those obtained from existing analytical models in order to have a validation of the test results. First of all, the average peak of pullout load measured during Test 1 was compared with that obtained from an analytical model for uncracked concrete (Kim and Smith, 2010). Secondly, the average maximum applied tensile force and the average maximum nominal stress on the FRP sheet were compared respectively with the maximum tensile force and the ultimate design strength, given by CNR-DT-200. Finally, the average deformations of the FRP sheet in the benchmark specimens measured during Test 3 by SG2 and SG3 were compared with those obtained from an existing analytical model. It investigates the load transfer mechanism between the substrate and the reinforcement under a tensile force (Carozzi, Colombi and Poggi, 2015).

4.1 Pull-out Strength of FRP Anchors in uncracked concrete

Experimental investigations have shown FRP anchors to be effective under tension (pullout) and shear loading. (Kim and Smith, 2010). Some analytical models exist to quantify the pullout strength of the FRP anchors; they were developed firstly for metallic anchors and than adjust for FRP anchors. These models are based on the following assumptions: single anchor behavior (no anchor grouping and multiple anchors do not interfere each other), monotonically applied tension load, idealized condition for epoxy cure (holes must be clean and dry before the installation, moderate temperature and proper curing of epoxy resin) and uncracked concrete (Kim and Smith, 2010). Under these assumptions, there were found similarities between the behavior of metallic anchors and FRP anchors. As a consequence, existing analytical

models, originally developed for metallic anchors, were critically reviewed and a best-fit and design model for FRP anchors was then provided (Cook et al., 1993; Ozdemir, 2005; Ozbakkalogu and Saatciolu, 2009)

Those pullout strength models, preliminarily developed for metal anchors, can be classified into four different types of model, depending on the type of failure.

The first one is the *Concrete Cone Model*. In this case, when the anchor is pull out from the concrete, the failure surface can form in the shape of a concrete cone. Two main type of failure can happen, concrete cone and concrete capacity design model (CCD). The first one assumes a circular projected area on the concrete surface based on a failure cone with side inclination of 45° to the concrete surface. The second one assume a projected square area on the concrete surface with a side dimension of three times the anchor embedment depth and a failure surface within the concrete of approximately 35° to the concrete surface (Kim and Smith, 2010).

The second model is the *Bond Model.* This model assumes that the failure surface is adjacent to the surface of the embedded portion of the anchor at the anchor-to-concrete interface. In this case, both the anchor diameter and the anchor hole diameter can be used for determine the bond resistance. It is also important to underline that in this case it is assumed to have a uniform bond stress.

The third type of model is the *Combined Concrete Cone and Bond Models.* This model assume a cone failure surface to form near the face of the concrete block with which the anchor is cast into with failure in the remaining portion occurring at the anchor-to-concrete interface. The pullout resistance in this case is the sum of the concrete strength contribution and the bonded interface strength contribution (Kim and Smith, 2010; Cook, 1993). Even in this case, the uniform bond stress model is the more appropriate for strength design and in particular adhesive anchors which may fail in concrete cone or combined failure mode.

The fourth type of model is the *Anchor Rupture Model.* It is based on the tensile capacity of the anchor. It was observed that 50% of the sutured anchors were composed by epoxy resin. Thus, to be conservative, an effective anchor section equal to the 50% of the real one was considered. Moreover, Kim and Smith showed that hand made FRP anchors usually have a tensile strength equal to the 65% of the tensile strength of the FRP sheet used to produce them. This is due to many misalignment and uneven straining of fibers during the manufacturing of anchors. (Ozbakkaloglu and Saatcioglu, 2009).

Based on the assumptions and the failure modes written above, the analytical model describing the pullout resistance (N_u) of a single FRP anchor can be formulated as follow (Kim and Smith, 2010):

$$N_u = \min (N_{cc}, N_{cb}, N_{ar})$$

$N_{cc} = \alpha_{cc} h_{ef}^{1.5} \sqrt{f_{cm}}$ (Concrete failure mode)

$N_{cb} = \tau_u \pi d_0 h_{ef}$ (Combined cone-bond failure)

$N_{ar} = 0{,}65(0{,}5\pi \frac{d_{anchor}^2}{4}) f_{FRP}$ (Anchor rapture)

Where:

h_{ef} is the effective embedded depth of the anchor
f'_c is the concrete cylinder compressive strength
d_0 is the diameter of the anchor hole
d_{anchor} is the diameter of the anchor
f_{FRP} is the flat coupon tensile strength rupture FRP strength

The key parameters for the analytical models are the calibration factors denoted by α_{cc} and τ_u. These parameters are fundamental and they were determined by a statistical analysis of different test data.
Based on statistical results, the design model recommendations are given as follow (Kim and Smith, 2010):

$$N_u = \min (N_{cc}, N_{cb}, N_{ar})$$

$N_{cc} = 9.68 h_{ef}^{1.5} \sqrt{f_{cm}}$ (Concrete failure mode)

$N_{cb} = 4.62 \pi d_0 h_{ef}$ $f_{cm} < 20Mpa$ (Combined cone-bond failure)

$N_{cb} = 9.07 \pi d_0 h_{ef}$ $f_{cm} \geq 20Mpa$ (Combined cone-bond failure)

$N_{ar} = 0{,}65(0{,}5\pi \frac{d_{anchor}^2}{4}) f_{FRP}$ (Anchor rapture)

The ranges of the parameters used to calibrate the analytical models are the following:

$17.5\ mm \leq h_{ef} \leq 100\ mm$, $10.4\ MPa \leq f_{cm} \leq 60.0\ MPa$ and $11.8\ mm \leq d_0 \leq 20.0\ mm$

Being:

h_{ef} = 101.6 mm

f_{cm} = 36 MPa

d_0 = 25.4 mm

d_{anchor} = 19,05 mm

t_f = 1.016 mm

f_f = 1339 MPa

- N_{cc} = 59.48 kN
- N_{cb} = 73.43 kN
- N_{ar} = 124 kN

$N_u = \min(N_{cc}, N_{cb}, N_{ar}) = 59{,}48\ kN$

Even if the proposed analytical model provides an accurate representation of the pullout resistance of the FRP anchors, not all the failure modes were always correctly predicted (Kim and Smith, 2010).

The analytical results are now compared with those obtained from Test 1. As written before, even if the dimensions of the concrete test specimens were considered sufficiently large to ensure that the failure was not due to the splitting tensile cracking

of concrete, this failure mode was observed in the 80% of the specimens. It means that the tension stresses in the concrete caused by the transfer of axial stresses from the anchor were higher than the splitting tensile strength of concrete (Ozbakkalogu and Saatciogli, 2013). For this reason, the average experimental peak load N_{exp} was largely lower than the pullout resistance obtained from the analytical model. In fact:

$N_{exp} = 33{,}5\ kN$

$N_u = \min(N_{cc}, N_{cb}, N_{ar}) = 59{,}48\ kN$

4.2 Optimal Bond Length of a generic external bonded FRP sheet/laminate

The Optimal Bond Length is the minimum bonded length that ensures the transmission of the bonding force and any longer bonded length does not produce any force increase.

This length is proportional to the axial stiffness of the reinforcement, in particular Young's modulus and thickness, and inversely proportional to the strength properties of the support

The CNR-DT-200 (2013) provides the following expression for it:

$$l_{ed} = min\left\{\frac{1}{\gamma_{Rd} \cdot f_{bd}}\sqrt{\frac{\pi^2 \cdot E_f \cdot t_f \cdot G_f}{2}}, 200\ mm\right\}$$

Where:

- E_f and t are the modulus of elasticity on the direction of force and the thickness of the FRP, respectively.
  In this case the FRP lamina has the following properties:

E_f = 74590 MPa

t_f = 1,016 mm

- $\gamma_{Rd} = 1.25$ is a corrective factor;

- G_f is the design value of the *specific fracture energy*; it depends on the strength properties of the concrete, adherents, adhesive and on the characteristic of the concrete surface. The fracture energy can be expressed as a function of the tensile and compressive strength in the concrete and of the shape factor depending on the FRP-to-concrete width ratio (*w/b*). It is the integral of the τ_b-s law (Lu et al 2005, Ferracuti et al. 2007, De Lorenzis et al. 2001) and, thus depends on the both the strength properties of the adherents, concrete, adhesive and on the characteristic of the concrete surface. When debonding occurs in the concrete layer, the fracture energy can be expressed as a function of the tensile and/or compressive strength in the concrete and of a shape factor depending on the FRP-to-concrete with ratio b_f/b.

CNR-DT200 (2013) provides the following expression for the *Design Fracture Energy*:

$$G_f = \frac{K_b K_G}{FC} \sqrt{f_{cm} f_{ctm}}$$

Where:

- f_{cm} and f_{ctm} are the mean values of the concrete's compressive and tensile strnghts, respectively, evaluated on-site (if experimental values are not available, the average concrete tensile strength can be computes using f_{cm} in accordance with the Building code specification).
  In this case the concrete has the following properties:

  $f_{ctm} = 0.27\sqrt[3]{f'^2_c}$ = 3 MPa

f_{cm}= 36 MPa

- FC is the confidence factor.
  Is assumed a confidence factor equal to 1.

- K_b is a geometrical corrective factor and function of the ratio between the FRP and the concrete width, b_f/b. K_b is defined with the following equation:

$$K_b = \sqrt{\frac{2 - \frac{b_f}{b}}{1 + \frac{b_f}{b}}} \geq 1$$

Where $\frac{b_f}{b} \geq 0.25$. If $\frac{b_f}{b} < 0.25$, K_b is equal to 1.18

Being:

$$\frac{b_f}{b} = \frac{6''}{8''} = 0.75$$

$$K_b = \sqrt{\frac{2 - \frac{b_f}{b}}{1 + \frac{b_f}{b}}} = 0.845$$

Due to the fact that K_b must be equal or greater then zero, it was taken:

K_b= 1

- K_G is an additional corrective factor calibrated from experimental results and equal to 0.023 mm for pre-cured or 0.037 mm for wet lay-up system.
  In this case:
  K_G = 0.037 mm for wet lay-up system

Thus, the value of the Design Fracture Energy is the following:

$G_f = \frac{K_b K_G}{FC}\sqrt{f_{cm} f_{ctm}}$ = 0.384515 MPa mm

- $f_{db} = \frac{2G_f}{s_u}$, with $s_u = 0{,}25\ mm$ is the Design *Bond Strength* between FRP and concrete.
  In this case:
  $f_{db} = \frac{2G_f}{s_u}$ = 3.07612 MPa

Based on the calculation, the Optimal Bond Length is equal to:

l_{ed} = 98 mm (3.8 in.)

The Optimal Bond Length given by CNR-DT200 (2004) was calculated and compared with that obtained from the latest version.
CNR-DT200 (2004) gives the following expression for the optimal bond length:

$$l_{ed} = \sqrt{\frac{E_f \cdot t_f}{2 \cdot f_{ctm}}} = 112\ mm$$

Being:
E_f = 74590 MPa
t_f = 1,016 mm
$f_{ctm} = 0.27\sqrt[3]{f'^2_c}$ = 3 MPa

As shown, The Optimal Bond Length given by 2004 version is greater than that given by 2013 version.
The FRP sheet bond length considered in Test 3 was 127 mm (5 in.), which is greater than both the two optimal bond lengths.

4.3 Maximum Tensile Force for a generic External Bonded FRP sheet/laminate

In general, before designing for flexural and shear, the evaluation of the maximum force transferred from the concrete to the FRP, as well as the evaluation of shear and normal stresses at the concrete-FRP interface, is required.

The *Maximum Tensile Force* in a generic FRP reinforcement with an infinite bonded length, F_{max}, can be calculated in the case of debonding failure as:

$$F_{max} = b_f \int_0^{\infty} \tau(x)dx \qquad \text{for externally bonded reinforcement system,}$$

where τ(x) is the bond shear between the FRP sheet and the concrete surface and b_f is the width of the FRP sheet. If we assume a linear elastic behavior for the externally bonded reinforcement system, the CNR-DT200 (2013) provides the following expression for the debonding load:

$$F_{max} = b_f \sqrt{2E_f t_f G_f} \qquad \text{for externally bonded reinforcement system,}$$

Where t_f and E_f are the thickness and the elastic modulus of the FRP reinforcement in the direction of the force and G_f is the fracture energy. When the debonding occurs, the fracture energy can be computed as follow (CNR-DT200, 2013):

$$G_f = \frac{K_b K_G}{FC} \sqrt{f_{cm} f_{ctm}}$$

where all the parameters have been already described before.

Being:

G_f= 0.384515 MPa mm

t_f = 1,016 mm

E_f = 74590 MPa

b_f = 152.4 mm

The Maximum Tensile Force is:

F_{max} = 36,8 kN

In the Test 3 (Shear test), the bond length was equal to 127 mm (5 in.). Being the bond length greater than the optimal bond length, the maximum tensile force was not reduced. This force was compared with the average peak load applied to a single FRP sheet during Test 3.

Average peak load (Test 3) = 42.2 kN
Maximum tensile force (CNR-DT-200) = 36.8 kN
Based on the comparison, the results obtained from Test 3 in case of benchmark specimens were considered consistent because the average maximum tensile force was just greater than the maximum tensile force given by CNR-DT 200.

4.4 Ultimate Design Strength for laminate/sheet end debonding (mode 1)

For laminate/sheet end debonding (mode 1), in cases in which the provide bond length is equal to or larger than the optimal bond length, the ultimate design strength, f_{fdd}, is defined as the maximum allowed strength before debonding of the ends. The CNR-DT-200 provides the following expression for it:

$$f_{fdd} = \frac{1}{\gamma_{f,d}} \sqrt{\frac{2E_f G_f}{t_f}}$$

where $\gamma_{f,d}$ is the partial factor and G_f is the fracture energy indicated previously.
For a bond length l_b shorter than the design optimal bond length $l_{ed,}$, the ultimate design strength shall be reduce according to the following equation:

$$f_{fdd,rid} = f_{fdd}\frac{l_b}{l_{ed}}\left(2 - \frac{l_b}{l_{ed}}\right)$$

In the Test 3 (Shear Test) the bond length was equal to 127 mm (5 in.). Being the bond length greater than the optimal bond length, the ultimate design strength was not reduced.

Being:

G_f= 0.384515 MPa mm

t_f = 1,016 mm

E_f = 74590 MPa

For the ultimate limit state, the value assigned to the partial factor of the FRP materials is the following: $\gamma_{f,d}$ = 1.10 (Section 3.4.1-CNR DT 200)

So the Ultimate Limit Strength for sheet end debonding is:

$$f_{fdd} = \frac{1}{\gamma_{f,d}}\sqrt{\frac{2E_f G_f}{t_f}} = 216\ MPa$$

Under the hypothesis of homogeneous distribution of the applied load along the section of the FRP sheet, the average maximum nominal stress in the FRP sheet in the case of benchmark specimens during Test 3 was compared with the Ultimate Design Strength for laminate end debonding (CNR-DT-200).

Average Nominal Stress (Test 3) = 273 N/mm^2

Ultimate Design Strength (CNR-DT200) = 216 N/mm^2

Based on the comparison, the results obtained from the shear test on the benchmark specimens were considered consistent because the average nominal stress was just greater than the ultimate design strength given by CNR-DT 200.

4.5 Analytical Debonding Model

The following calculations are based on several studies on FRP-reinforced masonry developed at Politecnico of Milan. In general, a refined debonding model is needed and experiment tests are required in order to achieve a refined calibration of the pertinent parameters, which influence the effectiveness of the FRP-repair system (Carozzi, Colombi and Poggi, 2015).

In this section an analytical models is presented. It investigates the load transfer mechanism between the substrate and the reinforcement under a tensile force F in the case of a double shear test. Even in this case, the provide bond length is equal to or larger than the optimal bond length. The following assumptions are made:

- Substrate and reinforcement are homogenous and linear elastic
- Linear kinematic relationships for the substrate and the reinforcement
- Interfacial linear ascending with sudden drop bond-slip relationship
- Adhesive layer is subjected to constant shear stress across the thickness
- Normal (peeling stress) in the adhesive layer are not taken into account
- Bending effect are neglected

The following table summarizes all the parameters considered in this paragraph. Then, a fully description of the analytical model is given.

δ	interfacial slip	δ_u	ultimate interfacial slip
u_s, u_f	substrate and reinforcement longitudinal displacement	K_b, K_G	reinforcement width and fracture energy corrector factor
N_s, N_f	substrate and reinforcement axial force	Γ_F	mode II fracture energy
A_s, A_f	substrate and reinforcement cross sectional area	f_{cm}, f_{ctm}	compressive and tensile strength of the clay brick substrate
ε_f	reinforcement longitudinal strain	b_f, b_s	reinforcement (bond) and surface width
F_{max}	maximum experimental transferable load	β_1	bond length corrector factor
τ, τ_{max}	tangential and maximum tangential stress at the interface	l_b, l_e	bond and effective bond length
E_s, E_f	substrate and reinforcement Young's modulus	t_f	reinforcement thickness

Table 4. 1 - parameters

The double shear test scheme adopted in the model is shown in the following figure.

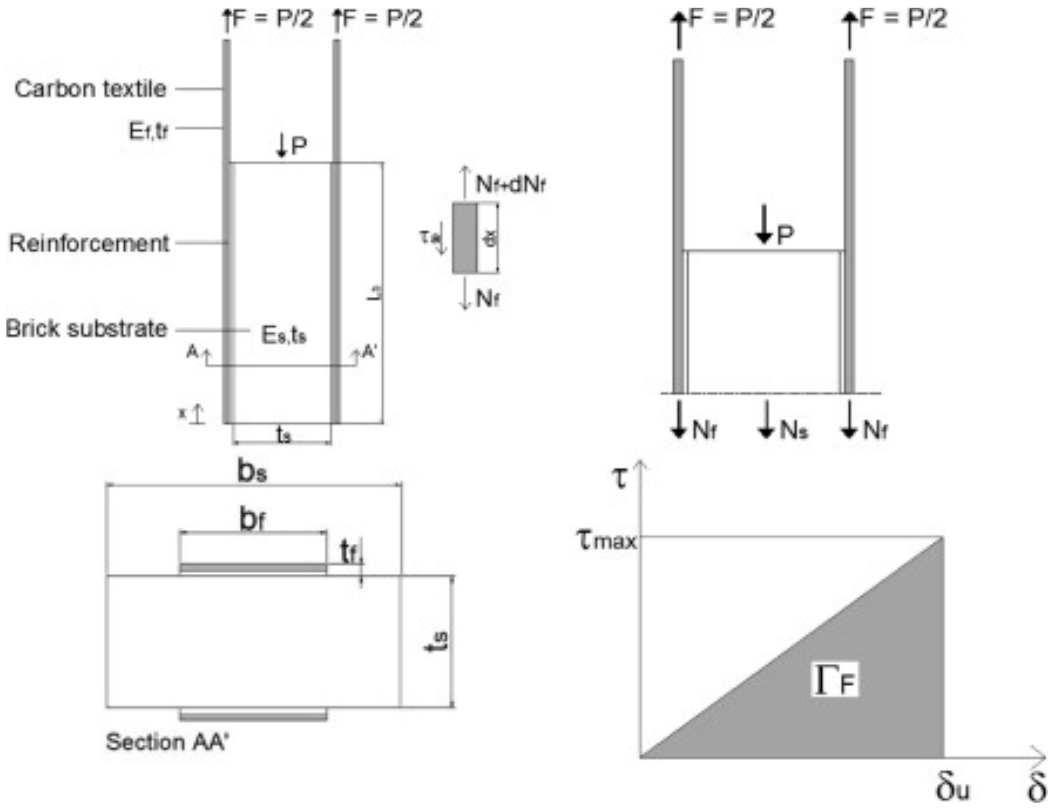

Fig. 4. 1 - Double shear test scheme (Carozzi, Colombi and Poggi, 2015)

The interfacial slip is defined as the relative longitudinal displacement between the reinforcement and the substrate.

1. $\delta = u_f - u_s$

where u_f and u_s are the reinforcement and substrate longitudinal displacement, respectively (Carozzi and Colombi, 2014).
The local equilibrium in the reinforcement in the longitudinal direction is given by:

2. $\frac{1}{b_f}\frac{dN_f}{dx} - \tau = 0$

where N_f is the reinforcement axial force, b_f is the reinforcement width and τ is the tangential stress in the adhesive layer.

The global equilibrium in the longitudinal direction is given by:

3. $N_s + 2N_f = 0$

where N_s is the substrate axial force.
According to the assumptions 1-3, the constitutive relationship for the reinforcement, the substrate and the interface are:

4. $N_f = A_f E_f \varepsilon_f = A_f E_f \frac{du_f}{dx}$
5. $N_s = A_f E_s \varepsilon_s = A_s E_s \frac{du_s}{dx}$
6. $\tau = \frac{\tau_{max}^2}{2G_F} \delta$

where A_f and A_s are the reinforcement and substrate sectional area respectively, ε_f and ε_s are the reinforcement and substrate longitudinal strain while E_f and E_s are the reinforcement and substrate Young's modulus. The shear stress-slip relationship is assumed linear up to the maximum allowable interfacial shear stress τ_{max}, that is before the occurrence of the interfacial fracture. The shear stress-slip is then assumed drop to zero when the value of the slip exceeds δ_u without consideration of the softening behavior. The shear stress-slip relationship above is a function of the Mode II Fracture Energy G_F, which is defined as the energy required for local bond fracture and is represented by the area under the shear stress-slip curve. G_f has been already in paragraph 4.3:

$G_F = \int_0^\infty \tau \, dx$ = 0.384515 Mpa mm

The maximum tangential stress at the interface τ_{max} can be calculated from the following expression based on Mohr-Coulomb failure criterion.

$$\tau_{max} = \frac{1}{2}\sqrt{f_{cm} f_{ctm}}$$

where f_{cm} and f_{ctm} are the compressive and tensile strength of the concrete substrate.

Inserting Eqs. (3)-(6) into Eq. (2) one gets:

$$\frac{d^2\delta}{dx^2} - \frac{f_2}{f_1}\delta = 0$$

where:

$$f_1 = \frac{2\Gamma_f}{b_f \tau_{max}^2} \;\; ; \;\; f_2 = \frac{2}{E_s A_s} + \frac{1}{E_f A_f}$$

Defining:

$$\lambda^2 = \frac{b_f \tau_{max}^2}{2\Gamma_F}\left(\frac{2}{E_s A_s} + \frac{1}{E_f A_f}\right)$$

with the following boundary conditions at the lower (x = 0) and upper (x = l_b) reinforcement ends:

- $N_f = \frac{1}{f_1}\frac{d\delta}{dx} = 0 \quad \text{at x} = 0$
- $N_f = \frac{1}{f_1}\frac{d\delta}{dx} = F \quad \text{at x} = l_b$

The expression of the *interfacial slip* is:

$$\delta = \frac{F}{\lambda \sinh(\lambda l_b)}\cosh(\lambda x)$$

The *longitudinal strain* in the reinforcement layer is equal to:

$$\varepsilon_f = \frac{F}{A_f E_f}\frac{\sinh(\lambda x)}{\sinh(\lambda l_b)}$$

The *tangential stress* on the interface is given by:

$$\tau = \frac{F\lambda}{b_f}\frac{\cosh(\lambda x)}{\sinh(\lambda l_{b)}}$$

Being:

$A_f = 154{,}83\ mm^2$

$E_f = 74590\ MPa$

$b_f = 152{,}4\ mm$

$A_s = 82580{,}48\ mm^2$

$E_s = 62145\ MPa$

$b_s = 203{,}2\ mm$

$l_b = 127\ mm$

$k_b = 1{,}13$

$k_G = 0{,}3$

$\Gamma_F = 0{,}353\ MPa\ mm$

$\tau_{max} = 5{,}196\ MPa$

$\lambda = 0{,}0123$

$l_b = 127\ mm$

$F = F_{max} = 36800\ N$

Where l_b represents the bond length of the FRP lamina considered in Test 3 while F_{max} is the maximum tensile force given by CNR-DT200.

The following figures represent the interfacial slip, the longitudinal debonding strain and the tangential stress along the FRP reinforcement lamina obtained from the expressions written above.

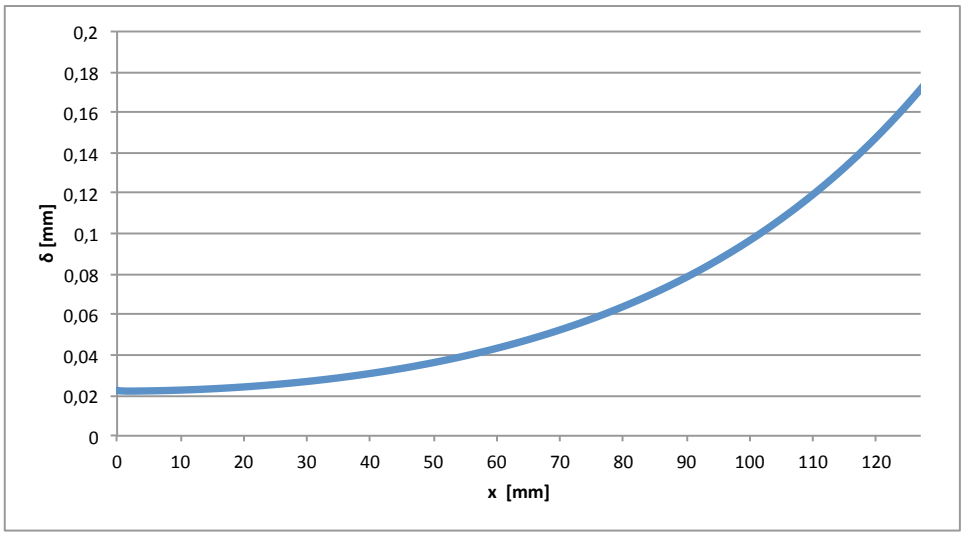

Fig. 4. 2 - Interfacial Slip

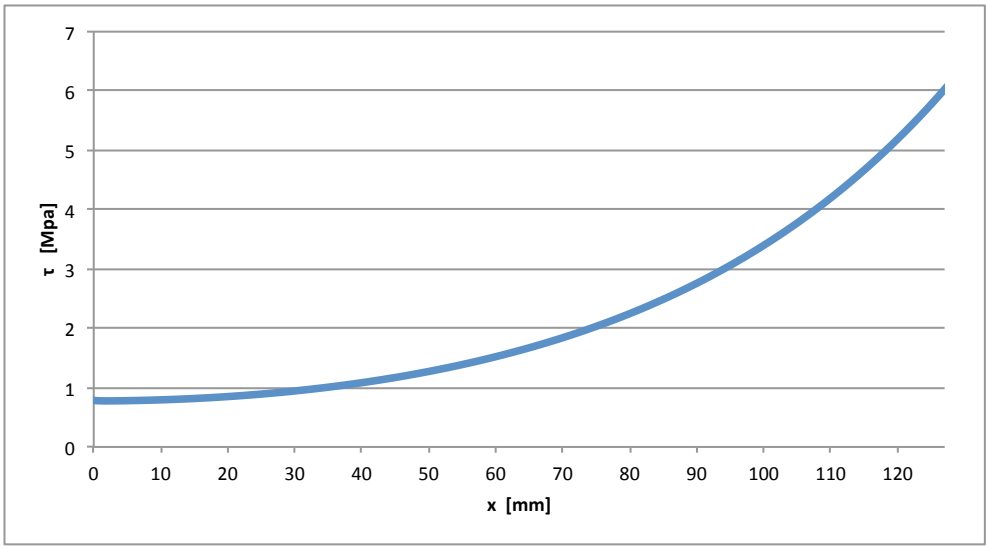

Fig. 4. 3 - Tangential Stress on the interface

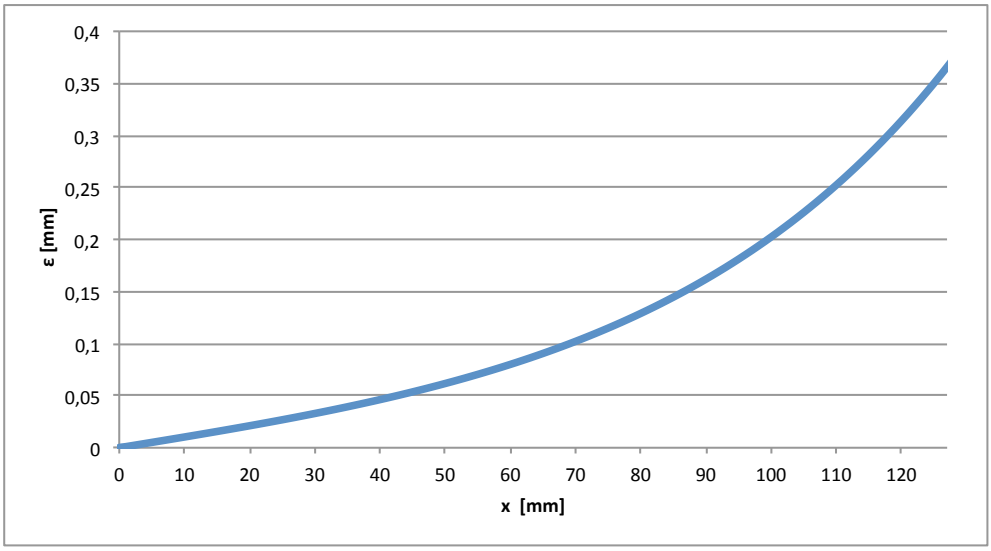

Fig. 4. 4 - Longitudinal Bond Strain

The experimental results obtained in Test 3 are now compared with those obtained from the analytical model described above. In particular, the strain measured by the strain gauges in the case of benchmark specimens is compared with that obtained from the analytical model.

In the following graph (Fig. 4.5), the curves represent the strain rates along the bonded FRP sheet for different applied loads obtained from the analytical model. F represents the maximum average tensile load applied to the FRP sheet during Test 3 and it is equal to 42,4 KN. Remember that F is half of the applied load P on the benchmark specimens. The dots represent the values of strain recorded during Test 3 by SG2 and SG3 at the same load intervals.

Fig. 4.6 illustrates the corresponding position of the strain gauges SG2 and SG3 on the bonded FRP sheet.

As shown in the graph below, for load intervals smaller than the 75 % of the average peak load, the analytical model and the experimental results assume very similar values. Increasing the load, the experimental results appears largely greater than those obtained from the analytical model.

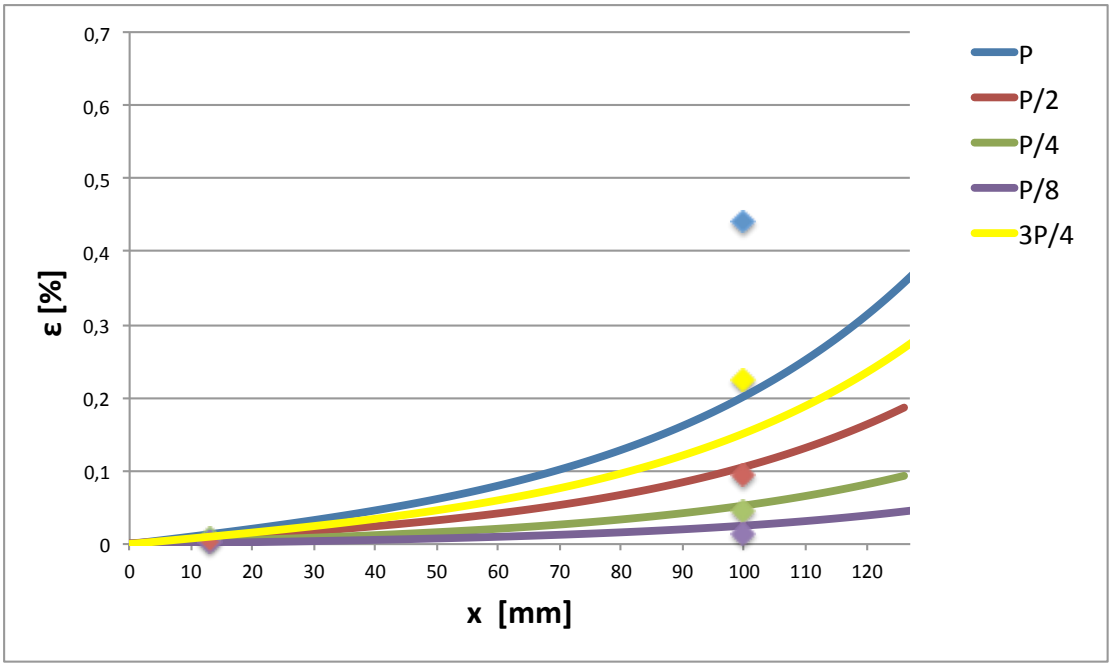

Fig. 4. 5 - Comparison between analytical and experimental results

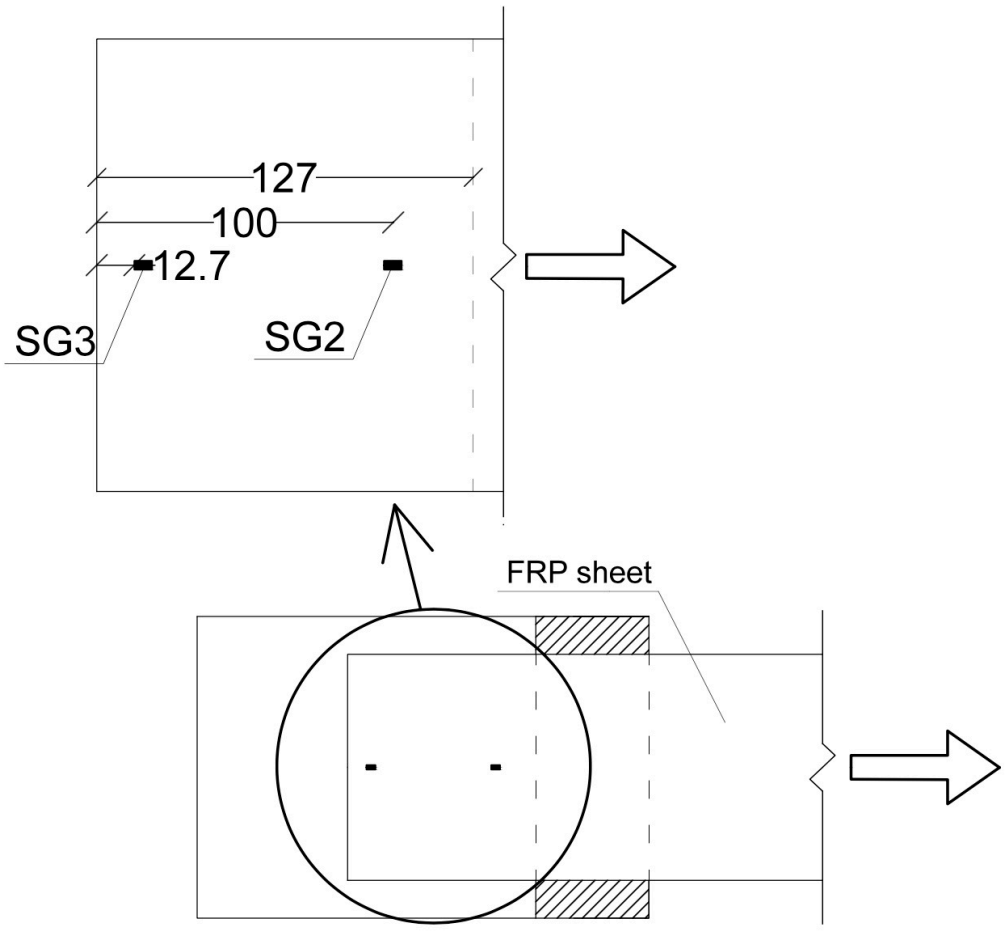

Fig. 4. 6 - SG2 and SG3 position

5. CONCLUSIONS

5.1 Comments

The FRP anchor spikes have been tested for many years with different levels of success, but a comprehensive understanding of their behavior is still lacking and hinders the development of design recommendations. The research presented in this thesis represents an initial study of the interaction that takes place between FRP anchor spikes and FRP sheets so that this anchoring system can be used more extensively. A complete experimental campaign has been developed in order to fully understand the behavior of this anchorage system. Three different tests were performed in order to characterize the parameters that affect the behavior of the anchors and fully understand the improvement on the global strengthening system. In general, the FRP anchor spikes are subjected to predominantly pullout forces or shear forces, depending on the orientation of the FRP anchors, as shown in Fig. 5.1 and 5.2. Anchor type "A" is mainly subjected to pull out force while anchor type "B" to a combination of pullout and shear forces. The first test was performed in order to measure the pullout resistance of the anchors subjected to a pure tensile force. The embedded length was kept constant end equal to 101 mm (4 inches) during the whole experimental program in order to study the capacity of the anchor subjected to both pullout and shear forces. The dimension of the embedded length was decided based on previous researches. In fact, many recommendations about it have been presented in the past. For example, according to tension tests conducted by Akyuz and Ozdemir (2004), an effective depth of 10 cm (approximately 3.9 inches) exists for CFRP anchors, beyond which the capacity of the anchor no longer increases. Moreover, according to Orton (2007), results from flexure tests have shown that an embedment of at least 2 inches into the concrete core is required. With the concrete cover included, the total embedment distance could reach a depth of 5 inches (Fig. 5.3). Kim (2008) also tested CFRP anchors similarly to Orton's tests, and recommended an embedment depth of at least 4 inches.

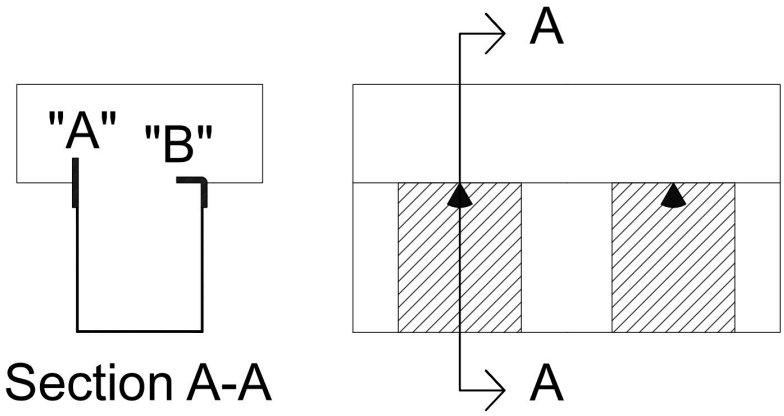

Fig. 5. 1 – Different FRP anchor spikes

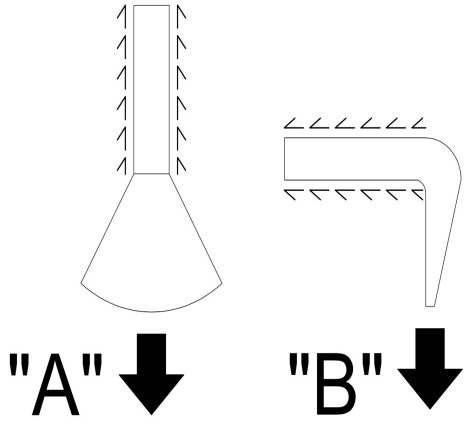

Fig. 5. 2– Different dowel angles

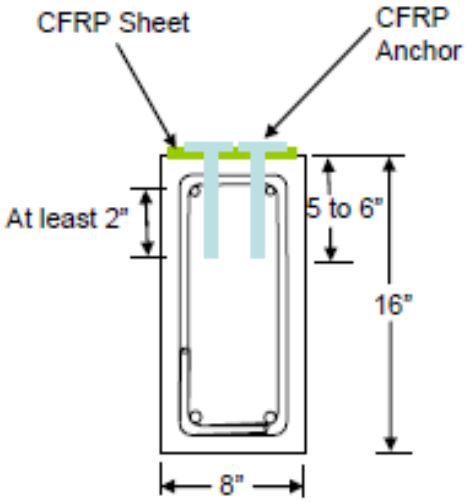

Fig. 5. 3- Embedded length in a RC member (Orton, 2007)

Another parameter that was kept constant during the experimental campaign is the anchor diameter. This size of the anchor greatly affects anchor performance since the strength of the anchor is dictated by the amount of material present. Likewise, the size of the anchor also determines whether the anchor has sufficient strength to allow the CFRP sheet to develop its full capacity. Kim (2008) tested a variety of anchor sizes and found that an anchor cross-sectional area 1.33 times that of the CFRP sheet was enough to develop the full capacity of the sheet. Therefore, he suggests a 1.50 ratio of anchor to sheet cross-sectional area as a conservative recommendation. Based on these recommendations, an anchor diameter equal to 19 mm (3/4 in.) was considered. In this way, the nominal section of the FRP sheets was 152 mm^2 while that of the

anchors 283 mm^2. In addition, based on previous researches, the thickness of adhesive layer does not appear to have a significant influence on the pullout strength of the anchor (Cook at al. 1998). For this reason, the holes were provided with a diameter 6.35 mm (0,25 inches) greater than the anchor diameter, just to have enough space for a correct installation.

The second test was performed in order to study a particular detail that may cause a decrease in the efficient of the strengthening system. Stress concentrations are likely to form in FRP anchor spikes where the anchor transitions from the edge of the hole to the strengthening sheet due to the sharp bend of the fibers. For this reason, the main goal of this test was to identify the best radius of curvature of the chamfer in order to avoid stress concentration. Three different types of specimens were analyzed, each one provided with a different chamfer radius. Based on the results of the test, the maximum average pullout force was measured in the specimens provided with the biggest chamfer radius (12.7 mm). In this case, the increment with respect to the specimen with no chamfer radius was of the 38%. On the other hand, the bigger is chamfer radius the more time is required for the preparation. Moreover, as shown in fig. 3.12, the effect of the chamfer radius on anchor capacity may not increase substantially more beyond a certain radius. Based on these considerations, 6.35 mm (0,5 inches) chamfer radius is considered the best solution in the field. The increment of the average pullout load with respect to the specimen without chamfer was of the 27%, in addition the time spent to prepare the chamfer was half of the time needed for the 12.7 mm chamfer radius. This means less time and cost for the preparation. The results were confirmed by many studies performed by researchers in the past. Pham (2009) explored this topic in greater detail through a series of tests using a 0 in. radius, 0.2 in. (6.35 mm) radius, and 0.5 in. (12.7 mm) radius, and reported a similar trend of increased capacity with increasing bend radius. Pham found that anchors with 0.25 in. (6,35 mm) bend radius had an 18% increase in capacity compared to the one with zero radius, and anchors with a 0.5” (12,7 mm) bend radius had a 23% increase in capacity compared with zero radius. Furthermore, more time is required to create larger bend radiuses. For this reason, a bend radius of at least 0.25 in. (6.35 mm) was recommended by him.

The last test was the most important part of the research campaign, even if the first two were determint for the final set up. In fact, the anchors were provided with an embedded length equal to 101 mm so that the pullout resistance was already known

based on Test 1. Moreover, each specimen was provided with a chamfer radius at the holes equal to 6,35 mm, based on the results of Test 2.

As explained in chapter 2, the double shear test set-up is only appropriate for the characterization of the peel-off type debonding associated mainly with interfacial shear stresses. Rip-off debonding mechanism, which is affected by other parameters, notably the presence of internal shear and flexural reinforcement and coexistence of shear and normal stresses, cannot be captured through such tests. Nonetheless, this test is useful for comparative purposes and can help towards the development of design guidelines for flexural FRP strengthening of RC beams.

First of all, the results in terms of average peak load obtained from the benchmark specimens were compared with the maximum tensile force in an external bonded lamina, given by CNR-DT200. Then, the average strain distribution was compared with an analytical model, as shown in paragraph 4.3 and 4.5. Both the two comparisons underlined the consistency of the results obtained from the benchmark, as described in chapter 4.

The results obtained from the anchored specimens show that there was always a large increase of the average tensile peak load with respect to the unanchored specimens (benchmark). In the case of benchmark specimens, debonding propagation develops fast with a small increase in FRP stress after initial debonding, underlining the brittleness of this failure mode. On the contrary, the presence of the anchors increased significantly both the strength and the ductility of the system. The failure was no more sudden once debonding started to propagate due to the action of the fan on the fibers of the laminate.

The most efficient anchorage system was the sandwich type, where the average peak load increased up to the 108%. Unfortunately, the presence of the cover did not allow both the recording of the strain distribution on the FRP sheet and the observation of the failure mode. For this reason, no comments can be developed and further shear tests should be done. The specimens provided with anchors having fan opening angle equal to 90° and 60° presented different results in term of average peak load and strain distribution on the FRP sheet. Based on the data obtained from the test, the maximum value of strain was measured in front of the anchor (position SG2, Fig. 5.5) in both the two specimens. In the case of 60° configuration specimens, this was greater than that measured in the 90° configuration specimens. Moreover, the strain recorded near the edge of the sheets (position SG5, Fig. 5.5) was always less than

0.1%. On the other hand, the average maximum applied tensile load measured in the 60° configuration specimens was lower than that recorded in the 90° configuration specimens. Based on the results, strain fields that develop in the FRP sheet appear to be not uniform in the transverse direction. For this reason, strains plotted longitudinally along the FRP sheet centerline are not representative of distributions near the edge of sheets and should be not taken as a design value. It is evidence that only sheet regions located within the anchor splay develop high stresses and strains. Due to the observations written above, a stress distribution model was supposed. It has the typical Gaussian distribution shape, symmetric with respect to the tension load The following sketch (Fig. 5.4) illustrates the supposed strain distribution while Fig. 5.5 shows again the position of SG2 and SG5.

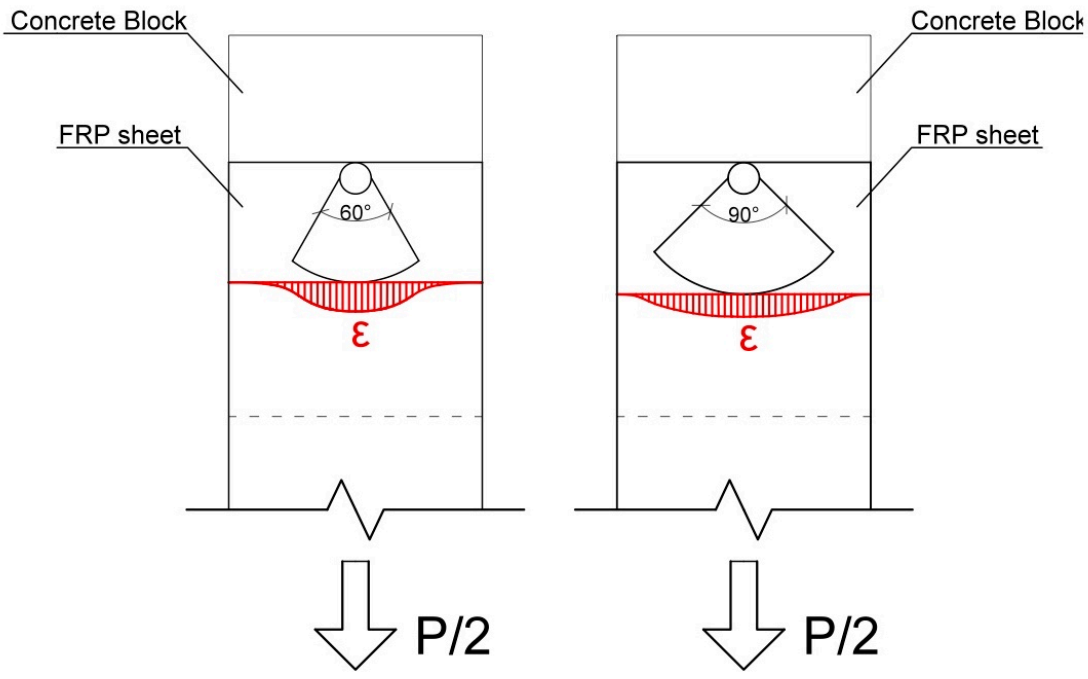

Fig. 5. 4 - Strain Distribution Model

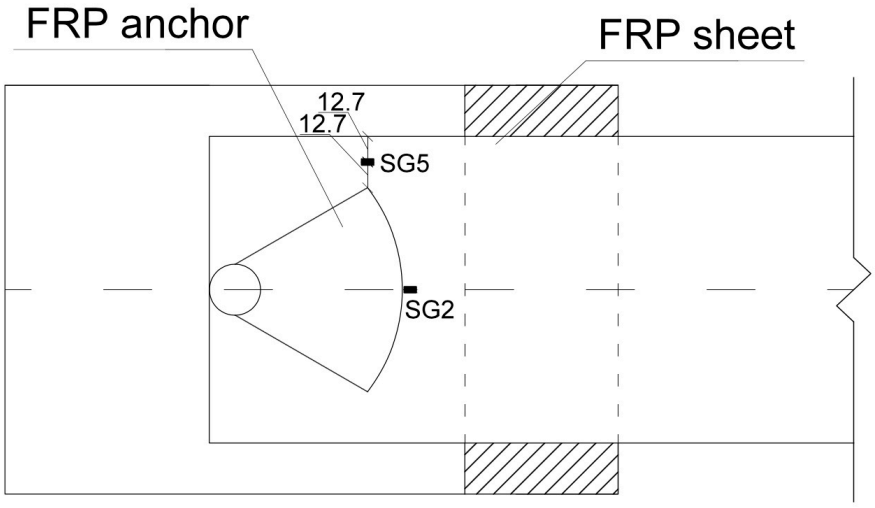

Fig. 5. 5 – Strain gauges position

The results show that the most effective configuration is achieved when the fan fibers are oriented in the direction of the tension force (pointing forward). In fact, the maximum strain was measured in the specimen provided with anchors having a fan opening angle equal to 60°. In this case, more fibers are oriented toward the tensile force, being all the anchors provided with the same number of fibers. On the other hand, even if the strain measured in the 90° configuration specimens was lower, the average peak load was greater. This is due to the fact that the area covered by the fan was larger than that covered by the anchor fan in the 60° configuration specimens.

Another important aspect of the test that has to be commented is the failure modes. Laboratory investigations performed by Niemitz et al. (2010) indicated three primary FRP anchor failure modes: FRP anchor fan delamination, FRP anchor shear rupture and FRP pullout. FRP anchor delamination is a failure mode that occurred between fibers forming the anchor fan and the FRP sheet surface. The FRP anchor shear rupture consists of anchor failure just below the FRP sheet surface while the fan remains attached to the upper face of the FRP sheet. It results in cases where the shear capacity of the anchors is lower than the rupture strength of the FRP sheet. FRP anchor pullout is not a common failure mode and occurred only in case where the holes in the concrete are not perfectly cleaned (Brena, McGuirk, 2013). In this research, the observed failure modes were always due to the failure of the FRP sheet. In all the specimens, the anchor dowel remained inside the hole and the fan in its position even after the failure of the system. Moreover, in the case of specimens

provided with anchors having fan opening angle equal to 60°, the failure was always due to rupture of the sheet around the fan, while in the case of fan opening angle equal to 90°, the failure was due to slippage of the sheet under the fan or substrate rupture.
Based on these results, many conclusions may be done. The anchors appear to be strong enough to develop the full capacity of the sheet. In fact, pullout and shear failure of the anchors were never observed during Test 3. From these observations, anchor may be considered really effective in securing only the width of sheet fibers approximately covered by the fans. Therefore, it is most effective to have anchor fans placed such that they cover the entire width of the FRP sheet, as demonstrated by the anchors provided with fan opening angle equal to 90°. On the other hand, the anchors provided with fan opening angle equal to 60° appeared to be more effective to develop the full capacity just of the FRP sheet directly engaged by anchor fibers.
Based on the comments given before, a draft of design guideline is provided in the following paragraph.

5.2 Guidelines

The aim of this research is to deepen the knowledge of externally bonded FRP laminate anchored with FRP anchor spikes. The parameters that govern the behavior of this anchorage system have been study through an experimental campaign composed by different types of test. Many conclusions have been listed in the previous paragraph and a draft of guideline is provided below that could help engineers to include FRP anchor spikes in the designing of the FRP strengthening systems.

- An anchor provided with an embedded length equal to 101 mm (4 inches) and a diameter equal to 19 mm (0,75 inches) may be enough in order to prevent shear or pullout failure. In this case in fact, the failure of the system is always due to the FRP rupture, debonding or slippage.
- A hole diameter 6.35 mm (0,25 inches) greater than the anchor diameter is enough in order to have a good installation, which is fundamental for the efficiency of the strengthening system. It allows the fibers to be straight inside the hole. The critical importance of correctly installing FRP anchor spikes lead to attempt to obtain also quality control guidelines for their use.

- A chamfer radius equal to 6.35 mm (0,25 inches) is enough in order to reduce stress concentration at the hole and increase the pullout resistance of the anchors. It is also easy to be created even in the field.
- The strain distributions and sheet stress development along the FRP sheet largely varied depending on the fan opening angle. The angle should be less than 90 degrees to be most effective, as shown in figure 5.6 and a fan opening angle equal to 60° is enough in order to achieve the full capacity of the FRP laminate. In addition, the fan should cover the entire width of the laminate in order to have improvement in terms of global strength of the system. If more than one anchor is used, they should not have an open space between the anchor fans, otherwise the sheet between the fans may debond prematurely. Moreover, based on previous research, anchors that are installed adjacent to each other should be overlap in the fan fibers of 10 mm or more (Kobayashi, 2001), as shown in Figure 5.7.

The anchors layouts shown in Figures 5.7 are representative of the final considerations of this research, while the Table 5.1 summarizes the properties of the FRP strengthening system, based on the guideline just described above.

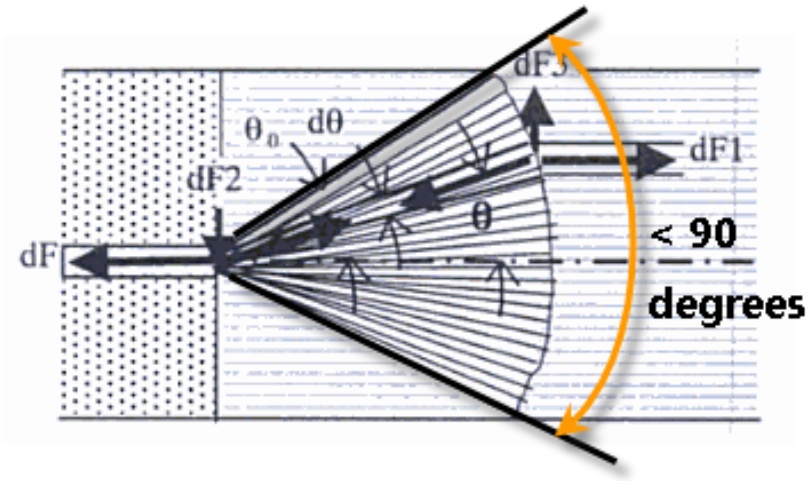

Fig. 5. 6 - Fan opening angle (Wang, 2013)

Table 5. 1 - Summary of the guideline

Hole			Anchor				Laminate	
			Dowel		Fan			
Diameter [mm]	Depth [mm]	Chamfer Radius [mm]	Diameter [mm]	Length [mm]	Radius [mm]	Opening Angle [Deg]	Width [mm]	Thickness [mm]
25,4	101,6	6,35	19	101	76,2	60	152	1

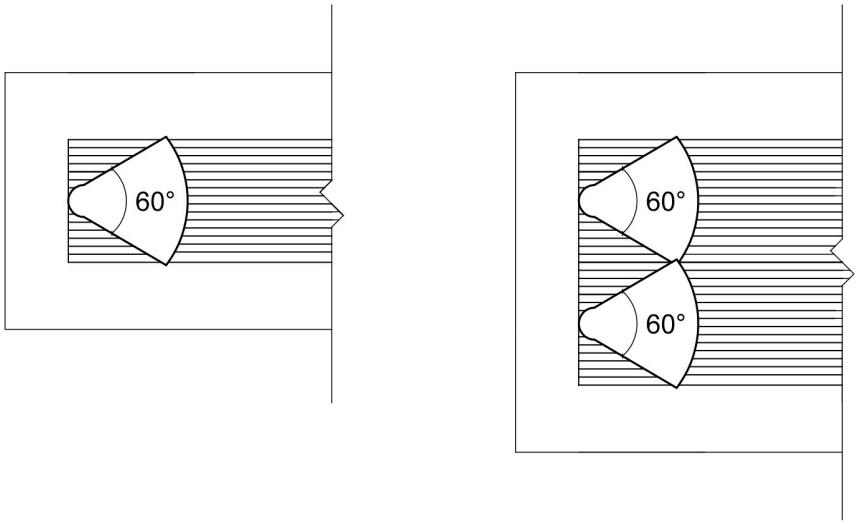

Fig. 5. 7 - Final anchors layouts

In general, the interest in FRP anchors has led to numerous studies and efforts to establish quality control techniques for their design and use. FRP anchors have proven very useful for developing the full tensile capacities of externally bonded reinforcing sheets and for increasing the ductility of the system. Many authors have suggested the need for more studies to further understand FRP anchors. One such suggestion is to study different anchor layouts, as shown in figure 5.8, or anchorage system on multiplies FRP laminates. Moreover, tests on real scale are needed in order to measure the improvement in terms of bearing capacity of the whole system.

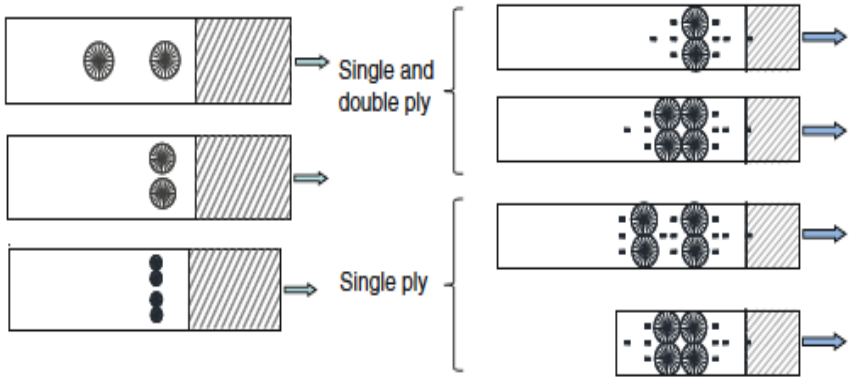

Fig. 5. 8 – Different anchors patterns

BIBLIOGRAPHY

AASHTO-2012 “Guide Specification for Design of Bonded FRP Systems for Repair and Strengthening of Concrete Bridge Elements”. American Association of State Highway and Transportation Officials (AASHTO) 2012.Washington, DC.

AC125-2012 “Acceptance criteria for concrete and reinforced and unreinforced masonry strengthening using externally bonded fiber reinforced polymer (FRP) composite systems”. International Code Council Evaluation Service. June 2012.

ACI 318-11 “Appendix D – Anchoring to Concrete” Reported by ACi Committee.

ACI 355.4-11 “Qualification of Post-Installed Adhesive Anchors in Concrete and Commentary”. Reported by ACi Committee 440.

ACI 440 R-07 “Report on Fibre-Reinforced Polymer (FRP). Reinforcement for concrete structures”. Reported by ACi Committee 440. ISBN 978-0-87031-259-5.

ACI Committee 440. “Guide for the design and construction of externally bonded FRP systems for strengthening concrete structures”. ACI 440.2 R-08. Farmington Hills (MI): American Concrete Institute; 2008. p.76.

ACI Committee 440. “Guide for the design and construction of structural concrete reinforced with FRP bars”. ACI 440.1 R-06. Farmington Hills (MI): American Concrete Institute; 2006.

ACS. “National historic chemical landmarks-Bacon’s breakthrough”. Washington (DC); 2007.

ASTM C31/C31M - 12 “Standard Practice for Making and Curing Concrete Test Specimens in the Field”. American Society for Testing and Materials (ASTM) 2012.

ASTM C39/C39M - 14 “Standard Test Method for Compressive Strength of Cylindrical Concrete Specimens”. American Society for Testing and Materials

(ASTM) 2014.

ASTM C143/143M – 12 “Standard Test Method for Slump of Hydraulic-Cement Concrete”. American Society for Testing and Materials (ASTM) 2012.

ASTM D3039/D3039M - 08 “Standard Tests Method for Tensile Properties of Polymer Matrix Composite Materials”. American Society for Testing and Materials (ASTM) 2008.

ASTM E4 – 13 “Standard Practice for Force Verification of Testing Machines”. American Society for Testing and Materials (ASTM) 2013.

ASTM E83 – 10a “Standard Practice for Verification and Classification of Extensometer Systems”. American Society for Testing and Materials (ASTM) 2010.

ASTM E178 – 08 “Standard Practice for Dealing With Outlying Observations”. American Society for Testing and Materials (ASTM) 2008.

ASTM E488/E488M – 10 “Standard Test Methods for Strength of Anchor in Concrete Elements”. American Society for Testing and Materials (ASTM) 2010

Bakis C.E., Bank L.C., Brown V.L., et al. “Fiber-reinforced polymer composite for construction-state-of the-art review”. ASCE-J Compos Constr 2002;6(2):73-87.

Bissonnette, Benoit, Alexander M. Vaysburd, and Kurt F. von Fay, “Best Practices for Preparing Concrete Surfaces Prior to Repairs and Overlays”. Report No. MERL 11-XX, Bureau of Reclamation, December 2011.

Bournas D.A., Pavese A. and Tizani W. “Tensile capacity of FRP anchors in connecting FRP and TRM sheets to concrete” Elvisier Ltd, 2014.

Brena S.F. and McGuirk G.N. “Advanced on the behavior characterization of FRP-anchored carbon fiber-reinforced polymer sheets used to strengthen concrete elements”, International Journal of Concrete Structures and Materials, March 2013, Vol.7, No.1, pp. 3-16.

Brosens K., Van Gemert D. “Anchorage design for externally bonded carbon fiber reinforced polymer laminates”. Proceedings of the FRPRCS4 International

Symposium, 1999 Nov; Baltimore. pp. 635-645.

Brosens K., and Van Gemert D. “Anchorage Design for Externally Bonded Carbon Fiber-Reinforcement Polymer Laminates”. Proceedings of the FRP RCS-4 SP-188, American Concrete Institute 1999, Farmington Hills, Mich.l. pp 635-645.

Caggegi C., Pensèe V., Fagone M., Cuomo M., Chevalier L. “Experimental global analysis of the efficiency of carbon fiber anchors applied over CFRP strengthened bricks”. Elvisier Ltd, 2013.

Carozzi F.G., Colombi P., Montalbano A. and Poggi C. “Utilizzo di connettori per l’incremento della forza di distacco del rinforzo in FRP di strutture in muratura o calcestruzzo”. 2° Convegno Nazionale Assocompositi, Torino 29-31 Maggio 2012.

Carozzi F.G., Colombi P., Poggi C. “Calibration of end-debonding strength model for FRP-reinforced masonry”. Elvisier Ltd, 2014

Chajes, M.J.; Finch, Jr., W.W.; Januszka, T.F.; and Thomson, T.A. “Bond and Force Transfer of Composite Material Plates Bonded to Concrete”. ACI Structural Journal, V. 93, No. 2, Mar.-Apr. 1996. pp. 295-303.

Chen J.F., Teng J.G., “Anchorage strength models for FRP and steel plates bonded to concrete”. J Struct Eng ASCE 2001. pp.127-784-791.

CNR (National Research Council). “Guide for the design and construction of externally bonded FRP systems for strengthening existing structures”. Rome, Italy: Advisory Committee on Technical Recommendation for Construction of National Research Council; 2004. pp. 154.

CNR-Advisory Committee on Technical Recommendations for Construction. “Guide for the Design and Construction of Externally Bonded FRP Systems for Strengthening Existing Structures”. Materials, RC and PC structures, masonry structures. CNR-DT 200 R1/2013. Roma – 10 Ottobre 2013.

De Lorenzis L., Miller B., Nanni A. “Bond of Fiber-Reinforced Polymer Laminates to Concrete”. ACI Materials Journal; May-June 2001.

De Lorenzis L., Teng J.G. “Near-surface mounted FRP reinforcement: an emerging

technique for structural strengthening". Compos Part B 2007;38: pp.119-143.

Fédération International du Béton (FIB). "Externally bonded FRP reinforcement for RC structures". Technical report prepared by Task Group 9.3, Bulletin 14, Lausanne, Switzerlad; 2001. pp. 130.

Ferracuti B., Savoia M., Mazzotti C. "Interface law for FRP-concrete delamination". Comp Struct 2007. 80(4): pp. 523-531.

Figeys W., Schueremans L., Van Gemert D., et al. "A new composite for external reinforcement: steel cord reinforced polymer". Constr. Build Mater; 2008; 22(9): pp. 1929-1938.

Grelle S.V. and Sneed L.H., "Review of anchorage system for externally bonded FRP laminates". Internation journal of concrete structures and materials, March 2017, Vol.7, No.1, pp. 17-33.

IStructE. "Interim guidance on the design of reinforced concrete structures using fibre composite reinforcement". London: Institution of Structural Engineers; 1999. pp. 116.

JSCE "Recommendation for the upgrading of concrete structures with use of continuous fiber sheet". Concrete engineering series nr 41. Tokyo: Japanese Society of Civil Engineers; 2001. pp. 250 (available in English).

JSCE. "Standard specification for concrete structures". Tokyo: Japanese Society of Civil Engineers; 1986. pp. 274 (English translation 1996).

Kim S.J. and Smith S.T. . Pull.out strength model for FRP anchors in uncracked concrete". ASCE; 2010, July/August, Vol. 14, No. 4, pp. 406-411

Kim S.J. and Smith S.T. "Pull-out test on FRP anchors". Asia-Pacific Conference on FRP in Structures, International Institute for FRP in Construction; 2007

Lamanna A.J. Bank L.C., Scott D.W. "Flexural strengthening of reinforced concrete beams using fasteners and fiber reinforced polymers strips". ACI Struct J 2001; 98(3): pp. 368-376.

Lopez A., Galati N., Alkhrdaji T., et al. "Strengthening of a reinforced concrete

bridge with externally bonded steel reinforced polymer (SRP)". Compos Part B; 2007. 38: pp. 429-436.

Lu X.Z., Teng J.G., Ye L.P., et al. "Bond-slip models for FRP sheets/plates bonded to concrete". Eng Struct 2005. 27: pp. 920-937.

Meier U. "Bridge repair with high performance composite materials". Mater Tech (Duebendorf, Switz.) 1987. 4: pp. 125-128 (in German).

Nanni A., Rizkalla S., Bakis C.E., et al. "Characterization of GFRP ribbed rod used for reinforced concrete construction". Proceedings of the international composites exhibition (ICE-98). Nashville (TN); 1998. pp.16A/1-6.

Nanni A. "Composite: Coming on Strong", Concrete Constuction, Vol.44, 199, p.120

Nanni A. "Composites: coming on Conc Constr". 1999. 44(1): pp. 120-124.

Nanni A. "Concrete repair with externally bonded FRP reinforcement". Concr Int 1995. 17(6): pp.22-26.

Neto P. Alfaiate J. Vinagre J. "A three-dimensional analysis of CFRP-concrete bond behavior". Composites: Part B 59; 2014. pp. 153-165.

Nicolais L., Borzacchiello A. "Wiley encyclopedia of composites". 2 (NJ): Wiley & Sons, 2012.

Niemitz C.W., James R. and Brena S.F. "Experimenta behavior of carbon fiber-reinforced polimer sheets attached to concrete surfaces using CFRP anchors" . Journal of composite for construction, ASCE, March/April 2010, pp. 185-194.

Obaidat Y.T., Heyden S., Dahlblom O. "Evaluation of Parameters of Bond Action between FRP and Concrete". Journal of Composites for Construction. ASCE. Reston (VA); September/October 2013. V. 17, No. 5, pp. 626-635.

Ozbakkaloglu T., Saatcioglu M. "Tensile Behavior of FRP Anchors in Concrete". Journal of Composites for Construction. ASCE. March/April 2011. V. 13, No. 2, pp. 82-92

Prota A., Tan K., Nanni A., et al. "Performance of shallow reinforced concrete beams

with externally bonded steel-reinforced polymer". ACI Struct J; 2006. 103(2): pp.163-170.

Serbescu A., Guadagnini M., Pilakoutas K. "Standardised double-shear test for determining bond of the FRP to concrete and corresponding model development" Elsevier Ltd, 2013.

Smith ST, Teng JG. "FRP-strengthened RC beams-I: review of debonding strength models". Eng Struct 2002;24(4):385-395.

Taljsten B. "Strengthening of beams by plate bonding". ASCE-J Mater Civil Eng; 1997. 9(4): pp.206-212.

Tamura T. "FiBRA, fiber-reinforced-plastic (FRP) reinforcement for concrete structures: properties and applications". In: Nanni A., editor. developments in civil engineering. Volume 42. Amsterdam: Elsevier; 1993. pp. 291-303].

Teng J. G. Smith S. T. Yao J. and Chean J. F. "Intermediate Crack Induced Debonding in RC Beams and Slabs",Construction and Building Materials, 2001, V. 17, No. 6-7 pp 447-462.

Teng J.G. et al. "RP composites in civil engineering". Hong Kong: Elsevier; 2001.

Teng J.G., Chen J.F., Smith ST, et al. "FRP strengthened RC structures". Chichester: John Wiley & Sons Ltd; 2002. pp. 11–101.

Ueda T., Sato Y., Asano Y. "Experimental Study on Bond Strength of Continuous Carbon Fiber Sheet". Proceedings of the FRP RCS-4 SP-188, American Concrete Institute; 1999, Farmington Hills, Mich., pp 407-416.

Zhang H.W. and Smith S.T. "Influence of FRP anchor fan configuration and dowel angle on anchoring FRP plates". Elsevier Ltd., 2011.

APPENDICES

5.3 Appendix A: Conversion Unit Table

Table A. 1 - Conversion of Units

Unit	Divisions	SI Equivalent
	UNIT FOR LENGTH	
1 inch (in)		25,4 mm
1 foot (ft)	12 in	0.305 m
1 yard (yd)	3 ft (36 in)	0.914 m
1 mile (mi)	1760 yd (5280 ft)	1.609 Km
	UNIT FOR AREA	
1 square inch (in^2)		645.16 mm^2
1 square foot (in^2)	144 in^2	0.093 m^2
1 acre (ac)	43560 ft^2	4046.873 m^2
	UNIT FOR VOLUME	
1 cubin inch (in^3)		16.387 mm^3
1 cubic foot (ft^3)	1728 in3	0.028 m^3
1 gallon (gal US)		0.004 m^3
	UNIT FOR MASS	
1 ounce (oz)		28.350 g
1 pound (lb)	16 oz	453.592 g
	UNIT FOR FORCE	
1 pound force (lbf)		4.448 N
1 kip force (kipf)	1000 lbf	4448.222 N
	UNIT FOR DENSITY	
1 pounds per cubic foot (b/ft^3)		16.018 Kg/m^3
	UNIT FOR SPEED	
1mile per hour (mph)		1.609 Km/h
	UNIT FOR MOMENT	
1 inch-pound force (in lbf)		0.113 Nm
1 foot-pound force (ft lbf)		1.356 Nm
	UNIT FOR PRESSURE	
1 pound per square inch (psi)		6894.757 Pa
	UNIT FOR TEMPERATURE	
1 degree Fahrenheit (°F)		°F = 9/5°C + 32

5.4 Appendix B: Steel Support Design

A steel support was specifically designed in order to compute the double shear test (Test 3). Three different types of steel section were used in order to create the final support:

- Section C10x25, length 13 in.
- Section HSS 14x0.500, length 10 in.
- Plate 15x18

The steel components were welded together by the writer. The dimensions of the weldings are illustrated in the following drawings. Moreover, Fig. B.4 and B.5 illustrate the operation of welding and the final steel support.

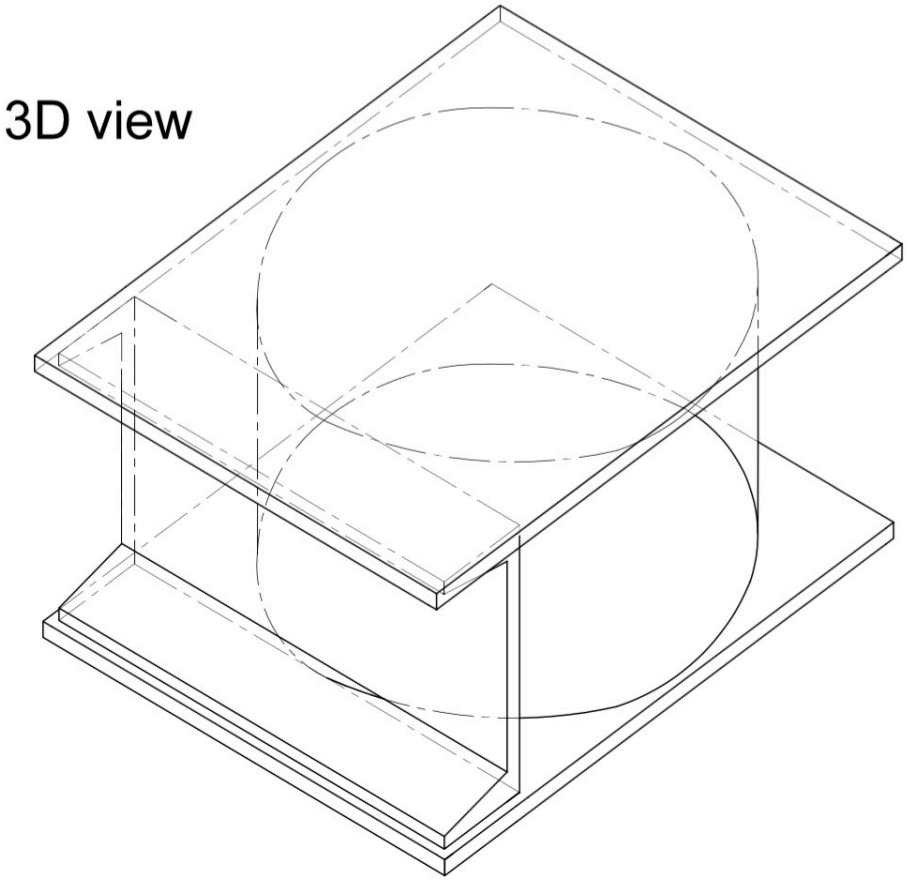

Appendix B. 1 - 3D view of the steel support

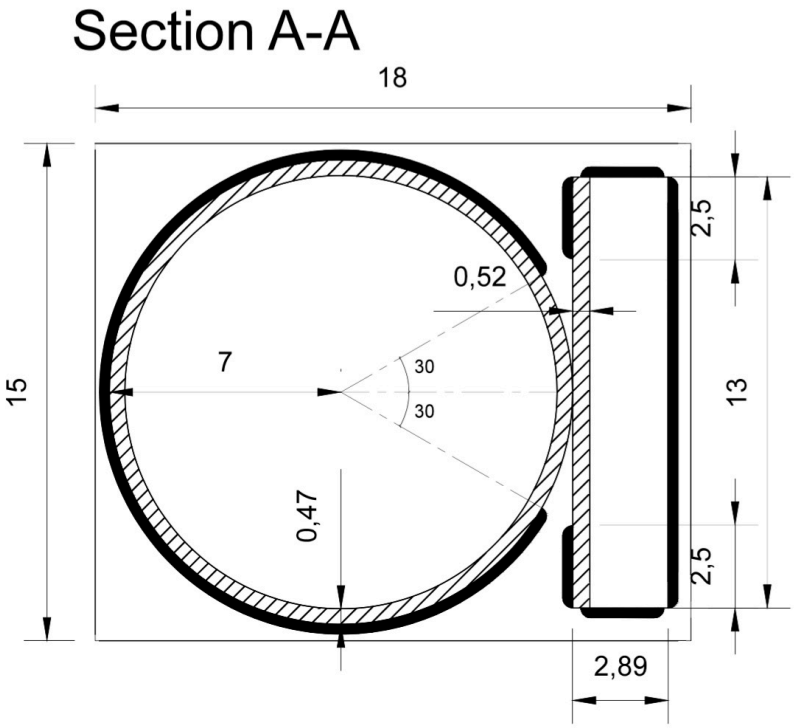

Appendix B. 2 - Section of the Steel Support

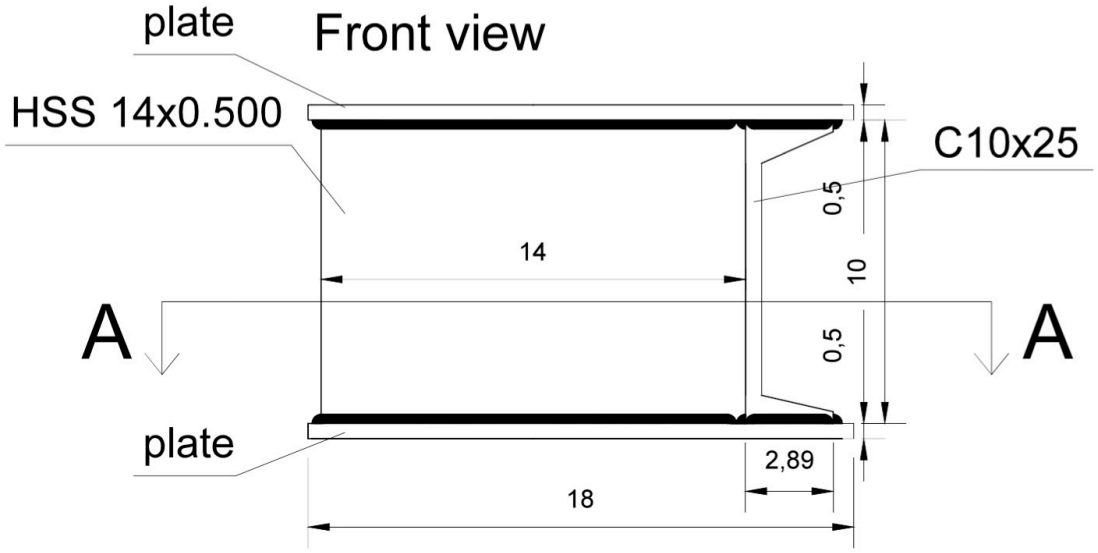

Appendix B. 3 . Fron View of the Steel Support

Appendix B. 4 - Operation of welding

Appendix B. 5 - Steel Support